Comparing calculation methods of deep excavations in soft clay

Comparison of analytical and numerical methods with field measurements for sheet pile wall excavations in soft clay

Master's thesis in the Master's programmes
Structural Engineering and Building Technology
Infrastructure and Environmental Engineering

Elin Johansson
Erica Larsson

Department of Architecture and Civil Engineering
CHALMERS UNIVERSITY OF TECHNOLOGY
Gothenburg, Sweden 2026
www.chalmers.se

Master's thesis 2026

Comparing calculation methods for deep excavations in soft clay

Comparison of analytical and numerical methods with field measurements for sheet pile wall excavations in soft clay

Elin Johansson

Erica Larsson

Department of Architecture and Civil Engineering
Division of Geology and Geotechnics
Chalmers University of Technology
Gothenburg, Sweden 2026

Comparing calculation methods for deep excavations in soft clay
Comparison of analytical and numerical methods with field measurements for sheet pile wall excavations in soft clay

ELIN JOHANSSON
ERICA LARSSON

Supervisor: Kajsa Alte, COWI
Supervisor: Leif Jendeby, COWI
Supervisor: Mats Karlsson, Department of Architecture and Civil Engineering
Examiner: Mats Karlsson, Department of Architecture and Civil Engineering

Master's Thesis 2026
Department of Architecture and Engineering
Division of Geology and Geotechnics
Chalmers University of Technology
SE-412 96 Gothenburg
Telephone +46 31 772 1000

Cover: Picture of the Lindome excavation 1997 (Leif Jendeby).

Typeset in LaTeX
Printed by Chalmers Reproservice
Gothenburg, Sweden 2026

Comparing calculation methods for deep excavations in soft clay
Comparison of analytical and numerical methods with field measurements for sheet pile wall excavations in soft clay
ELIN JOHANSSON
ERICA LARSSON
Department of Architecture and Civil Engineering
Chalmers University of Technology

Abstract

Using computational tools has become standard practice in all engineering fields. In geotechnical engineering, there are a large number of calculation programs available to capture the complex conditions associated with underground construction. These advanced models can achieve efficient and optimised designs in a short amount of time. But can the complicated conditions of soil construction be too complicated to capture in advance models? This thesis will try to answer when the implementation of numerical tools is the most appropriate option.

The thesis has studied three cases of sheet pile wall excavations, one of which is based on a real case with measured data from a single-strut excavation, and the other two are based on empirical values for typical Gothenburg clay. In the last two cases, one is a single-strut excavation, and the other has two levels of struts. The cases were assessed using four different calculation methods. Two of the four methods use a numerical approach, including the Mohr-Coulomb and NGI-ADP material models. Numerical results include a parametric study of certain stiffness parameters, such as the bending stiffness of the sheet pile wall, the soil stiffness, and the axial stiffness of the supporting strut. The results include active and passive earth pressures, horizontal displacements and waler reaction forces.

Results show that, in general, it is very difficult to create a model that accounts for all parts of a construction process, and that an advanced model does not always yield more realistic results than a simpler model. However, complicated models are more flexible to work with and easier to implement for finding optimised designs. The parametric study showed that earth pressures are not significantly affected by changes in stiffness inputs, whereas deflections and waler forces are more sensitive. Further, the soil stiffness input has a greater influence than the stiffness inputs of the structural elements. The effect of the strut stiffness in particular could be considered negligible, and the bending stiffness of the sheet pile wall only showed a minor influence on the results.

Keywords: Deep excavation, Soft clay, Retaining structure, Sheet pile wall, Numerical modelling, PLAXIS 2D, NGI-ADP, Mohr-Coulomb

Acknowledgements

This master's thesis was carried out during the spring of 2026 as a part of the master's programmes in Structural Engineering and Building Technology and Infrastructure and Environmental Engineering. The project has been conducted at the Department of Geology and Geotechnics at Chalmers University of Technology in collaboration with COWI AB.

We would like to thank COWI's Geotechnical department in Gothenburg for letting us work at your office and for all the valuable help and coffee breaks.

We express special appreciation to Kajsa Alte at COWI for all the great support and encouragement throughout this semester. We would also like to extend a special thank you to Leif Jendeby at COWI for introducing the subject and providing us with your work containing field measurements. We are deeply grateful for your incredible support and the knowledge you shared with us throughout the project.

Finally, we would like to express our gratitude to our supervisor and examiner at Chalmers, Mats Karlsson, for his valuable input, guidance, and support throughout this thesis.

List of Acronyms

Below is the list of acronyms that have been used throughout this thesis, listed in alphabetical order:

CRS	Constant rate of strain
DSS	Direct shear strength
FEA	Finite element analysis
FEM	Finite element method
FVT	Field vane test
MC	Mohr Coulomb
NC	Normally consolidated
OCR	Over-consolidation ratio
POP	Pre-overburden pressure
SF	Safety factor
SPH	Sponthandboken

Nomenclature

Below is the nomenclature of indices, sets, parameters, and variables that have been used throughout this thesis.

Latin letters

c	Cohseion	[kPa]
c_u	Undrained shear strength	[kPa]
c_{uv}	Uncorrected undrained shear strength from field vane test	[kPa]
D	Elastic material stiffness matrix	[kPa]
E'	Young's modulus	[kPa]
E_{oed}	Oedometer modulus	[kPa]
E'_{ref}	Referense soil stiffness	[kPa]
E'_{inc}	Increase of soil stiffnes with depth	[kPa]
EI	Bending stiffness	[kPa]
f	Yield function	[-]
F	Yield surface	[-]
G	Shear modulus	[kPa]
G_{ur}	Unload-reload shear modulus	[kPa]
H	Height of the excavation	[m]
I_P	Plasticity index	[%]
k	Hardening parameter	[-]
K_0	Coefficient of lateral earth pressure at rest	[-]
K_a	Coefficient of active lateral earth pressure	[-]
N_{cb}	Bearing capacity factor	[-]
K_p	Coefficient of passive lateral earth pressure	[-]

p_0	Lateral earth pressure at rest	[kPa]
p_a	Active lateral earth pressure	[kPa]
$p_{\mathrm{p,netto}}$	Net earth pressure below excavation bottom	[kPa]
p_p	Passive lateral earth pressure	[kPa]
q_d	Design surcharge load	[kPa]
q_k	Characteristic surcharge load	[kPa]
r	Adhesion	[-]
s_u^A	Undrained active shear strength	[kPa]
s_u^P	Undrained passive shear strength	[kPa]
s_u^{DSS}	Direct simple shear strength	[kPa]
u	Pore water pressure	[kPa]
w_N	Natural water content	[%]
w_L	Liquid limit	[%]
w_P	Plastic limit	[%]
z	Depth	[m]

Greek letters

γ	Unit weight	[kN/m^3]
γ_d	Partial coefficient for safety class	[-]
$\gamma_{\varphi'}$	Partial safety factor of effective friction angle	[-]
γ_{c_u}	Partial safety factor of undrained shear strength	[-]
ε	Strain	[-]
κ	Volumetric hardening parameter	[-]
μ	Correction factor	[-]
ν	Poisson's ratio	[-]
σ	Stress	[kPa]
σ'_{h0}	Lateral earth pressure at rest	[kPa]
σ'_c	Pre-consolidation pressure	[kPa]
σ_t	Cut-off tension and tensile strength	[kPa]
σ'_v	In-situ effective vertical pressure	[kPa]
φ	Friction angle	[$\circ$]
ψ	Dilatancy angle	[$\circ$]

Contents

List of Figures

List of Tables

1
Introduction

Retaining structures are a standard concept in construction and infrastructure projects that include deep excavations. In urban environments, space may be limited, and under these circumstances, there are strict requirements regarding anticipated deformations and stability. In such cases, unreliable results can lead to structural damage and significant economic consequences.

When designing a retaining structure, the standard practice is to use analytical calculations for stability and structural forces. This method is beneficial when simplicity, efficiency and cost-effectiveness are desired. It provides a simplification of the soil into a manageable and more easily evaluated structure.

However, with the increasing complexity of geotechnical problems and improved computational technology, numerical analysis programs are increasingly becoming more common in civil engineering. Numerical methods can provide a more detailed description of material behaviours and, therefore, more accurate results. However, the increasing accessibility and intuitive interfaces of these programs may contribute to improper use and misinterpretations of results, especially when the operator lacks sufficient knowledge.

Although numerical programs can significantly improve solution accuracy, the additional time and cost of running them may outweigh the benefits. Furthermore, due to the complexity of the soil and the complicated conditions of the surrounding environment, particularly in urban areas, the material models used in numerical analyses rely on several simplifications. Consequently, the calculated results may still contain uncertainties due to the advanced circumstances of the problem.

Hence, it would be beneficial to identify the circumstances under which a numerical approach would be most advantageous.

1.1 Aim and objectives

This study aims to investigate whether numerical analyses can provide more reliable and detailed results than analytical analyses, and to identify the conditions under which this may be the case. This includes investigating the assumptions and simplifications made in each method and evaluating how they affect the final results.

Furthermore, the study will also investigate the differences between the analytical and numerical models, as well as how different material models and input parameters affect the final results. The study will be conducted using two cases, one theoretical, mostly based on empirical values, and one based on measurements from an excavation in Lindome.

The list below presents the research questions and objectives that were applied to assist the report.

Research questions

1. Under which conditions are analytical analyses enough?
2. When is the use of numerical analyses necessary?
3. Which input parameters have the most influence on the results?
4. Will the accuracy of numerical results increase with increasingly complex problems?

1.2 Societal, ethical and ecological aspects

From an ecological perspective, an efficient design of deep excavations may contribute to reduced material consumption, shorter construction time and reduced impact on the surrounding environment. The choice of calculation method may influence both the design and sustainability of the projects. Numerical methods can provide more detailed results and therefore support a more optimised design. However, these methods often require greater computational effort, greater demand on user knowledge, and are more time-consuming. Consequently, the use of numerical methods should be evaluated (Plevris & Markeset, 2018).

Societal aspects may be related to the safety, especially when conducting excavations in urban environments. It is important to consider when designing and constructing geotechnical structures. Failure of retaining structures can have serious consequences for workers, nearby buildings and infrastructure. It is therefore important that the selected design methods provide reliable predictions of the structural behaviour of the retaining walls to minimise the risk of accidents and failure.

The ethical aspects are related to how the numerical models are created, interpreted and applied in practice. The results depend on the input parameters, modelling assumptions, and the model's limitations. It is therefore important that uncertainties and limitations are clearly reported rather than neglected or adjusted to obtain a desired result. Therefore, numerical methods should be used critically and as a complement to the engineering judgment. Ultimately, the engineer remains responsible for the design decisions and must be able to justify the chosen methods, assumptions and results.

1.3 Method

The methods that have been implemented in this project are briefly described by the flowchart in Figure 1.1.

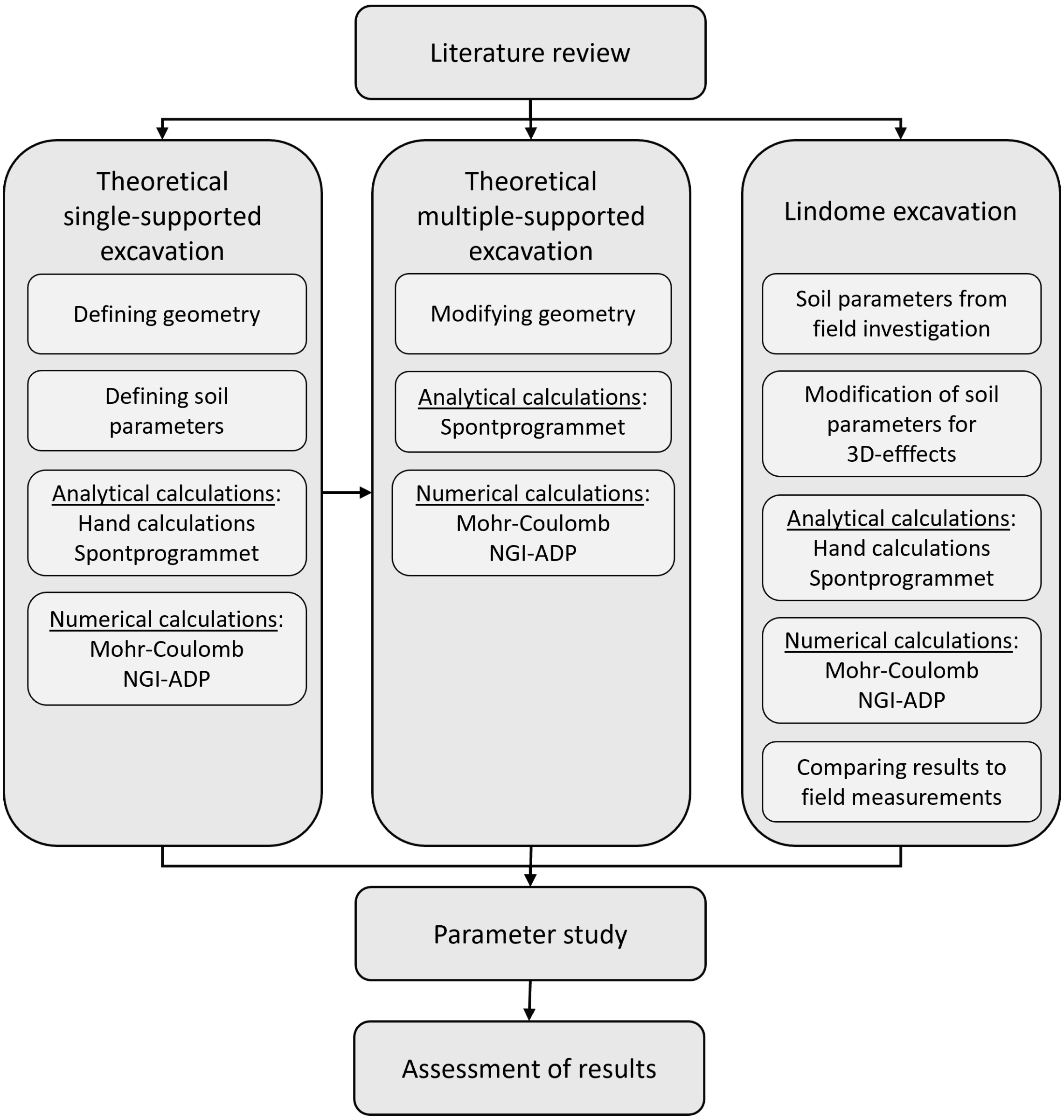

Figure 1.1: Overview of applied methodology

Four calculation methods have been applied during the study, two of which are analytical and two are numerical. The analytical methods are done according to the calculations presented in *Sponthandboken, Rapport 107* (SPH) by Fredriksson et al. (2024). The first analytical method was performed using SPH in an Excel spreadsheet and will be referred to as *hand calculations*. *Spontprogrammet* by Anders Ryner have been used as the second option for analytical calculations. The numerical calculations have been performed using PLAXIS 2D. The clay layers were modelled using Mohr-Coulomb (MC), which is a simple material model, and the more complex NGI-ADP material model.

The four mentioned models have been implemented three times. First, two theoretical cases have been used in a parametric study to compare the different methods. The theoretical cases are divided into a single-strut excavation and a multiple-strut excavation. The second is a further development of the first case, examining how parameters are affected as the complexity of the problem increases.

Lastly, in the Lindome case, with on-site parameters taken from the report by Edstam and Jendeby (1992). The input parameters have been modified to account for the 3D effects. The on-site measurements done in Lindome have been used to compare the four calculation methods to real-life measurements, along with a parametric study of the PLAXIS models.

1.4 Scope

This study will only focus on the numerical analysis conducted in PLAXIS 2D to compare analytical and numerical methods. For a simple rotationally stable case, the main purpose is to evaluate the differences between the different methods of analysis. For this reason, there will also be a comparison between different numerical material models.

The excavation described in the case report by Edstam and Jendeby (1992) will be replicated as closely as possible to obtain results that are as realistic as possible. However, some simplifications will be done to reduce workload and keep the main focus on different calculation methods. For this reason, the modelling of the stiffness of the temporary strut will not be included in this report. The excavation geometry is presented in more detail in Section 5.1.

The real excavation was performed in several horizontal steps due to the stabilising effects of 3D effects, but this project is limited to 2D numerical analyses. The report also focuses only on undrained conditions in soft cohesive soils. while long-term effects such as consolidation and creep are not considered.

2

Theory

2.1 Earth pressure and retaining structures

The purpose of a retaining structure is to resist retained soil masses from collapsing or deforming onto the construction site below. A retaining wall placed in the ground without excavation is subjected to horizontal pressure from the surrounding soil.

Excavation on one side of a retaining wall reduces lateral support, causing retained soil to deform towards the excavation. As the wall moves, shear strength is mobilised in the soil mass until it reaches the bearing capacity under active and passive earth pressures. Active earth pressure acts on the retained side and pushes the wall towards the excavation, whereas passive earth pressure is mobilised on the excavation side and acts in the opposite direction, providing resistance to wall movement (Fredriksson et al., 2024). The *active and passive Rankine states* form the two extreme boundary conditions in which equilibrium is maintained, see Figure 2.1.

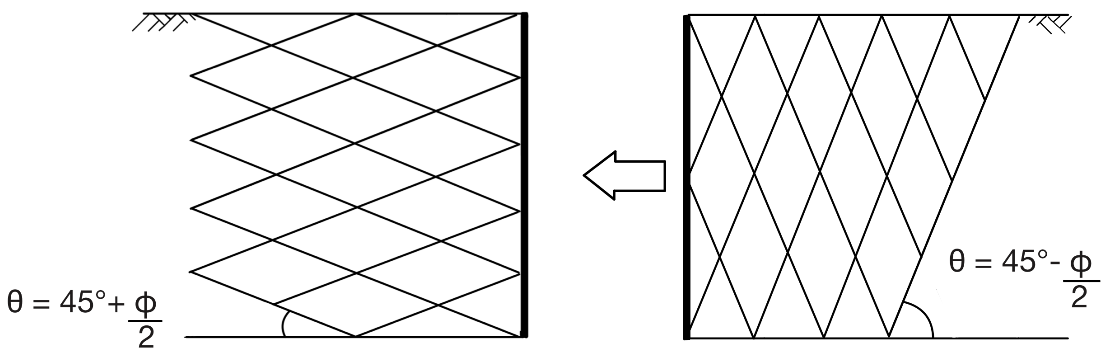

Figure 2.1: Rankine's active and passive states

Rankine's *Lateral earth pressure coefficients* (K) are used to describe different stress states of the soil (Tornborg, 2024), including the ultimate states. All intermediate states between the limiting conditions, including the state of rest, are referred to as a *state of elastic equilibrium* (Terzaghi & Peck, 1967). The relationships between lateral strain and earth pressure coefficients can be found in Figure 2.2.

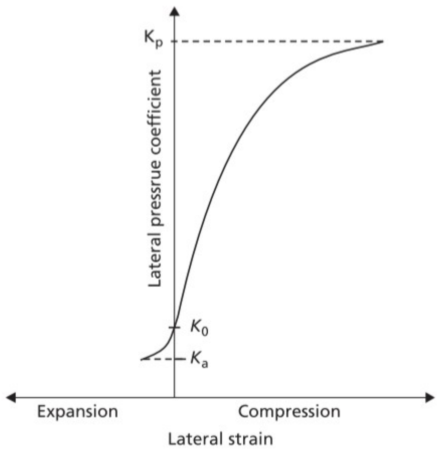

Figure 2.2: Relationship between lateral strain and lateral earth pressure coefficients (Knappett & Craig, 2012)

2.1.1 Initial earth pressure

Before any excavations of soil, a retaining structure can be assumed to be under an initial lateral earth pressure (σ_0) that corresponds to the total horizontal earth pressure at rest (σ_{h0}). The horizontal earth pressure is often expressed by the earth pressure coefficient, which at rest conditions is named K_0 and defined according to Equation (2.1).

$$K_0 = \frac{\sigma'_{\mathrm{h0}}}{\sigma'_{\mathrm{v0}}} \tag{2.1}$$

where σ'_{h0} = effective horizontal earth pressure at rest

σ'_{v0} = effective vertical earth pressure at rest

The initial horizontal earth pressure can then be calculated using Equation (2.2). This is the theoretical earth pressure acting on a sheet pile wall installed in the ground before any excavation.

$$p_0 = \sigma'_{\mathrm{v0}} \cdot K_0 + u \tag{2.2}$$

2.1.2 Retaining structures in cohesion-less soil

In cohesion-less soils, earth pressures can be estimated using Rankine´s earth pressure theory (Rankine, 1857). The theory describes the passive and active horizontal earth pressures on retaining structures based on a plastic equilibrium (Terzaghi & Peck, 1967). The theory states that the active and passive horizontal earth pressure can be calculated according to Equation (2.3) and Equation (2.4)

$$p_a = \sigma'_v \cdot K_a + u \tag{2.3}$$

$$p_p = \sigma'_v \cdot K_p + u \tag{2.4}$$

where K_a = Coefficient of active earth pressure
K_p = Coefficient of passive earth pressure

The earth pressure experienced by the retaining structure can be divided between pore water pressure (u) and effective earth pressure (σ'_v). To account for the anisotropy of the soil, K_a and K_p are multiplied by σ'_v. The earth pressure coefficients are defined according to Equations (2.5) and (2.6). When the active or passive pressures are fully developed, the soil has reached *active/passive Rankine state* (Terzaghi & Peck, 1967).

$$K_a = \frac{1 - \sin(\varphi)}{1 + \sin(\varphi)} = \tan^2(45° - \frac{\varphi}{2}) \tag{2.5}$$

$$K_p = \frac{1 + \sin(\varphi)}{1 - \sin(\varphi)} = \tan^2(45° + \frac{\varphi}{2}) \tag{2.6}$$

2.1.3 Retaining structures in cohesive soil

In cohesive soils, Rankine's theory can be combined with Terzaghi's principle to calculate the active and passive earth pressure according to Equation (2.7) and Equation (2.8) (Terzaghi, 1946).

$$p_a = \sigma'_v \cdot K_a - 2 \cdot c \cdot \sqrt{K_a} + u \tag{2.7}$$

$$p_p = \sigma'_v \cdot K_p + 2 \cdot c \cdot \sqrt{K_p} + u \tag{2.8}$$

In undrained conditions, the friction angle in Equation (2.5) can be assumed to φ=0 and when calculating the earth pressures in cohesive soils such as clay, the interface friction between the retaining wall and the adjacent soil can be taken into account by the equations (2.9) and (2.10) (Fredriksson et al., 2024).

$$p_a = \sigma_v - 2 \cdot c_u \cdot \sqrt{1 + r_a} \tag{2.9}$$

$$p_p = \sigma_v + 2 \cdot c_u \cdot \sqrt{1 + r_p} \tag{2.10}$$

where r_a = active relative adhesion factor
r_p = passive relative adhesion factor
c_u = undrained shear strength

Normally, when calculating the active and passive earth pressures, the adhesion can be assumed to be zero and the equations can then be simplified to those presented by Terzaghi and Peck, 1967, equations (2.11) and (2.12)

$$p_a = \sigma_v - 2 \cdot c_u \tag{2.11}$$

$$p_p = \sigma_v + 2 \cdot c_u \tag{2.12}$$

When the earth pressures have been obtained, a net earth pressure acting in the passive direction is calculated according to Equation (2.13) (Sahlström & Stille, 1979). This applies to excavations with soft soils, such as clay, below the excavation bottom.

$$p_{\text{net}} = N_{\text{cb}} \cdot c_u - (\gamma \cdot H + q) \tag{2.13}$$

where N_{cb} = Bearing capacity factor
H = Excavation depth
q = Surcharge load

The bearing factor N_{cb} depends on the number of support levels, the width of the excavation and the interaction between the retaining wall and the surrounding soil on the active and passive sides (Sahlström & Stille, 1979).

For retaining structures anchored at a single level, the factor N_{cb} mainly depends on the interface friction between the wall and soil. The coarseness of the retaining wall takes a value between $-1 \leq r \leq 1$, where r=1 indicates full adhesion between sheet pile wall and soil in an upwards direction. N_{cb} can be calculated according to Equation (2.14) (Fredriksson et al., 2024).

$$N_{cb} = 2 \cdot (\sqrt{1 + r_p} + \sqrt{1 + r_a}) \tag{2.14}$$

Retaining structures supported at multiple levels become statically indeterminate, and the design earth pressure is calculated differently. The horizontal earth pressures are calculated similarly to a single support excavation, but a redistribution of the earth pressure profile is done according to Equation (2.15)

$$\sigma_i = \frac{P_A}{0.9 \cdot H + d} \tag{2.15}$$

The stability of the excavation is determined by stability against bottom heave, where another term, N_b, is calculated (Sahlström & Stille, 1979). The safety factor against bottom heave only applies to excavations retained at multiple levels.

2.2 Analytical stability analysis

Retaining walls are normally designed and checked in the *Ultimate Limit state* (ULS) and in the *Serviceability Limit State* (SLS). In ULS, the excavation is designed to ensure overall stability under maximum loading conditions. For retaining walls, the analysis evaluates whether the structure can withstand lateral earth pressures.

In a ULS calculation, the partial safety factors are applied to the material parameters, overturning permanent loads such as earth pressures, and external loads. In this method, there is no need to apply any further factors to the final result for the waler force. The solution becomes lower-bound by the added partial factors, which means that the expected deformations and forces will be conservatively estimated. This ensures that the analysis takes uncertainties of the soil properties or modelling assumptions into account.

Stability calculations in SLS account for normal operating loads, meaning that no partial factors are applied to the resulting force. The resulting forces, according to Sponhandboken, should be corrected using the method by Stille (1976), which accounts for pre-stressing of the struts. If the strut is considered very stiff, the total dimensioning waler force reads according to Equation (2.16)

$$Q_{\text{tot}} = 1.12 \cdot Q_{\text{Fr(G)}} \tag{2.16}$$

where $Q_{Fr(G)}$ = Resultant of net active earth pressure acting on sheet pile wall

The SLS design approach also adds a model factor ($\gamma_{\text{S:d}}$) to stiff and weak elements. If a stiff strut is in place, the model factor should be applied to the force when pre-stresses are taken into account.

2.2.1 Stability calculation single support

For a retaining structure, the stability is governed by the static equilibrium. For an excavation supported at a single level, the problem is statically determinate and can be solved by force equilibrium.

The required length of the retaining wall is determined by the moment equilibrium about the centre of rotation. Thus, the sum of the overturning moments must be equal to the resisting moments, where the wall length defines the lever arm of the resisting moments (Sahlström & Stille, 1979).

The reactive force in the waler is determined by force equilibrium, where the resultant of the overturning forces is balanced by the stabilising forces and the force in the waler (Sahlström & Stille, 1979).

2.2.2 Stability calculation multiple supports

When installing additional supports, the excavation system becomes statically indeterminate and can no longer be solved by moment equilibrium.

After the ordinary earth pressures are calculated, the active design pressure is redistributed against the sheet pile wall. Afterwards, a cantilever moment can be calculated above the top support level, a moment between two support levels and a moment below the lowest support level (Sahlström & Stille, 1979). The load between two supports can be divided between the supports to calculate the reaction force in the waler (Fredriksson et al., 2024).

2.2.3 Spontprogrammet

Spontprogrammet 3.63 by RynSoft AB has been developed as an analytical computational program for the design of sheet pile walls. The calculations are based on the methods presented in Sponthandboken from 2018 (Ryner, 2022).

The computational tool uses Rankine's earth pressure theory to calculate the active and passive earth pressures in the soil. The length of the retaining structure and the load effects in the walers are determined by force and moment equilibrium, as described in Section 2.2.1. In Spontprogrammet, it is not possible to model time effects or multiple construction stages.

2.3 Numerical analyses in PLAXIS 2D

Numerical analyses are commonly applied to advanced mathematical problems that are difficult or impossible to obtain analytically. They will provide approximate solutions with an iterative approach until a satisfactory result is obtained. The analysis is performed incrementally to capture changes in stiffness, with each step subdivided into increments for which equilibrium must be achieved (Broo et al., 2008).

The Finite Element Method emphasises that, instead of analysing an entire domain, it can be divided into a finite number of smaller elements. The set of elements is called a *finite element mesh* and the elements are assembled with certain compatibility conditions to form the domain (Ottosen & Petersson, 1992).

It is assumed that the differential equations hold in a certain region, and instead of seeking a solution for the entire domain, an approximation is obtained over the elements. Even though the problem may vary non-linearly over the region, it is assumed that the approximation over the element is linear (Ottosen & Petersson, 1992). When approximations for all elements have been made, it allows for an approximate solution for the entire domain (Ottosen & Petersson, 1992).

PLAXIS 2D is a commercial software package that performs 2-dimensional analyses focused on deformations and stability in geotechnical engineering (Seequent, 2025a). PLAXIS 2D uses the Finite Element Method (FEM), a numerical method for solving complex problems described by systems of equations (Ottosen & Petersson, 1992).

2.3.1 Modelling elasto-plastic behaviour in soils

As shown in Figure 2.3, several types of constitutive models are used to describe the stress-strain relationship of elasto-plastic materials, these are collectively called *elasto-plastic constitutive models*. They all consist of four parts: an elastic law, a yield surface, a flow rule and hardening laws (Karstunen & Amavasai, 2017).

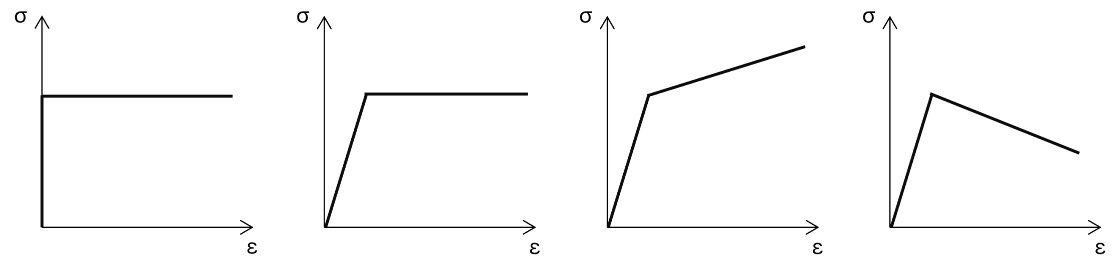

(a) Rigid perfectly plastic (b) Elasto-plastic perfectly plastic (c) Elasto-plastic hardening (d) Elasto-plastic softening

Figure 2.3: Idealised stress-strain responses figure taken from (Karstunen & Amavasai, 2017)

Elastic response

In the initial stages of retaining structure analysis, soil behaviour is typically assumed to be elastic. This is relevant in the early stages of excavation, where stress changes are relatively small, and the strains remain elastic (Knappett & Craig, 2012). The soil is typically assumed to be isotropic, and the relationship between stress σ and strain ε can be expressed by Hooke's law, see Equation (2.17) (Ottosen & Petersson, 1992).

$$\sigma = E \cdot \varepsilon \tag{2.17}$$

The expression requires two material parameters, which are Young´s modulus E, which defines the soil stiffness and Poisson´s ratio ν (Lees, 2016). In numerical analyses, the relationship is generalised to a matrix form described by Equation (2.18).

$$\boldsymbol{\sigma} = \mathbf{D} \cdot \boldsymbol{\varepsilon} \tag{2.18}$$

$$D = \frac{E}{2 \cdot (1 - \nu)} \begin{bmatrix} 1 & 1 & 1 \\ 1 & 1 & 1 \\ 1 & 1 & 1 \end{bmatrix} \tag{2.19}$$

The theory assumes that strains that develop during the stress state will return to zero when the imposed stress is removed, leaving no residual deformation. For retaining structures, elastic deformations only occur in the cross-sectional plane and not in the longitudinal direction (Knappett & Craig, 2012). The matrix **D** represents the elastic material stiffness matrix in two dimensions, where Young's modulus (E') and Poisson's ratio (v') are input parameters in the matrix (Ottosen & Petersson, 1992). However, the linear-elastic soil model is a simplification of the real soil behaviour. As excavation and analysis progress, stress levels increase, and the soil response becomes nonlinear.

Plastic response

During plastic response, the material has been subjected to permanent deformation, which is described in constitutive models by the yield functions, flow rule and hardening parameter.

The boundary in the principal stress space between elastic and elasto-plastic behaviour is made up of the *yield surface* (F) (Lees, 2016). The surface is constructed from several yield functions (f). If f = 0, the stress state lies on the yield surface, and the soil behaviour is plastic. If f<0, the current stress state has not reached the yield surface and the soil behaves elastically, while f > 0 is practically impossible to achieve (Jasoliya et al., 2024).

When the stress state of the soil reaches the yield surface and undergoes plastic deformation, a flow rule is used to define how plastic strain develops on the yield surface. An *associate flow* suggests that the plastic strain increment develops perpendicular to the yield surface. In a *non-associate* flow, the plastic strain develops independently from the yield surface (Karstunen & Amavasai, 2017). An associate flow is often assumed for soil with low friction angles.

The yield surface contains a hardening parameter (κ) that varies with plastic strain, the variation is described by the adopted hardening or softening law (Jasoliya et al., 2024). If k is constant, there is no defined hardening or softening law and the material is considered perfectly plastic, as in figure 2.3b.

2.3.2 Modelling a 3D problem in 2D

PLAXIS 2D has a modelling mode called *Plane strain*. This is an approximation which simplifies a three-dimensional problem into two dimensions. The approximation relies on the assumption that for cross-sections, the out-of-plane deformation is negligible. It means that the strains perpendicular to the cross-sectional plane are assumed to be zero, as well as the associated shear strains (Ottosen & Petersson, 1992).

In PLAXIS 2D, this assumption is implemented by prescribing the displacement in the out-of-plane direction to zero. Despite this restriction, PLAXIS will still calculate a three-dimensional stress state at each integration point.

This ensures that a three-dimensional material behaviour is calculated while simplifying the problem to two dimensions. The plane strain assumption is appropriate for geotechnical structures with constant geometry, material properties, and loading conditions along their longitudinal direction, such as retaining walls, sheet pile walls, and excavations (Lees, 2016).

Structural elements

In PLAXIS 2D, the structural parts of a construction, such as retaining walls and struts, can be simulated using structural elements. Among the most commonly used elements are the plate elements and the fixed-end anchors.

A fixed-end anchor is a spring element that connects a node to a fixed point (Lees, 2016). The fixed point has a prescribed displacement that is always zero (Seequent, 2025c). The stiffness in the spring element provides an axial stiffness between the connected nodes, which theoretically allows the anchor to extend or compress, creating compressive or tensile forces in the element (Lees, 2016).

Plates are elements that have displacement degrees of freedom as well as rotational degrees of freedom. However, in PLAXIS 2D, the plate elements are actually beam elements but designed to integrate the 3-dimensional effects in a 2-dimensional environment in plane strain (Seequent, 2025d). These elements have both axial and bending stiffness and are commonly used to model retaining walls (Lees, 2016).

Interface elements are elements that can be implemented to simulate the interaction between the retaining wall face and the adjacent soil (Lees, 2016). These are zero-thickness elements that have node pairs instead of a single node. The nodes share the same location, but each has its own three translational degrees of freedom. This allows for displacements between the pairs, which can occur in the form of gapping and slipping. Slipping represents the shear displacement of the soil along the wall, and gapping describes the separation between the wall and adjacent soil (Seequent, 2025d).

Drainage type

It can be appropriate to perform an *undrained analysis* in cases where the loading rate is high, the soil's permeability is low or if only short-term output effects are required (Seequent, 2025c). Undrained conditions assume that there is no dissipation or flow of water, which leads to a build-up of excess pore water pressure (Lees, 2016). However, for long-term behaviour, a *consolidation analysis* allows excess pore pressures to dissipate and long-term effects to develop (Lees, 2016).

There are three different drainage types available in PLAXIS 2D, Undrained A, B or C. Undrained A and B are both effective stress analyses that predict excess pore pressures. Undrained A provides c_u as a result, which might lead to overestimation of the undrained shear strength, while Undrained B has a specified c_u as input (Seequent, 2025b). Undrained C is a total stress analysis defined by total stress parameters as inputs, c_u is also entered as input to the model.

Model boundaries

The global boundaries of a FE mesh are the *model boundaries*. The purpose of the model boundaries is to define the model's spatial extent and simulate its interactions with the surrounding area. The boundaries should be placed sufficiently far away from the area of interest so that it does not affect the outputs. To simplify a symmetric geometry, only one side of the excavation needs to be modelled. This means that there will be a vertical model boundary at the axes of symmetry that represents that all aspects of the model are symmetrical, including, for instance, time steps, loads, ground conditions, etc. (Lees, 2016).

2.3.3 Material models

When modelling geotechnical problems in PLAXIS 2D, there are various material models available. In this study, the Mohr-Coulomb (MC) material model and the NGI-ADP material model have been applied to the clay layers. The MC model is an isotropic model recommended to be used as a basic reference model for first approximations. While the NGI-ADP model is more advanced by considering annisotropic soill behaviour. It also requires a more extensive set of input parameters (Seequent, 2025b).

Mohr-Coulomb model

The Mohr-Coulomb model in PLAXIS 2D is a linear elastic perfectly plastic model in which the linear elastic part follows Hooke's law as described in Equation (2.18). The plastic part is based on the Mohr-Coulomb failure criterion, with a yield surface usually formulated as in Equation (2.20).

$$F = \frac{\sigma_i' + \sigma_j'}{2} sin\phi - \frac{\sigma_i' - \sigma_j'}{2} - c \cdot cos\phi \leq 0 \tag{2.20}$$

The yield surface forms a hexagonal cone in the principal stress space, see Figure 2.4. If the stress state of a certain node lies within the criterion, the soil remains elastic, while a stress state on the yield surface indicates plastic failure.

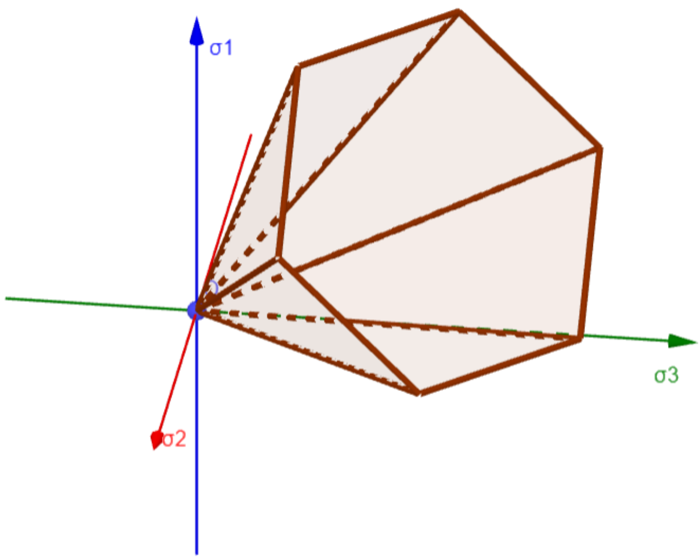

Figure 2.4: Yield surface of the Mohr-Coulomb material model plotted in principal stress space

The MC model keeps a non-associated flow rule defined by a plastic potential function in drained conditions. However, in undrained conditions, the flow rule becomes equal to the yield function and associated flow is adopted.

The required input data in PLAXIS 2D is at least 2 stiffness parameters and 3 strength parameters (Seequent, 2025b). All possible input parameters are listed in Table 2.1. The tensile strength (σ_t) is defined as the allowable tensile stress and is typically set to zero. It can be included when cohesion is considered. However, this may result in unrealistic predictions of tensile strength in the soil.

The three stiffness modules (E_{ref}, G, E_{OED}) are directly connected in the material model according to Hooke's law in Equations (2.21) and (2.22) (Seequent, 2025b).

Changing one of the inputs automatically changes the other two.

$$G = \frac{E}{2 \cdot (1 - \nu)} \tag{2.21}$$

$$E_{\text{OED}} = \frac{E \cdot (1 - \nu)}{(1 - 2 \cdot \nu) \cdot (1 + \nu)} \tag{2.22}$$

Table 2.1: Input parameters with standard units to the Mohr-Coulomb material model in PLAXIS 2D for non-dynamic applications (Seequent, 2025b)

Input parameters			
Stiffness	E_{ref}	Young´s modulus	[kPa]
	v	Poisson's ratio	[-]
	G	Shear modulus	[kPa]
	E_{oed}	Oedometer modulus	[kPa]
Strength	c	Cohesion	[kPa]
	φ	Friction angle	[°]
	ψ	Dilatancy angle	[°]
	σ_{t}	Cut-off tension and tensile strength	[kPa]

NGI-ADP

NGI-ADP is a constitutive model developed by the Norwegian Geotechnical Institute (NGI) that can be implemented in PLAXIS 2D and is commonly used for undrained conditions in clay (Grimstad et al., 2012).

The model is a non-linear elasto-plastic model that incorporates anisotropy in undrained soil modelling based on the concept of ADP-zones introduced by Bjerrum and Aitchison, 1973. These zones, the active (A), direct simple shear (D) and passive zones (P) represent the active and passive earth pressures acting on a sheet pile wall (Bjerrum & Aitchison, 1973). They simplify the stress states in the soil, and the zones can be directly related to direct simple shear tests and to triaxial tests in compression and extension as shown in Figure 2.5 (Skredkommissionen, 1995).

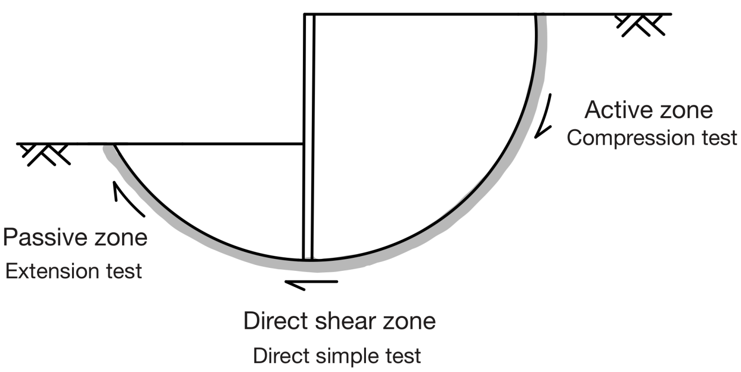

Figure 2.5: Active, direct shear and passive zones in an excavation with a retaining wall

The model uses Tresca´s yield criterion with a modified von Mises plastic potential function to avoid potential corner problems. These functions are independent of the mean stress, which results in no plastic volume strains developing. Choosing a Poisson´s ratio close to 0.5 results in a restriction of zero plastic volumetric strains (Grimstad et al., 2012). The yield criterion can be expressed as shown in Equation (2.23).

$$F = \sqrt{H(\omega) \cdot \hat{J}_2} - \kappa \cdot \frac{s_u^A + s_u^P}{2} = 0 \tag{2.23}$$

where $H(\omega)$ = Approximation of the Tresca criterion
$\hat{J}_2$ = Second deviatoric invariant
κ = Volumetric hardening parameter
s_u^A = Undrained active shear strength
s_u^A = Undrained passive shear strength

The active and passive shear strengths (s_u^A, s_u^P) are commonly obtained from triaxial compression and extension tests, while the direct shear stress (s_u^{DSS}) is obtained from the direct simple shear test. If triaxial tests are unavailable, empirical relations can be used to estimate the model's shear strength. The undrained shear strength can be estimated according to Equation (2.24) by Ladd and Foott (1974).

$$c_u = a \cdot \sigma'_{cv} \cdot OCR^{-(1-b)} \tag{2.24}$$

where a = Factor of load direction and liquid limit, Equation (2.25)
b = Material constant

The factor a is described by Lundström et al. (2025) in Equation (2.25). It is based on empirical relations of liquid limit and takes the direction of loading into account.

$$\begin{aligned} a &= 0.271 + 0.12 \cdot w_L \quad \text{for active direction of shear} \\ a &= 0.169 + 0.12 \cdot w_L \quad \text{for direct shear} \\ a &= 0.126 + 0.12 \cdot w_L \quad \text{for passive direction of shear} \end{aligned} \tag{2.25}$$

The NGI-ADP model has a non-associated flow rule and a non-linear hardening relationship that correlates with the plastic shear strain (γ^p), the shear strain at failure in triaxial compression and extension (γ_f^C, γ_f^E), and the direct simple shear (γ_f^{DSS}) (Grimstad et al., 2012). All the input parameters in PLAXIS 2D are listed in Table 2.2.

Table 2.2: Input parameters with standard units and some default input values to the NGI-ADP material model in PLAXIS 2D (Seequent, 2025b)

Input parameters			
Stiffness	G_{ur}/s_u^A	Ratio unloading / reloading shear modulus over (plane strain) active shear strength	[-]
	γ_f^C	Shear strain in triaxial compression	[%]
	γ_f^E	Shear strain in triaxial extension	[%]
	γ_f^{DSS}	Shear strain in direct simple shear	[%]
	ν_u	Undrained Poissons ratio	[-]
Strength	$s_u^{A,ref}$	Reference (plane strain) active shear strength	[kPa]
	$s_u^{C,TX}/s_u^A$	Ratio compressive shear strength over active shear strength (default = 0.99)	[-]
	y_{ref}	Reference level	[m]
	$s_{u,inc}^A$	Increase of shear strength with depth	[kPa/m]
	s_u^P/s_u^A	Ratio of passive shear strength over active shear strength	[-]
	τ_0/s_u^A	Initial mobilisation (default = 0.7)	[-]
	s_u^{DSS}/s_u^A	Ratio of direct simple shear strength over active shear strength	[-]

2.3.4 Output of structural forces

Structural forces in PLAXIS 2D depend on the magnitude of displacements and the material properties assigned to the structural elements. See the global equilibrium equation used for calculations Equation (2.26) (Seequent, 2025d).

$$\mathbf{K}^i \Delta\nu = f^i \tag{2.26}$$

where $\mathbf{K}$ = Stiffness matrix

$\Delta\nu$ = Incremental displacement vector

f^i = Residual force

i = Step number

Equilibrium is considered reached when the residual force, which is the difference between the external applied force and the internal boundary force, is smaller than the allowed margin of error. Because of non-isotropic behaviour, the procedure of reaching equilibrium is iterative. $\Delta\nu$ is the sum of several smaller incremental displacement vectors (Seequent, 2025d).

When extracting a structural force for a given element, the program solves the equation and extracts the displacements from $\Delta\nu$ at the requested nodes. The extracted displacements are inserted into the equations governing the behaviour of a specific structural element, using its material properties to determine the structural force.

3

Comparison of different methods of analysis for a single-strut excavation

The first part of the study evaluated different calculation methods in a theoretical excavation scenario. The chapter describes the methodology used to define the geometry and input parameters, and to perform the stability calculations. The obtained results are then used to evaluate and compare different analysis methods.

Firstly, a theoretical idealised single-supported excavation is created with typical geotechnical parameters based on conditions in Gothenburg. The soil consists of a fill layer and very soft, sensitive clay underneath.

The theoretical scenario is analysed for stability in the serviceability and ultimate limit states to assess how the different design approaches influence the different calculation methods. The reason for using an idealised general case is to compare the different methods in a controlled environment.

3.1 Geometry

The excavation is located in a very soft, very sensitive clay. The soil consists of a 1 m thick fill layer on top and the soft, sensitive clay underneath. The sheet pile wall is assumed to be a PU12 section, with a strut at the very top of the excavation. The soil parameters were assumed to be standard values for Gothenburg conditions.

The final geometry in Figure 3.1 was created using SLOPE/W. The excavation depth (H) was assumed to be 4 m, and the retaining wall was calculated to be 7 m long to achieve rotational stability. For a more detailed description of the SLOPE/W-model, see Appendix C.

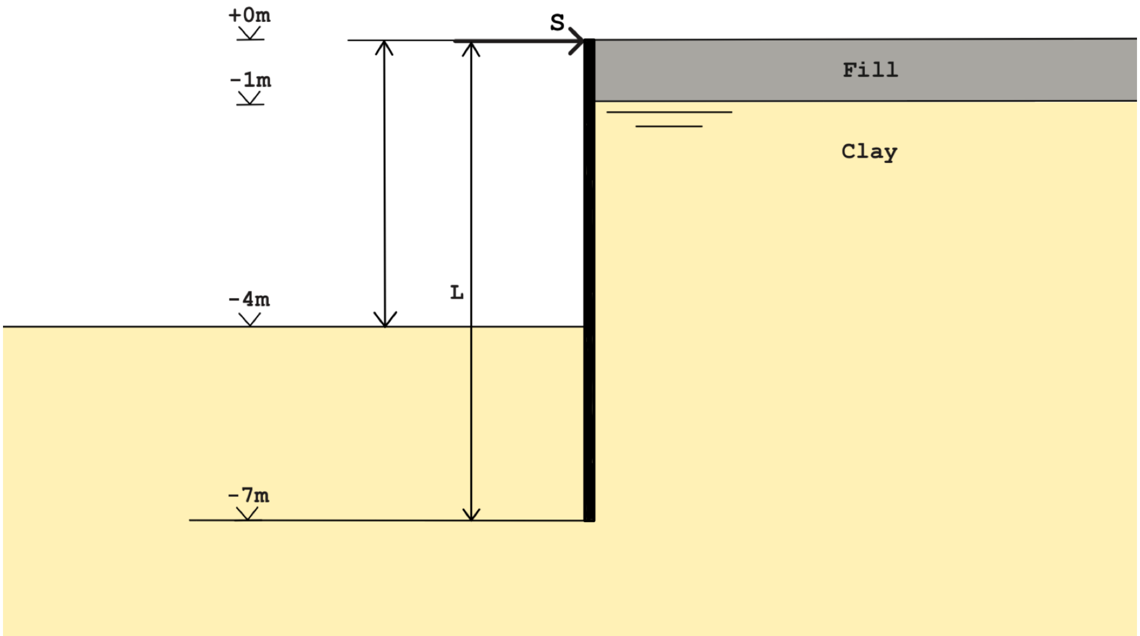

Figure 3.1: Cross-section of the theoretical case

The soil parameters for the theoretical case are based on empirical values for typical conditions in Gothenburg. The soil stiffness and friction angle are taken as characteristic values from TKGEO 11 (Trafikverket, 2011). However, the undrained shear strength was selected as a representative value, considered typical for a clay in western Sweden.

3.2 Methodology

This section describes how the four calculation procedures were carried out. First, analytical calculations are described, followed by the numerical calculations in PLAXIS 2D.

3.2.1 Analytical calculations

Analytical calculations have been carried out using two different approaches. Calculations in an Excel spreadsheet will be referred to as *hand calculations*, while calculations in the program Spontprogrammet will be referred to as *Spontprogrammet*. Both of the analytical calculations are based on the guidelines presented in Sponthandboken by Fredriksson et al. (2024).

Hand calculations

The first part of the analysis was to define the soil properties of the theoretical case. The characteristic soil properties were selected as representative values of typical soft clay conditions in western Sweden. The soil properties for the fill layer were chosen from typical empirical values presented by TKGEO11 (Trafikverket, 2011). The selected characteristic input parameters are presented in Table 3.1.

Table 3.1: Characteristic soil properties

		Fill	Clay	
Unit weight	γ	18	16	[kN/m^3]
Friction angle	φ_k	42	-	[°]
Undrained shear strength	c_{uk}	-	15	[kPa]
Rate of change	$c_{uk.inc}$	-	1.3	[kPa/m]

To evaluate the problem in the *Ultimate Limit State*, the chosen strength parameters are recalculated to design values according to Equations (3.1) and (3.2) with partial safety factors following the Swedish standards (Swedish Standards Institute [SIS], 2005).

$$\varphi'_d = \arctan\left(\frac{\tan(\varphi_k)}{\gamma_{\varphi'}}\right) \tag{3.1}$$

$$c_{ud} = \frac{c_{uk}}{\gamma_{cu}} \tag{3.2}$$

$$\text{where} \quad \gamma_{\varphi'} = 1.3$$
$$\gamma_{cu} = 1.5$$

The earth pressures were obtained using Rankine´s theory of earth pressure. The force in the waler and the excavation depth were calculated with moment equilibrium and force equilibrium following the method by Sahlström and Stille (1979) as suggested by SPH (Fredriksson et al., 2024).

The waler forces and earth pressures have been achieved using both SLS and ULS calculations. The SLS calculations include a partial factor that accounts for the prestressing force and a model factor of 1.274, according to Sponthandboken 2024.

Spontprogrammet

In addition to the hand calculations, results were also obtained by using the calculation tool Spontprogrammet. The same input material parameters were used as for the hand calculations, see Table 3.1. The user-defined partial factors are applied automatically by the program, depending on whether the calculation is performed in ULS or SLS.

The results obtained from Spontprogrammet were later plotted in Excel alongside the results from the hand calculations for comparison.

3.2.2 Numerical analyses

The numerical calculations were performed in PLAXIS 2D using two different approaches. In the first approach, the clay layer has been modelled using the Mohr-Coulomb material model. The second approach uses the NGI-ADP material model to model the clay. The chosen material models for the fill material were the same in both attempts. The generated mesh is the same for both material models, and a mesh sensitivity study is presented in Appendix E.

Table 3.2 contains material parameters for the top soil layer referred to as the fill layer. The parameters are defined based on empirical values. The inputs for all numerical material models have been chosen to replicate the material used in the analytical calculation model as closely as possible.

The sheet pile wall was modelled with a length of 7 m. The length of the retaining wall has been calculated using the SLOPE/W model. The calculations for acquiring a rotationally stable wall are presented in Appendix C. The plate element material was chosen as *PU12 - 240*, imported from a Geostudio, PLAXIS knowledge base (Papavasileiou, 2024). The strut was defined as a fixed-end anchor and assumed to have an elastic material with an axial stiffness (EA) of $6.5 \cdot 10^6 kN/m$. The length between struts was set to 1 m to get results comparable to the waler forces from analytical calculations.

Table 3.2: Fill material parameters used in PLAXIS 2D for the general case

Material set: Fill			
Soil model	Mohr-Coulomb		
Drainage type	Drained		
Dry unit weight	γ_{sat}	18	[kN/m^3]
Wet unit weight	γ_{unsat}	21	[kN/m^3]
Young's modulus	E'_{ref}	10 000	[kN/m^2]
Poisson's ratio	ν	0.33	[-]
Friction angle	ϕ'	42	[°]
Earth pressure coefficient at rest	K_0	0.44	[-]

Mohr-Coulomb

Assumed input values in the clay layer material parameters are presented in Table 3.3. The earth pressure coefficient (K_0) was set to 0.65, representing a typical empirical value for clay in western Sweden. Young's modulus (E'_{ref} and E'_{inc}) was estimated based on c_u according to Trafikverket (2025).

Table 3.3: Clay material parameters used in PLAXIS 2D for the general case

Material set: Clay			
Soil model	Mohr-Coulomb		
Drainage type	Undrained B		
Dry unit weight	γ_{sat}	16	[kN/m^3]
Wet unit weight	γ_{unsat}	16	[kN/m^3]
Initial Young's modulus	E'_{ref}	3750	[kN/m^2]
Increase of Young's modulus	E'_{inc}	325	[kN/m^2]
Poisson's ratio	ν'	0.2	[-]
Initial undrained shear strength	$c_{\text{u,ref}}$	15	[kPa]
Increase of undrained shear strength	$c_{\text{u,inc}}$	1.3	[kPa]
Earth pressure coefficient at rest	K_0	0.65	[-]

The construction was modelled in several steps, which is shown in Table 3.4. Each phase has a time span of one day to ease the evaluation of results, it is not expected to influence the results because of the chosen material models. Long-term effects, such as consolidation or creep, are not studied.

Table 3.4: Construction phases for Mohr-Coulomb and NGI-ADP material models in PLAXIS 2D

Phase	Description	Calculation type
Initial phase	Activation of soil and generating initial stresses	K_0-procedure
Phase 1	Installation of sheet pile wall	Plastic
Phase 2	Excavation to -1m	Plastic
Phase 3	Installation of strut at ground surface	Plastic
Phase 4	Excavation down to -2m	Plastic
Phase 5	Excavation down to -3m	Plastic
Phase 6	Excavation down to -4m	Plastic

The study was performed with characteristic values and with design values in ULS. The result obtained with design values has been calculated using the *Design approach* in PLAXIS, where partial factors have been applied to the soil properties. The parameters are modified according to equations (3.1) and (3.2).

NGI-ADP

The study was also conducted using the NGI-ADP material model for the clay layer. The study was conducted with the same phases as for the MC study, which can be found in Table 3.4.

The materials in the NGI-ADP model were designed to be as similar as possible to the Mohr-Coulomb model to enable comparison of the two outputs. This was done by simulating PLAXIS SoilTests. Generally, the model requires a DSS test and a triaxial test to determine the soil's strength and failure strains in all stress states in Figure 2.5.

In this case, triaxial tests could not be simulated in PLAXIS SoilTest because of the isotropic strength and stiffness of the MC material model. Instead, the shear strength ratios (s_u^P/s_u^A, s_u^{DSS}/s_u^A) where estimated based on the empirical relations described in Equation (2.25). It was also determined that the direct simple shear strength (s_u^{DSS}) was equal to the undrained shear strength (c_u) of the soil in the MC model.

The PLAXIS DSS SoilTest was used to estimate failure plastic strains (γ_f^C, γ_f^F, γ_f^E) and the stiffness ratio (G_{ur}/s_u^A) by plotting shear stress (τ_{xy}) against shear strain (γ_{xy}), see the DSS-study in Figure B.1. The final parameters can be found in Table 3.5.

Table 3.5: Clay material parameters used in PLAXIS 2D for the general case

Material set: Clay			
Soil model	NGI-ADP		
Drainage type	Undrained c		
Wet unit weight	γ_{unsat}	16	$[\frac{kN}{n^3}]$
Dry unit weight	γ_{sat}	16	$[\frac{kN}{m^3}]$
Ratio unloading/reloading shear modulus over active shear strength	G_{ur}/s_u^A	160	[-]
Undrained Poisson's ratio	ν_u	0.495	[-]
Initial active undrained shear strength	$s^A_{\text{u,ref}}$	20	$[kPa]$
Increase of active undrained shear strength	$s^A_{\text{u,inc}}$	1.7	$[kPa]$
Ratio of passive shear strength over active shear strength	s_u^P/s_u^A	0.67	[-]
Ratio of direct shear strength over active shear strength	s_u^{DSS}/s_u^A	0.77	[-]
Shear strain in triaxial compression	γ_f^C	3	[%]
Shear strain in triaxial extension	γ_f^E	6	[%]
Shear strain in direct simple shear	γ_f^{DSS}	4	[%]
Initial mobilization	τ_0/s_u^A	0.7	[-]
Earth pressure coefficient at rest	K_0	0.65	[-]

It was not possible to implement the Design approach to the NGI-ADP materials for ULS calculations. For this reason, the shear strength of the NGI-ADP clay layer was manually corrected using the partial factors before it was entered into the program. It was assumed that γ_{cu} would be applied to the shear strengths in all directions, for this reason, the partial factor was added to $s^A_{\text{u,ref}}$ and $s^A_{\text{u,inc}}$ and the other shear strength directions were automatically adjusted thanks to the strength ratios.

3.3 Results

In this section, the results from the theoretical case are presented. The study investigates whether there are differences between the two analytical methods and between the analytical and numerical results. The purpose is to determine whether there is any advantage to using a specific method.

3.3.1 Evaluation of analytical calculations

Both the calculations done by hand and by Spontprogrammet follow the procedure presented by Sponthandboken. The purpose of this chapter is to present and compare results from the two methods and determine the differences and the reliability.

The equations are presented in Section 2.1. Since both methods rely on the same theory and equations to calculate the earth pressures on the retaining wall, they should yield identical results. Complete results from Spontprogrammet are available in Appendix D. In Figure 3.2, the active and passive earth pressures are shown, and, as expected, they are identical.

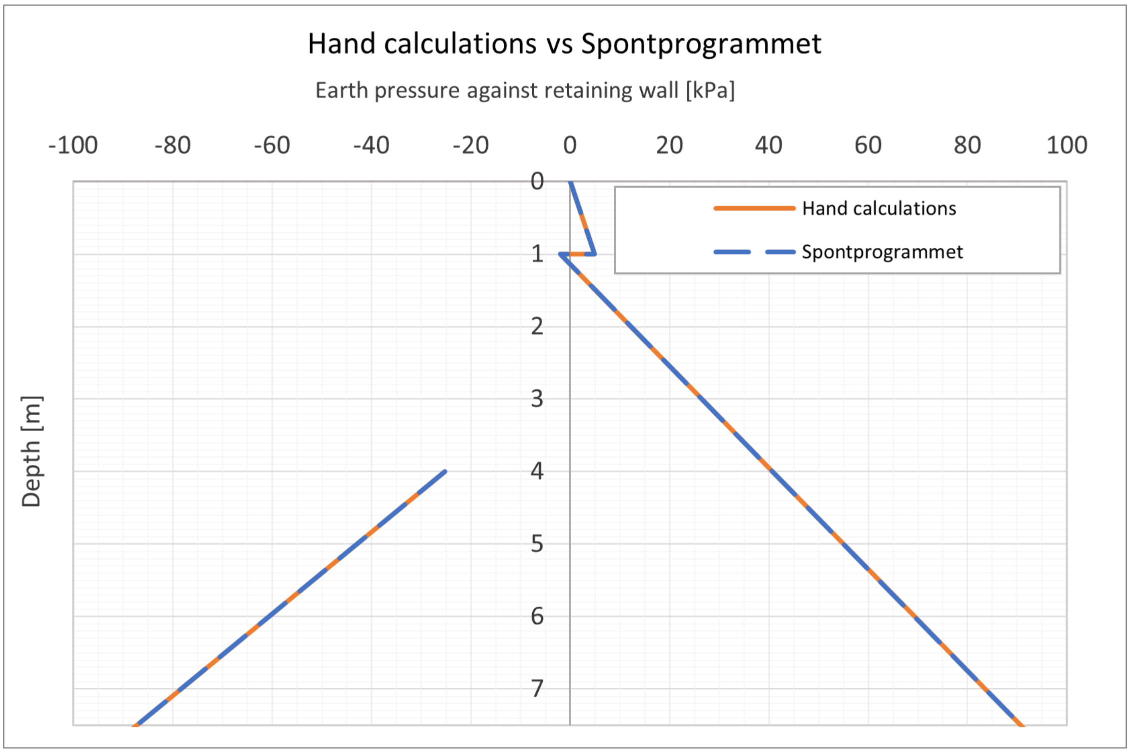

Figure 3.2: Comparison between the hand calculation and the calculations from Spontprogrammet

Other results of interest are the waler force and required length of the wall. Similar to the earth pressures presented above, the results are expected to be identical. The results are presented in Figure 3.3, which shows that the design earth pressures and waler forces are identical. The results are essentially identical, with only a negligible discrepancy observed in the required sheet pile wall length. However, the small discrepancy in the required wall length may be due to rounding error in the hand calculations.

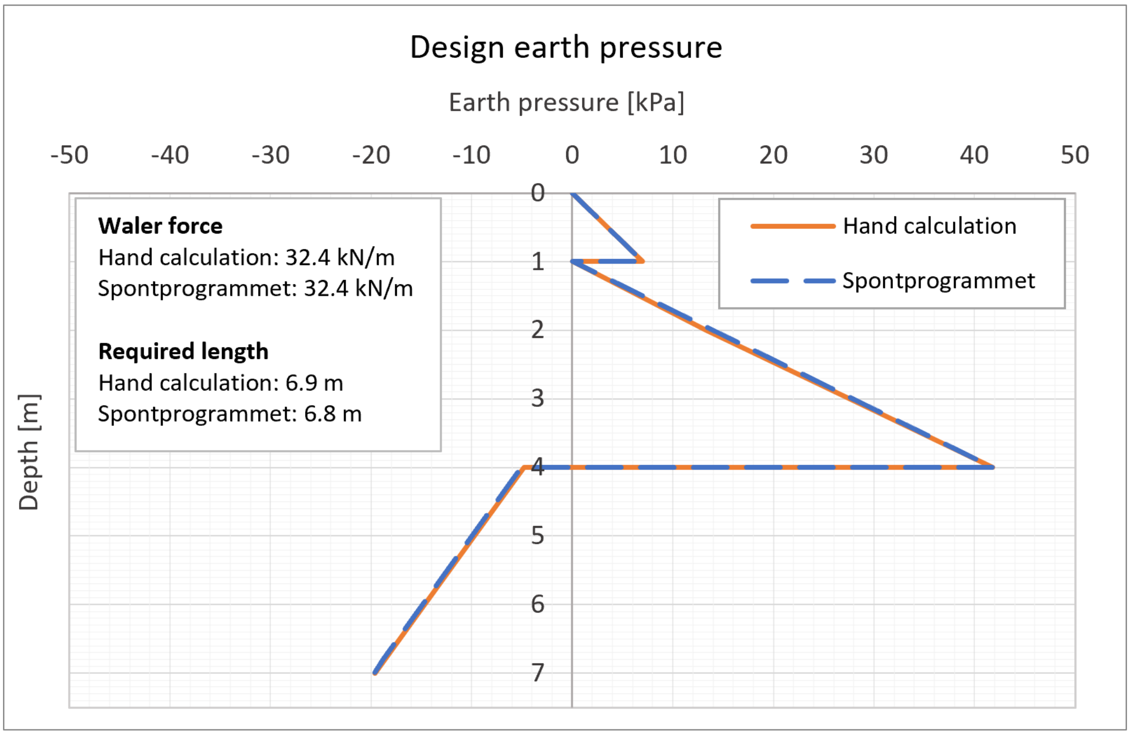

Figure 3.3: The design earth pressure, waler forces and required wall length for the hand calculations and the calculations from Spontprogrammet

As expected, the hand calculations and Spontprogrammet predict identical results because they rely on the same assumptions and simplifications. This indicates that for simple cases, such as the general case, hand calculations and Spontprogrammet are equally reliable and provide consistent results. This means that either method could be used when designing the retaining wall.

3.3.2 Comparing analytical and numerical earth pressures

The results from the earth pressure calculations are presented below. The active and passive earth pressures are calculated using two analytical and two numerical methods.

Since the results from the hand calculations and Spontprogrammet are identical, they are presented as a single result, referred to as *analytical calculations*, in the figures 3.4b and 3.4a, where the earth pressures from the analytical and the two numerical methods are shown.

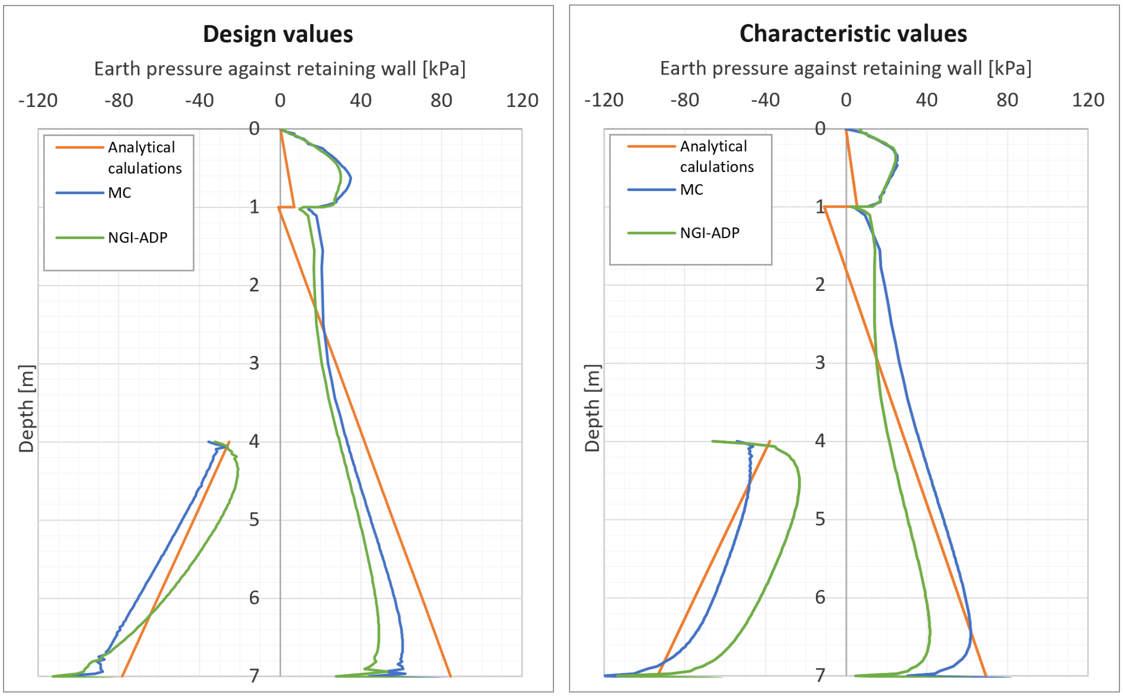

(a) Earth pressures calculated with design values

(b) Earth pressures calculated with characteristic values

Figure 3.4: Comparison between the earth pressures with design and characteristic values for analytical and numerical models.

The figures above show large differences between the analytical and numerical models when calculating the earth pressures. Both the characteristic and design calculations predict big differences between the analytical and numerical calculations.

The analytical solution generally predicts lower earth pressures near the ground surface compared to the numerical models. This is likely caused by how the FEM program redistributes pressures as the waler becomes increasingly loaded.

Both numerical models use the Mohr-Coulomb model in the fill layer and were expected to predict identical earth pressures, as shown in the SLS calculations. However, the ULS calculations show slightly different behaviours, believed to be due to the redistribution of forces when the partial factors are applied to the soil materials.

Looking at the clay below the excavation bottom, the NGI-ADP model generally predicts lower earth pressures. One possible explanation may be due to the different material formulations. The MC assumes an isotropic strength while the NGI-ADP differentiates between the active, passive and direct shear strengths. Therefore, the resistance below the excavation bottom may depend on the loading direction and deformation pattern. This may result in a lower degree of passive mobilisation and consequently lower earth pressures along the embedded part of the wall.

When comparing the design results with the characteristic results, the NGI-ADP model shows similar behaviour in both calculations. In contrast, the MC model predicts a much more linear earth pressure distribution in the SLS calculations. However, for the ULS calculation, its shape is similar to that of the NGI-ADP model. In addition, the figures show that the earth pressures calculated using design values are higher than those calculated using characteristic values. As mentioned before, this may be due to the deformation-dependent behaviour.

3.3.3 Waler forces

The waler forces from the different methods of analysis are presented in Table 3.6. It can be observed that the analytical methods will predict the same design waler force, which is expected since the two methods rely on the same theory. The SLS calculation differs slightly between the analytical approaches because Spontprogrammet has taken time effects into account by consolidation at the bottom of the excavation. The numerical models predict waler forces that are almost twice as large as those from the analytical methods. These differences are important because they can indicate that the analytical methods may underestimate the structural forces in the system. The results can also imply that the numerical methods are overestimating the forces.

Table 3.6: Waler forces for the different methods of analysis.

	Waler force [kN/m]	
	Characteristic	Design
Hand calculation	23	32
Spontprogrammet	27	32
PLAXIS MC	54	64
PLAXIS NGI-ADP	46	63

The reason the numerical analyses predict significantly higher waler forces may be that the analytical methods are based on simplified equilibrium assumptions in which the interaction between the soil and the retaining wall is not considered. In contrast, the numerical methods can account for the redistribution of stresses caused by the excavation. These stresses cause deformations in the soil according to the selected material model, which in turn causes deformations in the sheet pile wall as well. The wall and soil deformations cause deformations in the strut, and consequently, the waler force is obtained. The final force is also a result of the stiffness of the structural elements, rather than assuming an infinitely stiff construction.

The analytical design calculations assume that the soil's strength is fully mobilised. In the numerical models, the soil cannot become fully mobilised, and the addition of partial factors only reduces the soil strength. For this reason, the results from the numerical models are considered more accurate and reliable. However, results need to be carefully considered, especially since the numerical characteristic results are higher than the analytical design results.

3.3.4 Horizontal displacements

Analytical calculation methods cannot capture the displacement of the retaining wall because they rely on equilibrium conditions and simplified assumptions. This is because the soil-structure interactions are deformation-dependent. Since deformations are not included in the analytical analyses, wall displacement and stress redistribution cannot be evaluated analytically.

To predict the deformation of the retaining wall, numerical methods were used. In Figure 3.5, the displacements at each calculation step from the numerical analyses are presented.

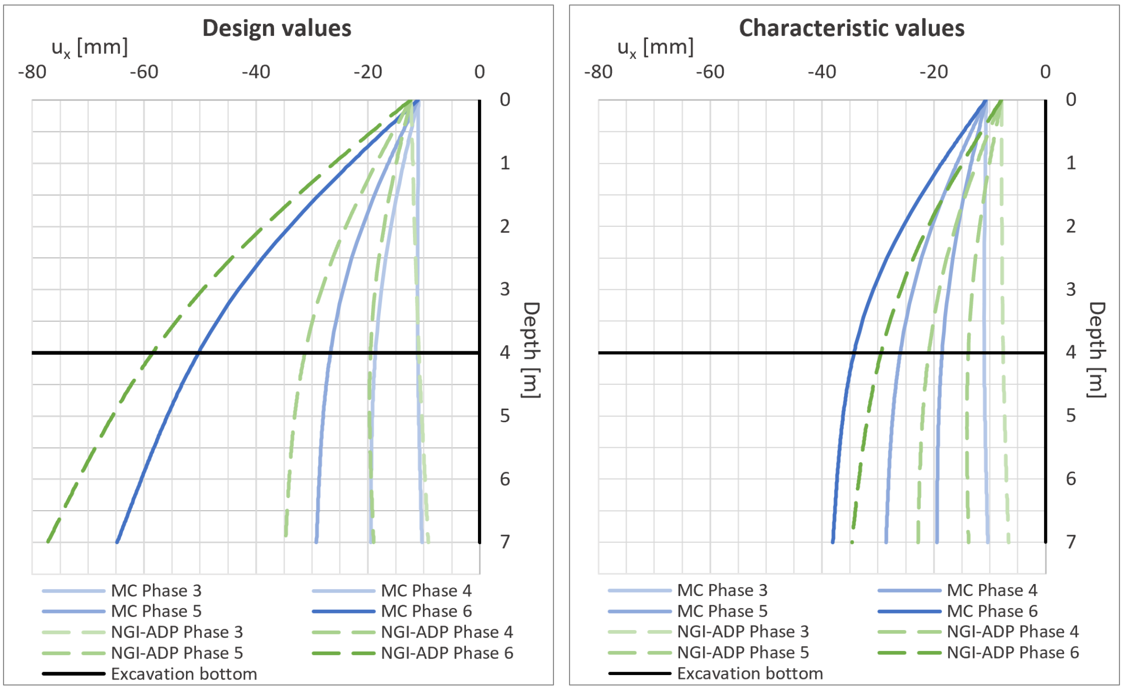

(a) Horizontal displacements calculated with design values.

(b) Horizontal displacements calculated with characteristic values.

Figure 3.5: Comparing the development of horizontal displacements calculated with design and characteristic values

In the analysis using the design values, Figure 3.5a, the NGI-ADP model predicts notably larger displacements than the MC model. Displacements from both models increase with depth, with the largest occurring at the bottom of the retaining wall. The larger displacements predicted by the NGI-ADP model may be explained by its anisotropic behaviour, indicating that it has a greater influence in regions subjected to higher stresses.

Another possible explanation may be that, due to the displacement and the shape of the wall, the soil will mobilise the passive shear strength. The NGI-ADP model describes the soil behaviour anisotropically by considering that the passive shear strength is lower than the direct shear or active shear strength. This would result in greater displacements at the bottom of the sheet pile wall. As the NGI-ADP also takes stiffness degradation into account, this may also be a possible explanation. As the inserted design values have decreased shear strength, the stiffness degradation becomes more evident.

Furthermore, the linear elastic behaviour of the MC model before yielding would also contribute to a stiffer response, resulting in smaller strain and, subsequently, smaller displacements. In contrast, the NGI-ADP model has a more advanced stress-strain behaviour, in which stiffness degradation and stress-path dependency may allow larger strains to develop. This would result in larger predicted displacements, as observed in the displacements calculated using design values in Figure 3.5a.

However, the analysis using the characteristic input data predicts the opposite, indicating that displacements are smaller in the NGI-ADP model. In this case, the difference between the displacements is also significantly smaller and more similar in terms of shape and curvature. This could indicate that the predicted wall response is less sensitive to the choice of soil model regarding characteristic values. These results show that the choice of soil model and selected parameters can influence the predicted response of the wall to different degrees.

4

Comparison of different methods of analysis for a multiple-strut excavation

This chapter contains a development of the theoretical case presented in Chapter 3. The geometry has been modified to evaluate how the models differ on a more complex structure with an additional support level.

The analysis aimed to evaluate how the additional strut level influences the wall displacement, structural forces, and the stability of the excavation. As in Chapter 3, the analytical approach will be compared to the two numerical material models to establish whether an excavation of increasing complexity gets better results from increasing complexity in the applied calculation model.

In the case of a single strut level, the system is statically determinate. However, introducing additional strut levels creates a statically indeterminate system, leading to a redistribution of forces. This case is expected to provide further insight into how the properties of the structural elements affect the results.

4.1 Geometry

This case study will investigate a modified version of the first theoretical case geometry. The modification includes the first geometry but will contain a longer sheet pile wall. Furthermore, after reaching the bottom of the previous excavation at a depth of 4 m, another support level will be incorporated at 3.5m depth. The excavation will then continue to the new excavation depth of 7 m.

The length of the sheet pile wall has been extended to 10 m. The location of the first strut remains unchanged, and the stratigraphy and soil properties are also consistent with the original design.

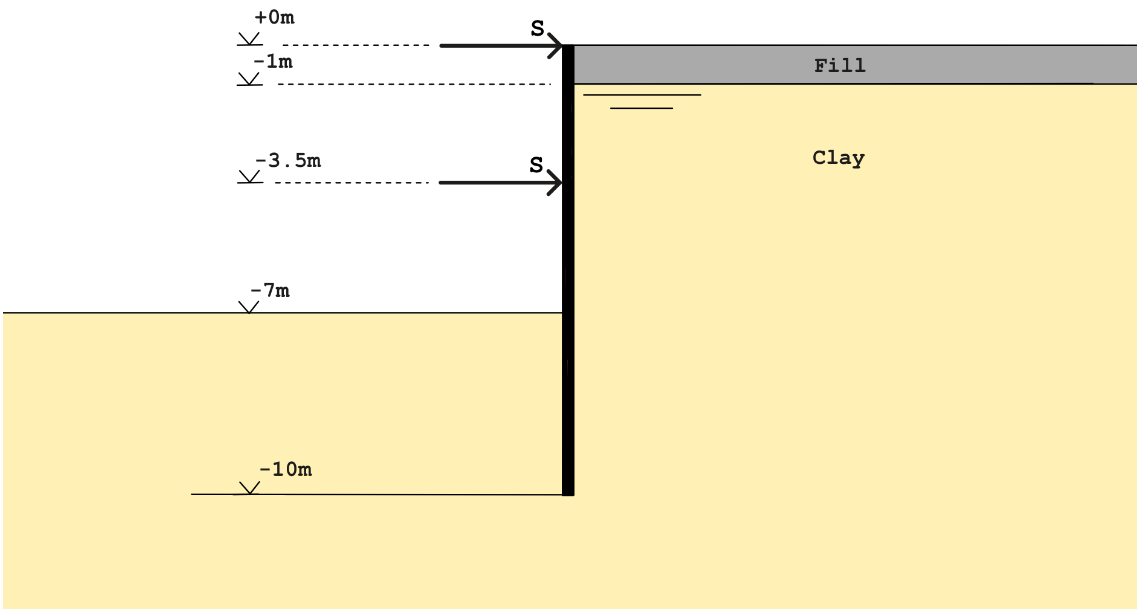

Figure 4.1: Geometry of the modified case study incorporating an additional support level

4.2 Method

This chapter will describe the methodology used to analyse the retaining wall. In this case study, only one analytical calculation method will be carried out, while the same numerical methods will be applied. Also, a simplification has been made to study the results with no partial factors applied. This is to be able to fully compare the calculation methods in themselves to each other without added factors influencing the results.

4.2.1 Analytical calculations

In Section 3.3, it was confirmed that the hand calculations and Spontprogrammet will provide the same results. Because of this, it was decided that Spontprogrammet would be used as the only analytical method in the following analysis to reduce the number of calculations.

4.2.2 Numerical calculations

The numerical calculations were performed in PLAXIS 2D using the Mohr-Coulomb and NGI-ADP model. As in the previous study, the fill layer will be modelled only with the Mohr-Coulomb model, whereas the clay layer will be varied.

The soil properties are the same as in the previous study. The fill properties can be found in Table 3.2, and the clay properties can be found in Table 3.3 and Table 3.5.

The excavation was carried out in several steps, as shown in Table 4.1, with time intervals of 1 day per step. This was to evaluate the results in the correct order, but since the analysis is undrained, long-term effects will not be taken into account. A new mesh sensitivity study was performed, and it is presented in Appendix E.

Table 4.1: Calculation steps used in PLAXIS for the multiple-strut scenario

Phase	Description	Calculation type
Initial phase	Activation of soil and generating initial stresses	K_0-procedure
Phase 1	Installation of sheet pile wall	Plastic
Phase 2	Excavation to -1m	Plastic
Phase 3	Installation of strut at ground surface	Plastic
Phase 4	Excavation down to -2m	Plastic
Phase 5	Excavation down to -3m	Plastic
Phase 6	Excavation down to -4m	Plastic
Phase 7	Installation of strut at -3.5m	Plastic
Phase 8	Excavation down to -5m	Plastic
Phase 9	Excavation down to -6m	Plastic
Phase 10	Excavation down to -7m	Plastic

4.3 Results

This section presents the results of the analytical calculations and evaluates the differences between the calculation methods based on the selected parameters from the first theoretical case. This includes the active and passive earth pressures, waler forces and horizontal displacements.

4.3.1 Active and passive earth pressures

The active and passive earth pressure distributions are presented in Figure 4.2. For the first theoretical case, the earth pressures were relatively similar, particularly for those with characteristic values used in this analysis. It was expected that, for this multi-supported case, the results would show larger differences in magnitude, but it could also be observed that the gradients of the curves were very different.

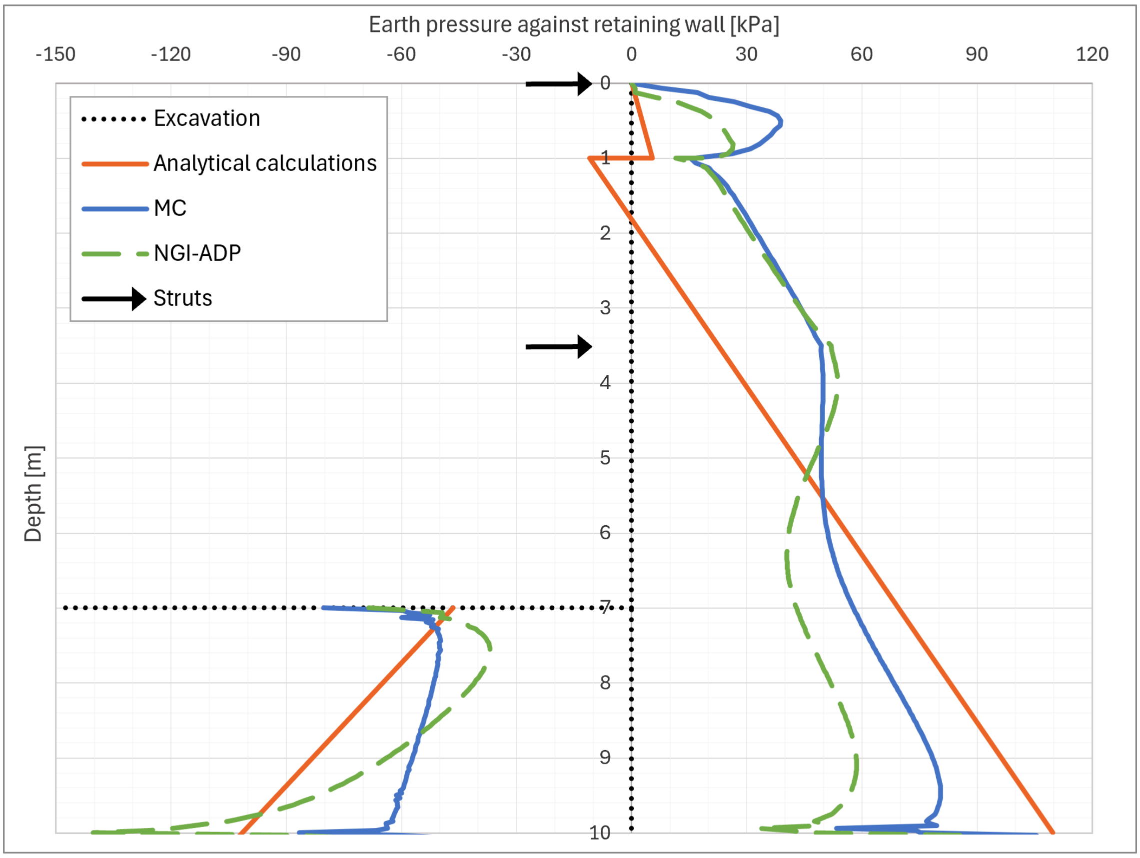

Figure 4.2: Comparison between differences between analytical and numerical methods

The largest differences occur within the clay layer. From approximately 1 m to 3.5 m depth, the curves follow a relatively similar gradient. Since the two supports limit soil deformation, the earth pressure may not reach the full active state and may remain closer to its at rest value. The differences between the analytical and numerical can therefore be related to the deformation-dependent response. Another possible difference is that the earth pressure that is calculated analytically does not take the excavation process of the soil into account. For the NGI-ADP model, the lower pressures may also be influenced by the anisotropic soil response, while the difference for the MC model most likely is related to the stress redistribution rather than differences in strength.

Below the bottom support, the differences decrease, and the curves intersect. However, at the intersection, the curves have distinctly different gradients and diverge, resulting in increasing differences towards the bottom of the wall. In this area, the sheet pile wall is not as restricted of movement and as a result, the numerical results show that the soil strength have become mobilised. Simultaneously, the analytical results keeps its linear behaviour and the earth pressure keeps growing with depth.

For the passive earth pressure, all three results show distinct behaviours. The analytical results is strictly linear while the numerical approaches show how the passive earth pressure mobilises directly at 7m. The MC model yields a roughly linear result after that point, whereas the NGI-ADP model shows a curved distribution. NGI-ADP accounts for a weaker passive shear strength in the soil at the excavation bottom and a direct shear strength ($s_u^{DSS} = c_u$) around the bottom of the sheet pile wall. How the soil is deformed affects its mobilised shear strength and consequently its earth pressure distribution.

It could also be observed that the shape of the earth pressures from the numerical analyses differs from the linear distribution assumed in analytical calculations. Instead, the numerical results show a more nonlinear distribution, indicating that stress redistribution may occur due to wall deformations. This redistribution resembles the shape of the earth pressures for a redistributed earth pressure described in Section 2.2.2.

4.3.2 Waler forces

The waler reaction forces after final excavation are presented in Table 4.2. Strut one is placed at the ground surface, and strut two sits 3.5 m below. The results in the first strut are representative of the acting forces after the excavation is finalised, meaning they are not the maximum forces occurring throughout construction.

The analytical and Mohr-Coulomb calculations provide 24-28 kN/m in the first strut. While the NGI-ADP model gets about 5 kN/m, which is likely because of the high active strength of the NGI-ADP soil. However, in the second strut, Mohr-Coulomb and NGI-ADP are between 226-234 kN/m and the analytical calculations give about half.

The analytical calculations have been done in one step and are based on the resulting forces of a redistributed dimensioned earth pressure at the moment of finished excavation. They are, for this reason, expected to have a smaller difference between Struts 1 and 2 compared to the numerical results. Since the numerical models take displacements into account when estimating the waler forces, the lower struts need to take more load from the displacements that develop while excavating to full depth.

Table 4.2: Waler forces for the different methods of analysis.

	Waler force [kN/m]	
	Strut 1	Strut 2
Analytical calculations	28	111
PLAXIS MC	24	226
PLAXIS NGI-ADP	5	234

4.3.3 Horizontal displacements

The horizontal displacements after finalised excavation are presented in Figure 4.3. The two material models follow the same shape and are relatively similar down to a depth of 7.5 m. Afterwards, the curves diverge, and the largest difference appears at the bottom of the sheet pile wall.

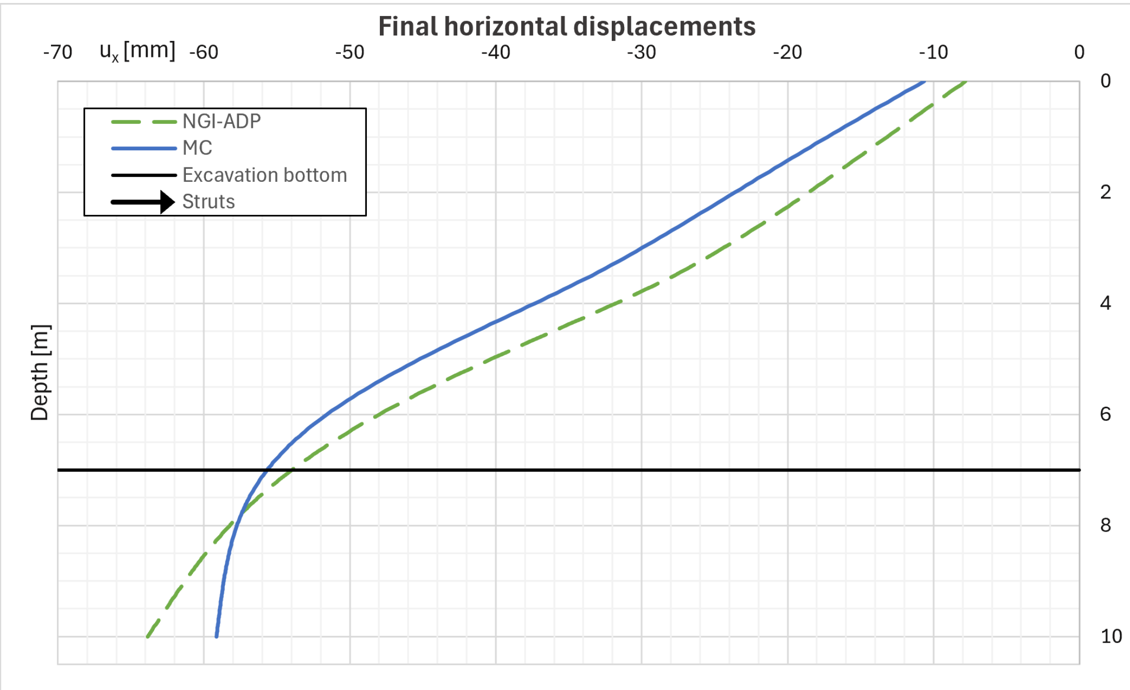

Figure 4.3: Comparison of final horizontal displacement for the numerical material models

It can be observed that for both material models, the sheet pile experiences deflection around the excavation bottom and toward the bottom of the retaining wall. The reason may be because of the anisotropy of the lower passive strength of the NGI-ADP model. With weaker retaining soil, more displacements can occur towards the lower end of the wall.

Another possible explanation is that, because the MC model uses a linear elastic representation of the stress-strain relationship, it allows for less strain development, leading to smaller displacements at the bottom. The NGI-ADP model includes a non-linear elastic representation of the stress-strain relationship, which reduces soil stiffness with increasing strain, and, because of anisotropy, different amounts of strain can develop in different directions.

The horizontal displacements calculated in PLAXIS depend on the amount of load or soil mass removed in each calculation phase. Figure 4.4 shows the development of displacements during the course of excavation. The installation of the struts appears to influence the magnitude and deflection of the displacements.

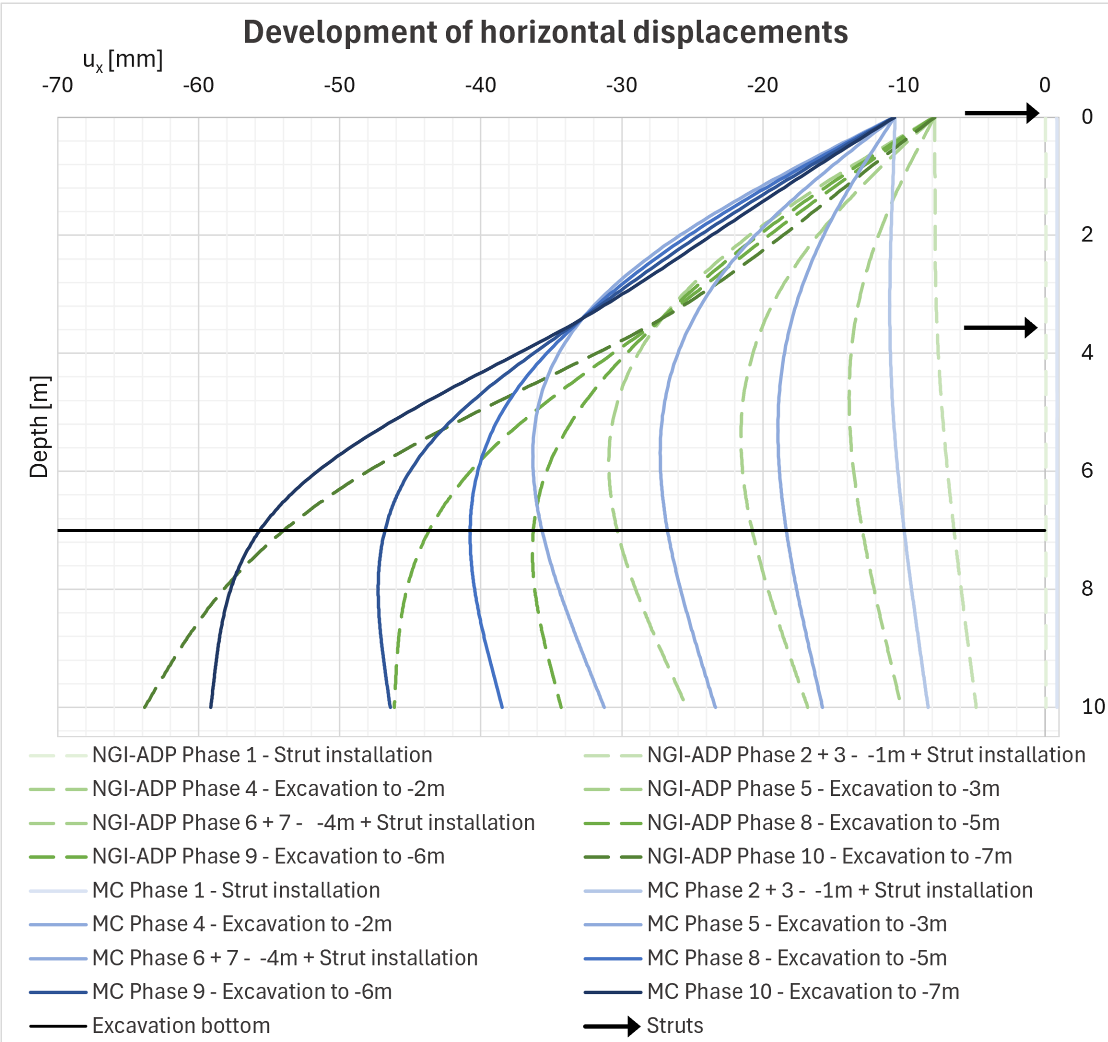

Figure 4.4: Development of horizontal displacements during PLAXIS excavation steps. Lighter graphs represent earlier stages.

There is a translateral displacement before the first strut was installed, which affects the magnitude of the final displacements. Since the NGI-ADP model maintains higher strength in the active zone, the displacements are slightly lower until the passive soil strength becomes more utilised at the bottom in the later stages. Since the NGI-ADP model has a lower passive shear strength, more displacements become evident at the bottom of the sheet pile wall.

While the shape of the wall is relatively similar, it could be assumed that both models will predict reasonable displacements. This should, however, be approached with caution, as other factors could affect the horizontal displacement, which cannot be accounted for in numerical models.

A study of the displacements affected by the bending stiffness of the sheet pile wall has been done, and it is presented in Chapter 6.

5

Comparing calculation results and field measurements

This section of the report will focus on calculations done based on field measurements from a case study presented in the report by Edstam and Jendeby (1992). The case is described in more detail below, and calculations have been performed to compare with real-world measurements and assess which calculation method predicts the most realistic results.

The same four calculation methods that were used in the theoretical case have been implemented in the Lindome case as well. The analytical and numerical methods will be presented, followed by the results. The methodology of the Lindome case study is similar to that of the previous chapter for the theoretical case.

Results from the different calculation models are compared with each other, as in the theoretical case. However, since the Lindome case already has measured field data, the results will also be evaluated against them.

5.1 Lindome case study

The study will investigate an excavation in the small town of Lindome on Sweden's west coast. Retaining structures were installed as part of the reconstruction of a railway crossing, where the road was rebuilt to pass beneath the railroad (Edstam & Jendeby, 1992). The road that was relocated is called Industrivägen and runs east-west, while the railway Västkustbanan runs primarily north-south, as shown in Figure 5.1.

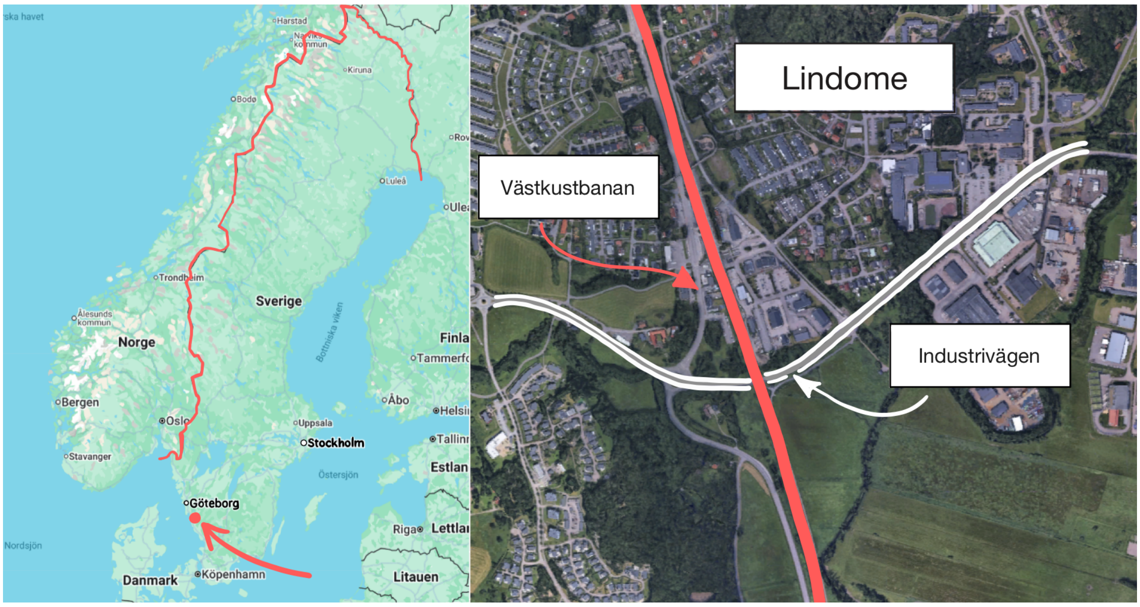

Figure 5.1: Location of the studied area, with Industrivägen och Västkustbanan highlighted

The excavation at the site was 19 m wide and up to 7 m deep at certain points since the railroad lies 1 m above the surrounding ground levels. The new crossing is below ground level and was achieved through a *through-structure*. Three boreholes have been used to collect soil data, one located directly on the east side of the railway and the other two on either side of Industrivägen on the west side of the railway.

5.1.1 Geometry

The investigated retaining structure is shown in Figure 5.2. The retaining structure consists of a PU®12 sheet pile wall installed to a depth of 10.45 meters below the ground surface, with an excavation depth of 6.25 meters. Soil was first excavated to a depth of 2 m, and then lateral supports consisting of bracing and struts were installed at ground level. The final excavation down to 6 meters was conducted in sections from west to east, and a concrete slab was successively cast at the excavation bottom. This method provided stability of the excavation during construction by utilising 3D effects. All vertical excavation steps are presented in Figure 5.3.

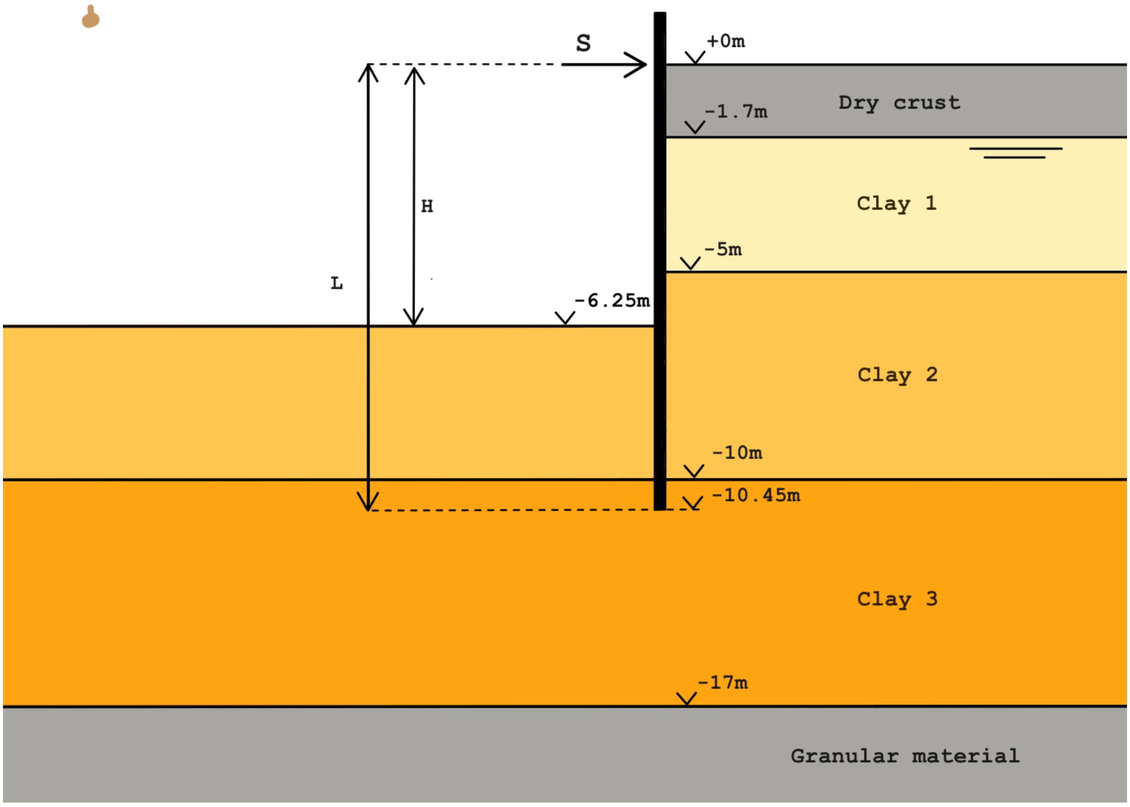

Figure 5.2: Cross-section of the excavation in Lindome

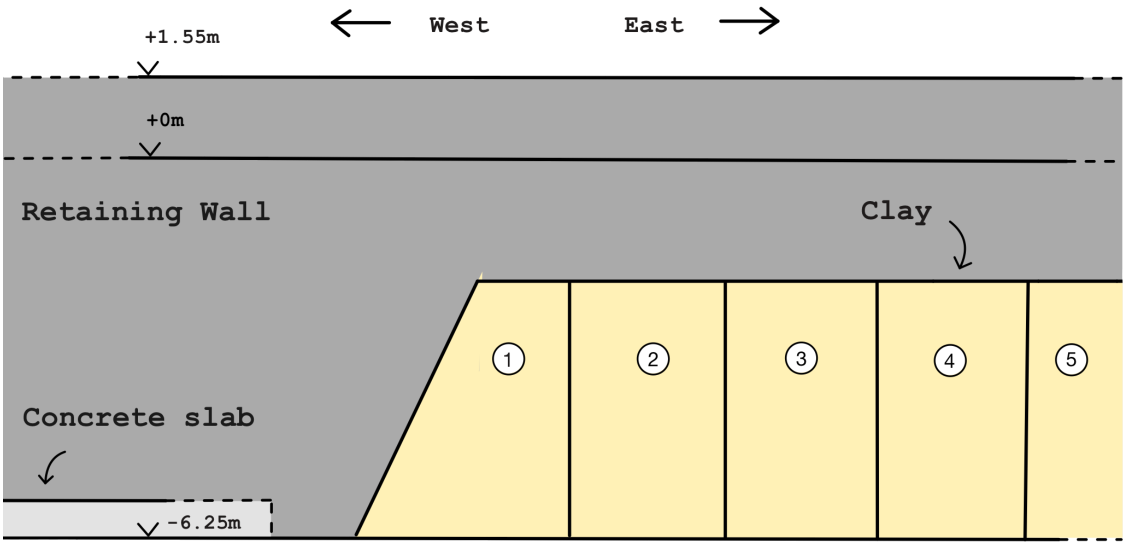

Figure 5.3: Illustration of the excavation steps, the excavation step to 6m depth was executed over a period of one month from section 1 to 6 (Edstam & Jendeby, 1992)

5.1.2 Soil properties

The soil profile consists of a 1.7 m thick dry crust overlying a 15 m thick layer of normally consolidated clay. In some locations, a thin layer of frictional soil is present above the bedrock.

Field vane tests (FVT) and a fall cone test were done on the soil field sample data and are presented in the original report by Edstam and Jendeby (1992). Soil parameters have been determined based on undrained shear strength (c_{uv}), natural water content (w_N) and liquid limit (w_L), presented in Figure A.1 in Appendix A. The fall cone test results have been neglected in the evaluation of c_{uv} due to possible sample disturbance. The top 5 m of the clay layer has a high water content, and at depths of 6-8m, it is considered extremely sensitive.

The starting point for the calculations was the evaluation of the previously mentioned soil samples. The clay was divided into three layers based on liquid limit and water content from the field data. The undrained shear strength from FVT was corrected using a correction factor (μ) according to equations (5.1) and (5.2). Selected soil layers are present in Figure 5.2.

$$\mu = (\frac{0.43}{w_L})^{0.45} \tag{5.1}$$

$$c_u = \mu \cdot c_{\text{uv}} \tag{5.2}$$

where c_{uv} = Undrained shear strength from FVT

The dry weight of the clay was estimated to 16 kN/m^3 by Edstam and Jendeby (1992). It has been assumed that the clay in the third layer is 17 kN/m^3 due to the weight of the overlying soil. The value of K_0 has been estimated from the provided field measurements of initial earth pressure according to Equation (2.2); it is around 0.7-0.75.

CRS tests were also conducted by Edstam and Jendeby (1992), who provided an oedometer modulus for stresses below the preconsolidation pressure ($M_{0,\text{CRS}}$) of about 1000-1500 kPa at the top of the clay and 3500 kPa at the bottom. Empirical relations have been used to determine the soil stiffness input parameters in PLAXIS 2D from $M_{0,\text{CRS}}$.

The parameters of the dry crust and frictional material were chosen based on empirical values. Respective dry weights were estimated to 19 and 18 kN/m^3 and friction angles to 34° and 40°.

Modifying the undrained shear strength based on 3D-effects

The Lindome excavation reached full depth and rotational stability due to resisting 3D effects from the immediate surroundings, as excavation was performed in horizontal steps. However, calculations were performed only in a 2D plane-strain model, assuming an infinite excavation in the out-of-plane direction. To achieve rotational stability without changing the excavation geometry, c_u was modified. It was assumed that the 3D effects from the horizontal excavation can be modelled by an increase in shear strength. This assumption increases the strength of the entire soil domain, whereas in reality, the 3D effects contributed to shear resistance only along the short ends of the slip surface. Thus, the modified strength parameters should not be interpreted as representative soil properties, but rather as a modelling assumption introduced to ensure stability in a 2D analysis.

The undrained shear strength was investigated as an input to a new SLOPE/W model, with a desired factor of safety for total stability of the construction of 1.3. The retaining wall was aimed to be rotationally stable when the rotation centre was placed at the ground surface, at the level of the strut. The undrained shear strength was then iteratively increased until the safety factor was reached. See the SLOPE/W model in Appendix C. The recalculated undrained shear strengths are subsequently used in the following analyses, and the soil properties are presented in Table 5.1.

Table 5.1: Soil parameters with modified undrained shear strengths for analytical (hand) calculations

	Dry crust	Clay 1	Clay 2	Clay 3	
Unit weight γ	19	16	16	17	[kN/m^3]
Friction angle φ	34	-	-	-	[°]
Undrained shear strength c_u	-	29	26	26	[kPa]
Rate of change $c_{u.inc}$	-	-1	-	-	[kPa/m]
Resting earth pressure coefficient K_0	0.44	0.7	0.7	0.75	[-]

5.2 Methodology

The calculations for the Lindome excavation have been similar to those used in the previous theoretical case studies. Two analytical and two numerical methods will be presented. For this case study, only one support level is considered because the sheet pile wall was found to be rotationally stable due to the modified soil properties. The temporary strut is therefore excluded from the analysis to simplify the model and focus on the main support system.

5.2.1 Analytical analysis

The analytical calculations for the Lindome case study have been conducted similarly to those for the theoretical case studies. The calculations for the excavation have been conducted by hand and with Spontprogrammet. The hand calculations have been executed using an Excel spreadsheet. The analytical calculations are based on the soil properties modified in Section 5.1.2.

Hand calculations

Similar to the general case study, the earth pressures were obtained using Rankine´s earth pressure theory and the standard methods for calculating earth pressures in clay in Sweden, as described in Section 2.1. The forces in the walers and the excavation depth were calculated using moment equilibrium and force equilibrium, following the method described in Section 2.2.1.

For the Lindome case study, the soil parameters are not corrected with partial safety factors. The study emphasises the comparison between the measured field values and the calculated results. Consequently, no structural element design was performed, and the study was carried out using characteristic soil values.

Calculation of waler force

The purpose of this calculation is to achieve the actual force acting on the waler. In reality, the full passive earth pressure is not utilised and will therefore be reduced in the hand calculations. This has been done using two different assumptions. There are no measured results concerning waler forces, which makes it less important. However, it can provide a clearer indication of how the calculation models differ.

The first assumption calculates the net earth pressure below the excavation bottom that acts over the full length of the sheet pile wall, as shown in Figure 5.4a. In theory, the full passive pressure acts over the entire length, but in practice, only a portion of the full pressure is mobilised. To determine the amount of mobilised net earth pressure, a percentage of the full pressure was calculated for which moment equilibrium around the waler was achieved.

The second method will calculate the required length of the sheet pile wall for which moment equilibrium around the waler is achieved if the full net earth pressure is utilised, see Figure 5.4b. This method is considered less likely to capture the actual acting waler force since the sheet pile wall will utilise its entire installed length to some extent. However, this method is used by Spontprogrammet and was implemented for confirmation of the two analytical methods.

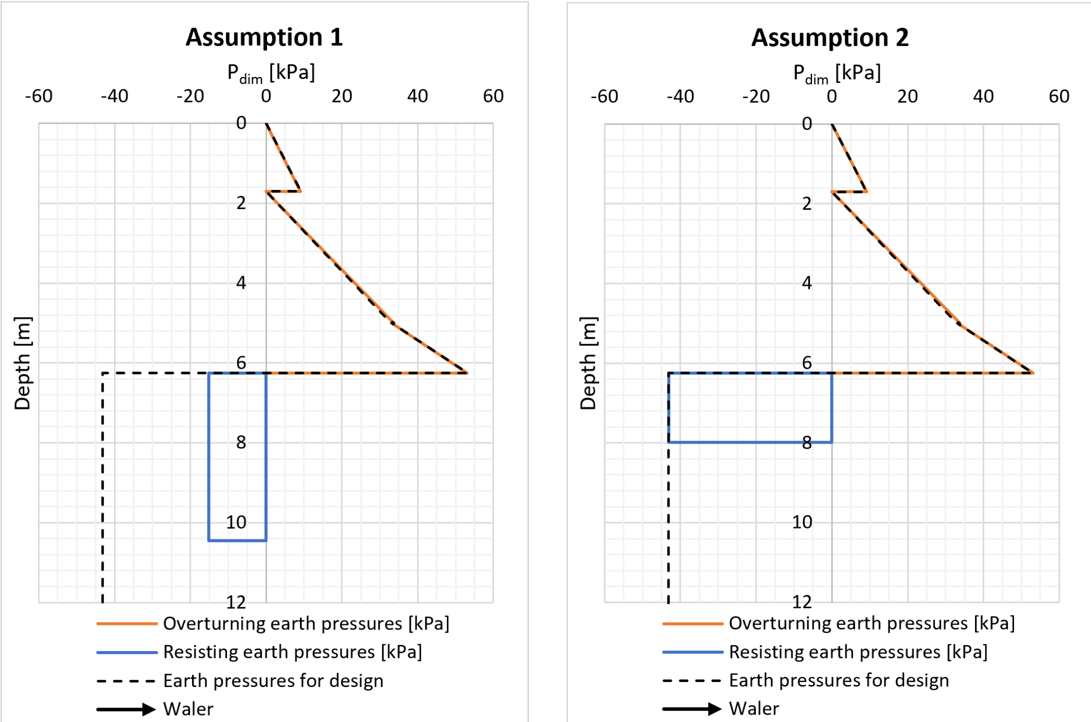

(a) Passive earth pressure reduced until moment equilibrium

(b) Sheet pile wall length reduced until moment equilibrium

Figure 5.4: Methodologies of estimating acting waler force

Spontprogrammet

With the computational tool Spontprogrammet, similar calculations have been made as for the hand calculations.

If a characteristic approach is used in Spontprogrammet, the resulting waler force is adjusted according to the methodology in Sponthandboken. To obtain the actual waler force without any partial factors, the program's design approach has been used instead. The characteristic inputs in Table 5.1 in the design approach are automatically changed with partial factors according to Equations (3.1) and (3.2). The inputs for the friction angle and undrained shear strength have, for this reason, been adjusted to account for the partial factors added by Spontprogrammet.

The bottom layer of frictional material, along with parts of Clay layer 3, has not been included in the modelled section because it would not affect the final results.

5.2.2 Numerical calculations

The numerical calculations were performed in PLAXIS 2D using two different approaches. In the first approach, the entire section was modelled using the Mohr-

Coulomb model, including the dry crust, friction material, and clays. The second approach uses the NGI-ADP material model for the clays. All soil materials, except the clay layers, have been assumed to be identical for both approaches and are listed in Table 5.2. The material parameters are based on empirical values.

Table 5.2: Input parameters for the fill material in Lindome

Material set: Dry crust		
Soil model	Mohr-Coulomb	
Drainage type	Drained	
Dry unit weight γ_{sat}	19	[kN/m^3]
Wet unit weight γ_{unsat}	22	[kN/m^3]
Young´s modulus E'_{ref}	15 000	[kPa]
Poisson´s ratio ν	0.33	[-]
Friction angle φ'	34	[°]
Earth pressure coefficient at rest K_0	0.44	[-]

The sheet pile wall was modelled as a plate element down to a depth of 10.45 m with interfaces on either side. The wall material was chosen as PU12-240, imported from the Geostudio, PLAXIS knowledge base (Papavasileiou, 2024). The strut was defined as a fixed-end anchor and assumed to behave elastically with an axial stiffness (EA) of $6.5 \cdot 10^6$ kN/m. The length between struts was set to 1 m to get results comparable to the waler forces from analytical calculations.

Mohr-Coulomb

The input data for the clay layers are summarised in Table 5.2. A CRS test was conducted in Lindome that provided an uncorrected oedometer modulus ($M_{0,CRS}$). $M_{0,CRS}$ was corrected for uncertainties and used as the oedometer modulus used by PLAXIS (E_{OED}). The reference stiffness modulus E'_{ref} was then estimated according to Equation (5.3) from Seequent (2025b).

$$E_{OED} = \frac{(1-\nu)E}{(1-2\nu)(1+\nu)} \tag{5.3}$$

$$\text{where} \quad E = E'_{ref} = \text{Young's modulus}$$

K_0 of the clay was estimated by back-calculating measurements of initial earth pressure and comparing them with empirical relations; see Appendix A for further details. The NGI-ADP material model described below uses the same K_0.

Table 5.3: Input parameters for the Mohr-Coulomb clay layers for the Lindome case

Material set	Clay 1	Clay 2	Clay 3	
Drainage type	Undrained B			
Dry unit weight γ_{sat}	16	16	17	[kN/m^3]
Wet unit weight γ_{unsat}	16	16	17	[kN/m^3]
Initial Young´s modulus E_{ref}	5600	8600	11300	[kPa]
Poisson´r ratio ν	0.2	0.2	0.2	[-]
Initial undrained shear strength $c_{\mathrm{u,ref}}$	29	26	26	[kPa]
Increase of undrained shear strength $c_{\mathrm{u,inc}}$	-1	-	-	[kPa]
Earth pressure coefficient at rest K_0	0.7	0.7	0.75	[-]

The model was constructed and calculated in several steps, displayed in Table 5.4. The time intervals were set to one day per step to evaluate results in the correct order. However, the analysis is undrained, and the study considers only short-term effects. Consequently, creep, consolidation or other time-dependent effects have not been taken into account.

Table 5.4: Construction phases with Mohr-Coulomb material model in PLAXIS 2D

Phase	Description	Calculation type
Initial phase	Activation of soil and generating initial stresses	K_0-procedure
Phase 1	Installation of sheet pile wall	Plastic
Phase 2	Excavation to -2m	Plastic
Phase 3	Installation of strut at ground surface	Plastic
Phase 4	Excavation down to -4m	Plastic
Phase 5	Excavation down to -6m	Plastic

NGI-ADP

The material parameters for the Mohr-Coulomb model were modified to represent the NGI-ADP model. The input parameters differ, so the soil properties have been altered. This includes the shear strength ratios (s_u^p/s_u^A, s_u^{DSS}/s_u^A) which were calculated according to empirical relations by Tornborg (2024). The evaluated relations were then used to assess $s^A_{\mathrm{u,ref}}$ and $s^A_{\mathrm{u,inc}}$.

The failure plastic strains and the stiffness ratio were estimated by performing a DSS test in PLAXIS 2D SoilTest and plotting shear stress against shear strain. The input parameters were iteratively adjusted to obtain a soil model that corresponds to the MC model as closely as possible. The DSS tests are presented in Figure B.2 in Appendix Chapter A. The final input parameters obtained from the calibration procedure are summarised in Table 5.5.

Table 5.5: Clay material parameters for the NGI-ADP clay layers for the Lindome case

Material set	Clay 1	Clay 2	Clay 3	
Drainage type	Undrained C			
Wet unit weight γ_{unsat}	16	16	17	[kN/m^3]
Dry unit weight γ_{sat}	16	16	17	[kN/m^3]
Void ratio $\mathrm{e}_{\mathrm{init}}$	0.495	0.495	0.495	[-]
Ratio unloading/reloading shear modulus over active shear strength G_{ur}/s_u^A	120	180	240	[-]
Undrained Poisson's ratio ν_u	0.495	0.495	0.495	[-]
Initial active undrained shear strength $s^A_{\mathrm{u,ref}}$	38	36	37	[kPa]
Increase of active undrained shear strength $s^A_{\mathrm{u,inc}}$	-1.7	-	-	[kPa]
Ratio of passive shear strength over active shear strength s_u^P/s_u^A	0.67	0.62	0.58	[-]
Ratio of direct shear strength over active shear strength s_u^{DSS}/s_u^A	0.77	0.73	0.70	[-]
Shear strain in triaxial compression γ_f^C	3	3	3	[%]
Shear strain in triaxial extension γ_f^E	6	6	6	[%]
Shear strain in direct simple shear γ_f^{DSS}	4	4	4	[%]
Initial mobilization τ_0/s_u^A	0.7	0.7	0.7	[-]
Earth pressure coefficient at rest K_0	0.7	0.7	0.75	[-]

5.3 Results

This section presents the results of calculations for the Lindome case study. The results from the four calculation methods are presented and compared to each other and with the field measurements.

The measurements in Lindome were conducted across three sheet pile sections using earth pressure cells. Two of the pressure cells measured the pressure on the crest of the sheet pile wave, these two sections are compared to the calculated results below.

5.3.1 Active and passive earth pressures

Figure 5.5 shows the active and passive earth pressures calculated from each calculation method, along with field measurements from the earth pressure cells in Lindome. Measurements have only been made on the active earth pressure, and the passive side is therefore excluded from the discussion. The results from hand calculations and Spontprogrammet were identical and are presented together as *Analytical calculations*.

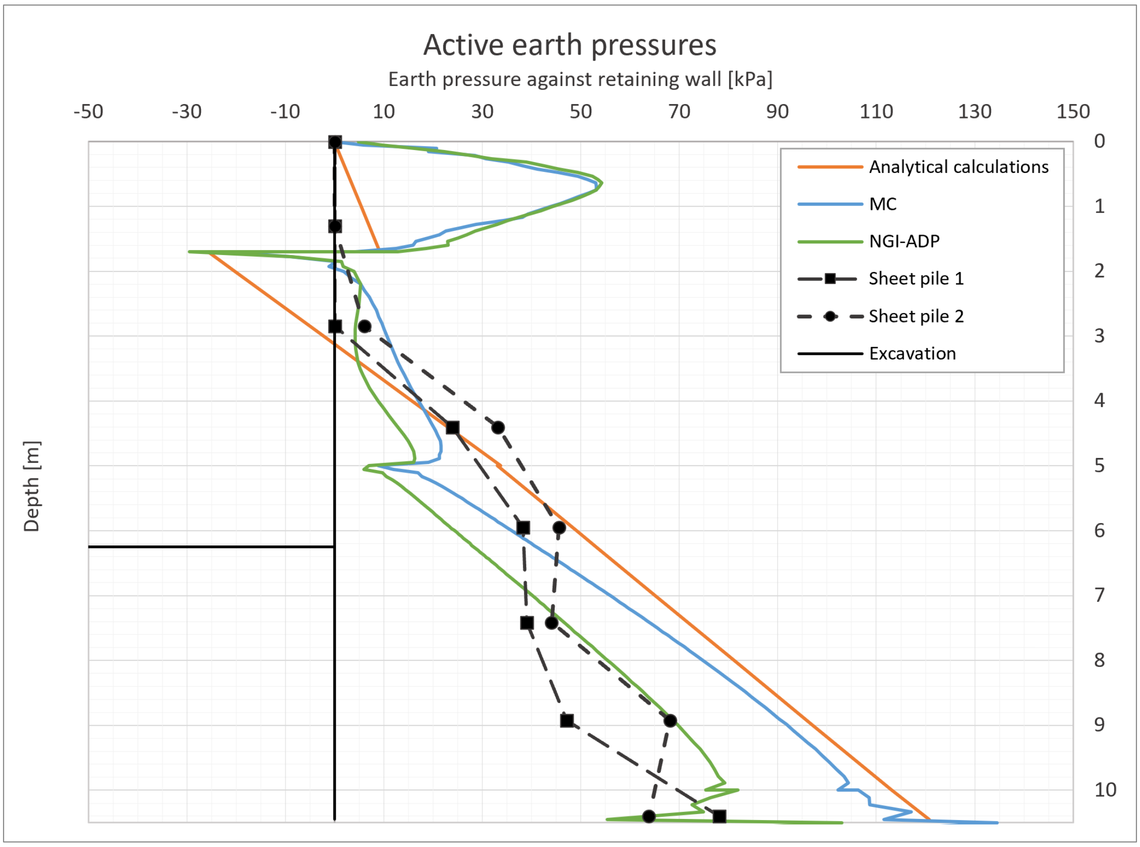

Figure 5.5: Comparing calculated results of active earth pressure to measured data

In the dry crust layer, the numerical models yield earth pressures of up to 50 kPa, whereas the analytical solution increases linearly with depth. The numerical results, as mentioned in Section 3.3.2, are likely due to how PLAXIS predicts the redistribution of loads. Measurements have not been made in the top layer and cannot be used to confirm which model provides the best representation. However, it is assumed that the earth pressures from the numerical models are largely overestimated.

Between 2 m and the bottom of the excavation, the measured earth pressures are slightly bigger than the calculated values. The inclinations of the earth pressures are fairly consistent with the Rankine active earth pressure theory.

Below the excavation bottom, the NGI-ADP model shows the closest agreement between results. This may be because the model's ability to capture anisotropy and stiffness degradation allows the redistribution of stresses under certain conditions. However, the model underestimates the earth pressure between approximately 3 m and 7 m. One possible explanation is that the surrounding conditions of the real excavation restrict wall movement, thereby causing earth pressures to remain closer to the resting state in that region. None of the calculation models has been able to capture the effects causing the changing inclination of the measured plots.

The analytical model provides conservative results of the full active earth pressure. The results indicate that the increase in undrained shear strength used to account for 3D effects did not lead to unrealistically high earth pressures compared with the measured results. However, the aim of the modification was to recreate the acting earth pressures and should not be used as an approach for design. Calculated results should be interpreted as idealised estimates rather than exact representations of the earth pressure.

5.3.2 Waler forces

All calculated forces from the waler are presented in Table 5.6. Hand calculations have been done following the two methods presented in Section 5.2.1.

Both assumptions used in the analytical hand calculation are compared in the results section. The assumption of reduced utilisation of the passive earth pressure is included mainly to compare the hand calculations with Spontprogrammet, whereas the assumption of utilised wall length will be the main focus, as it is also implemented by Spontprogrammet, which follows SPH.

Table 5.6: Calculated reaction forces acting from the waler on the sheet pile wall

Calculation method	Waler force [kN/m]
Hand calculations (Reducing passive earth pressure)	54
Hand calculations (Reducing sheet pile length)	43
Spontprogrammet	47
MC	82
NGI-ADP	77

Looking only at the analytical results, the calculated waler force is larger when the entire sheet pile wall length is used than when only the required length is used. This is expected because a longer wall provides a longer lever arm and requires a larger counterweight to achieve equilibrium. For the second option, the results and Spontprogrammet should be theoretically identical. Instead, there is a slight difference, which can be explained by the fact that Spontprogrammet also considers consolidation effects at the excavation bottom. The consolidation effects reduce the net earth pressure on the passive side, which increases the lever arm against the strut. Since the hand calculations do not include time-related effects, a minor difference is expected.

When comparing the analytical and numerical methods in Table 5.6, the differences are much larger. The numerical models predict almost 50% larger than the analytical ones. This may be explained by the fact that the analytical calculations are based on moment equilibrium, whereas the numerical forces depend on mobilised deformations. However, the difference between the numerical models is relatively small, approximately 5 kN/m. This indicates that the choice of material model has a limited effect on the waler force in this case.

5.3.3 Horizontal displacements

The measured displacements are plotted along with the numerical results in Figure 5.6. The numerical models have been unable to predict the displacements of the sheet pile wall. The results show significant differences, with the measured values nearly 10 times larger than the calculated values.

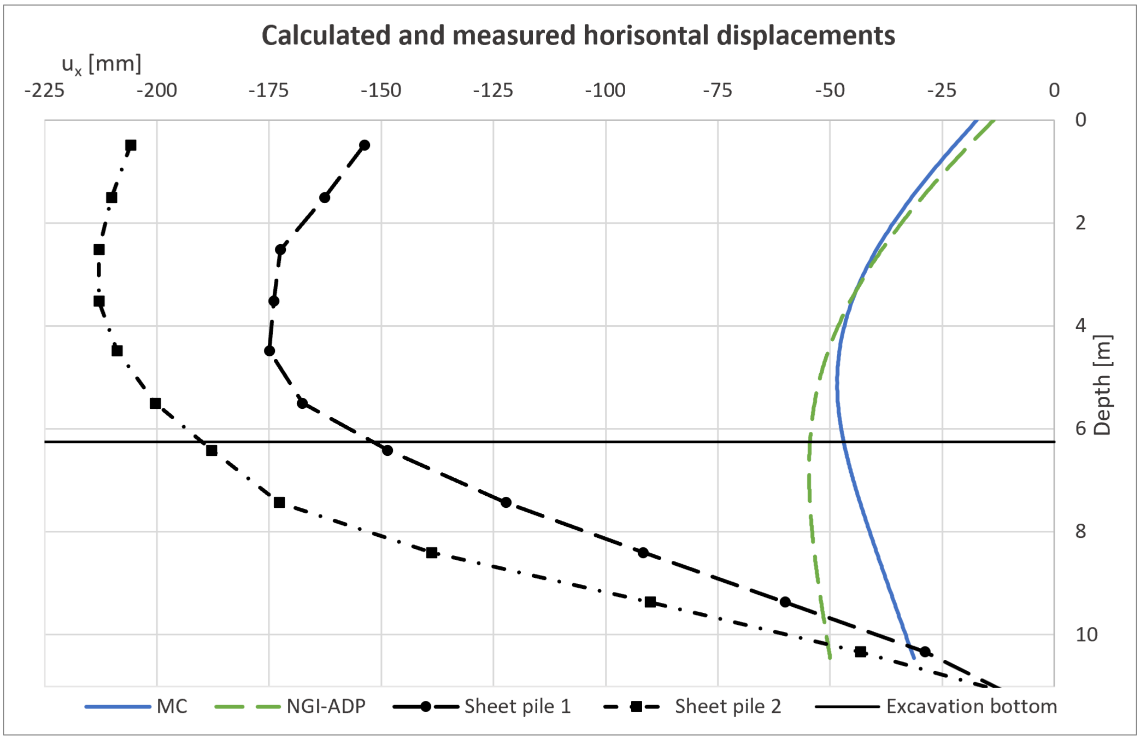

Figure 5.6: Comparing the calculated results of horizontal displacement to the measured field data

One possible explanation for the large displacements near the ground surface for the measured results is that imperfections may have occurred during construction. For example, if the strut was installed with slightly insufficient length or did not provide full support immediately, the wall could have rotated inwards and developed displacements of 15-20 cm before the support became fully active. In practice, such construction-related events are difficult to incorporate into calculations.

At the bottom of the wall, the measured displacements were almost negligible. In contrast, the numerical models predicted significantly smaller displacements near the ground surface, but slightly larger displacements towards the bottom of the sheet pile wall. This indicates that the calculated deformation shape differs from the measured behaviour, even though the overall displacement magnitude is underestimated.

Further, the increased soil strength could have led to an underestimation of the displacement in the clay layer. It is, however, unlikely that this is the only explanation, given the large difference in displacements and the relative agreement of the earth pressure distribution.

Another possible source of uncertainty may have been the measuring method. The displacements were measured using inclinometers, and errors related to the calibration, installation or interpretation of these instruments may also have affected the measured values. However, the difference between the measured and calculated displacements is likely due to additional uncertainties other than only measuring errors.

6 Parametric study of theoretical cases

For simplicity, many assumptions are made in analytical calculations. Numerical calculation methods offer greater flexibility to implement a larger number of soil and structural parameters. This can contribute to more detailed and flexible results, but it also requires more extensive field investigations or parameter assessments, which may not always be available.

The basic analytical calculations of earth pressure simplify the structural elements to rigid bodies. This section presents a PLAXIS 2D parametric study of the bending stiffness of the plate element simulating the sheet pile wall and the axial stiffness of the fixed-end anchors simulating the struts. The study has been conducted using the Mohr-Coulomb and the NGI-ADP analyses to assess how the two material models interact with surrounding structures. Further, the soil stiffnesses have also been varied in the parametric study to assess their effect on the two material models.

The input parameters will be varied by -50%, -25%, +25%, and +50% of the original stiffness.

By varying the stiffness ratio (G_{ur}/s_u^A) in the NGI-ADP model, it is assumed that the unload-reload shear modulus (G_{ur}) is changed in the same proportion since the active undrained shear strength is an input of its own. In the Mohr-Coulomb model, Young's modulus is varied. Since it is connected to the shear modulus by Hooke's law in Equation (2.21), the variation of E_{ref} is considered comparable to the change of the stiffness ratio in the NGI-ADP material model.

The importance of varied input parameters will be evaluated in terms of effects on the result's horizontal displacements, earth pressures and waler forces.

6.1 Single-strut excavation

This section of the study investigates the importance of certain input parameters in the theoretical single-supported excavation. The study will investigate the effects of varying the bending stiffness of the sheet pile wall, the soil stiffness and the stiffness of the fixed-end anchor. The parametric study will evaluate only the results using characteristic input parameters.

6.1.1 Varying stiffness of sheet pile wall

The bending stiffness of the retaining wall is an input parameter that is not considered in the analytical calculations. It is typically assumed that the sheet pile wall is infinitely stiff, implying that no displacements will occur.

The study investigated the effect of the bending stiffness (EI) by performing the analysis multiple times and varying the parameter. The study also separated the soil models with individual analyses for the MC and NGI-ADP models.

Displacements

The results are shown in Table 6.1, along with plotted results of displacements in Figure 6.1. All results from the variations are compared as percentages of the original results, indicating increases or decreases.

The study shows that the stiffness of the retaining wall generally has little to no effect on wall displacement. The largest mean relative change is approximately 6% for the MC model when the stiffness is reduced by 50%. However, this corresponds to a change in the MC model at about 2 mm, which is considered very small. For the NGI-ADP model, the variation is even smaller, indicating that it is slightly less sensitive than the MC to sheet pile wall stiffness.

Two points of interest are considered for each analysis, the maximum deflection at the midpoint of the retaining wall and the displacement at the bottom of the wall. The maximum mid deflection occurs at a depth of 2.8-3.0 m for both models. Similar to the results for the mean displacements, the relative change is somewhat larger, where the maximum is almost 11 % for the MC model. However, the actual change is only 3.2 mm, which again can be considered very small for a 7 m long retaining wall. The trend also appears to be that the NGI-ADP is more stable and less sensitive to variations in wall stiffness.

Table 6.1: Results showing the changes in horizontal displacements from the sheet pile stiffness sensitivity analysis

parametric study					
Bending stiffness [kNm^2/m]	22680	34020	45360	56700	68040
Change [%]	-50	-25	±0	+25	+50
MC					
Mean displacement [mm]	31	30	29	29	28
Relative change [%]	+6	+2	0	-2	-3
Maximum mid disp. [mm]	+3.2	+1.3	-	-0.9	-1.6
Relative change [%]	+10.8	+4.2	0	-3.0	-5.2
Bottom disp. [mm]	-0.9	-0.4	-	+0.3	+0.6
Relative change [%]	-2.4	-1.1	0	+0.8	+1.5
NGI-ADP					
Mean displacement [mm]	26	25	25	25	24
Relative change [%]	+5	+2	0	-1	-2
Maximum mid disp. [mm]	+2.2	+0.9	-	-0.7	-1.1
Relative change [%]	+8.8	+3.4	0	-2.5	-4.4
Bottom disp. [mm]	-1.0	-0.4	-	+0.3	+0.6
Relative change [%]	-2.9	-1.2	0	+1.0	+1.8

When observing the figures of the retaining wall shown in Figure 6.1, it can be seen that, as mentioned, the MC model shows larger differences with variations in bending stiffness. It can also be seen that, while the magnitude is small, the wall's deflection is mainly affected, leading to a larger or smaller curvature.

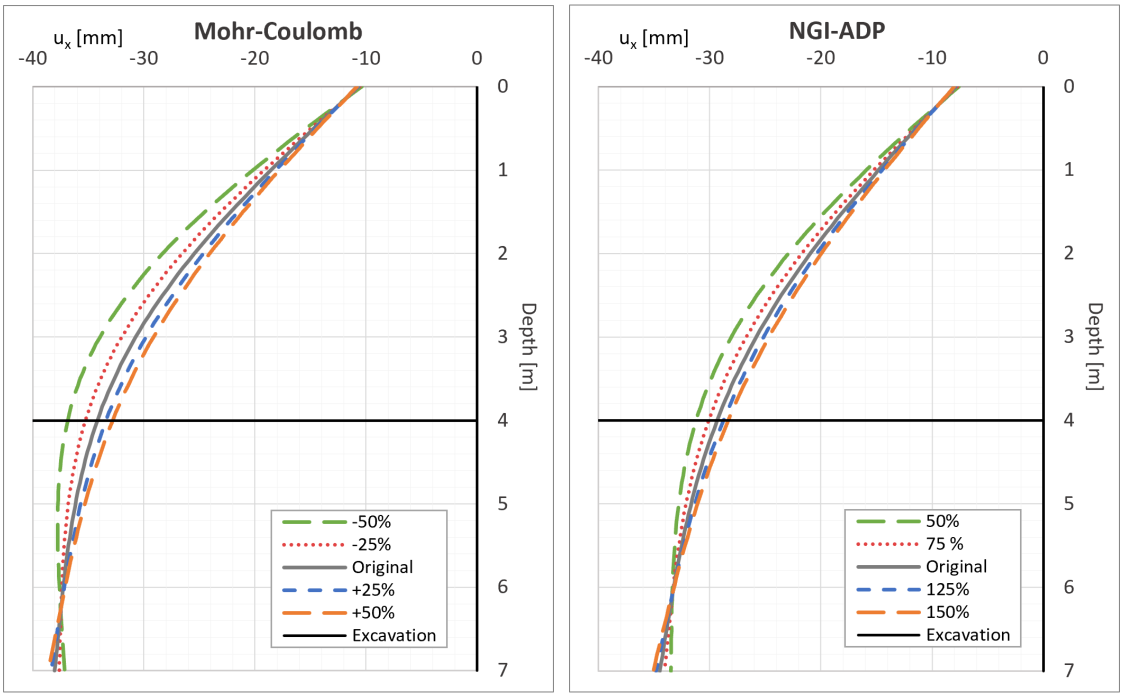

(a) Horizontal displacements calculated using the Mohr-Coulomb material model

(b) Horizontal displacements calculated using the NGI-ADP material model

Figure 6.1: Comparison of horizontal displacements for varying bending stiffness of the sheet pile wall.

Waler forces

The waler force shows a slightly larger variation, and the results are shown in Table 6.1. However, there is no difference between the material models, where the largest relative change is approximately 12%. This corresponds to a reduction of 5-6 kN/m and occurs when the bending stiffness is reduced by 50 %. In contrast, increasing the stiffness by 50 % only results in a relative change of approximately 6 %, for both models.

Table 6.2: Results for the whaler forces for varying the bending stiffness of the sheet pile wall.

parametric study					
Bending stiffness [kNm^2/m] Change [%]	22680 -50	34020 -25	45360 ±0	56700 +25	68040 +50
MC					
Waler force [kN/m] Relative change [%]	48 -12	52 -5	54 0	56 +3	58 +6
NGI-ADP					
Waler force [kN/m] Relative change [%]	41 -12	44 -5	46 0	48 +4	49 +6

It can be concluded that bending stiffness has a greater effect on the waler force than displacements when stiffness is reduced. As mentioned previously, the increased stiffness may not provide additional restraint, which in turn decreases displacement and the waler force.

Earth pressures

For the earth pressures, the pressure distribution along the depth appears to be the same. The earth pressures have been plotted and are shown in Figure 6.2. Overall, the differences are relatively small across all analysed cases, suggesting that sheet pile stiffness has a limited effect on earth pressures. The Mohr-Coulomb model shows a wider variety at the bottom of the wall, and the NGI-ADP model appears more stable. However, it cannot be fully trusted, as the assessment in Section 5.3.1 also shows numerical difficulties in the NGI-ADP model.

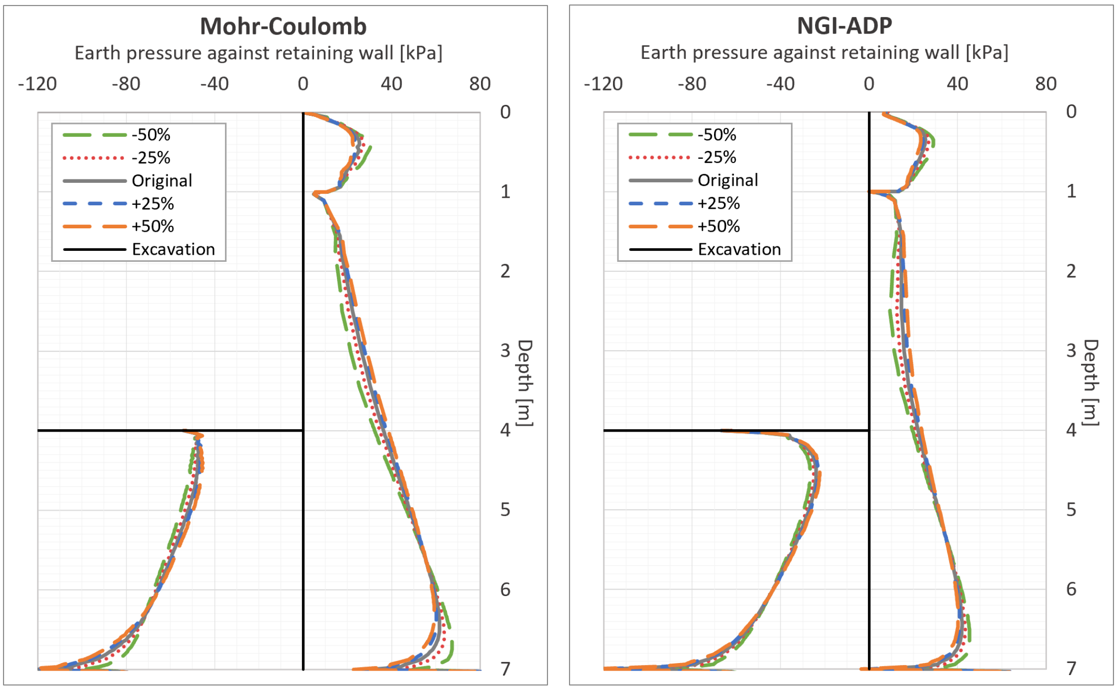

(a) Earth pressures calculated with the MC material model

(b) Earth pressures calculated with the NGI-ADP material model

Figure 6.2: Effect of varying the sheet pile wall stiffness on the earth pressure distribution.

It should be noted that the result is only dependent on the bending stiffness of the retaining wall. Additional parameters, such as axial stiffness and buckling effects, could also be investigated. Furthermore, the limited sensitivity observed may also be a consequence of the studied geometry. Overall, it can also be concluded that the influence of sheet pile stiffness is negligible. The results of this parametric study support the assumption made for analytical calculation that the wall stiffness has no significant influence.

6.1.2 Varying soil stiffness

In addition to varying the bending stiffness of the plate element in PLAXIS, another parametric study was conducted in which the soil stiffness was varied. The original stiffness parameters have been scaled with the same factors as previously. E'_{ref} and E'_{inc} have been adjusted in the Mohr-Coulomb material model and G_{ur}/s_u^A in the NGI-ADP material model. As this study changes the soil properties, it is expected to show more varied results than the previous study.

Displacements

For the horizontal displacements, it can be observed that varying the soil stiffness has a much greater effect, which is as expected. Both the MC and NGI-ADP models show large changes in the displacement profiles, where decreasing the stiffness results in larger displacements, while increasing the stiffness reduces them. Results are presented in Table 6.3 and figure 6.3

Table 6.3: Results showing the changes in horizontal displacements from the soil stiffness sensitivity analysis

parametric study					
MC					
Soil stiffness [kPa]	1875	2813	3750	4688	5625
Increase	163	244	325	406	488
Change [%]	-50	-25	±0	+25	+50
Mean displacement [mm]	55	38	29	24	20
Relative change [%]	+89	+30	0	-19	-31
Maximum disp. [mm]	+40	+13	-	-8	-13
Relative change [%]	+104	+34	0	-21	-34
NGI-ADP					
Stiffness ratio [-]	80	120	160	200	240
Change [%]	-50	-25	±0	+25	+50
Mean displacement [mm]	37	29	25	22	21
Relative change [%]	+49	+17	0	-10	-18
Maximum disp. [mm]	+18	+6	-	-4	-6
Relative change [%]	+53	+18	0	-111	-18

When the stiffness is decreased, the largest relative change in the mean displacement is approximately +89% for the MC model, whereas the corresponding change for the NGI-ADP model is only about +49%. A similar trend can be observed for the maximum displacement, with the MC model predicting a relative change of nearly +104%, compared to approximately +53% for the NGI-ADP model.

Since the MC model is linear elastic, a reduced soil stiffness is expected to provide much larger displacements. The NGI-ADP model, however, appears less affected, likely due to its nonlinear behaviour. A reduction in stiffness changes the stress-strain curve and the way displacements develop. This, in combination with the anisotropic soil strength, provides a greater stability towards changes in soil stiffness.

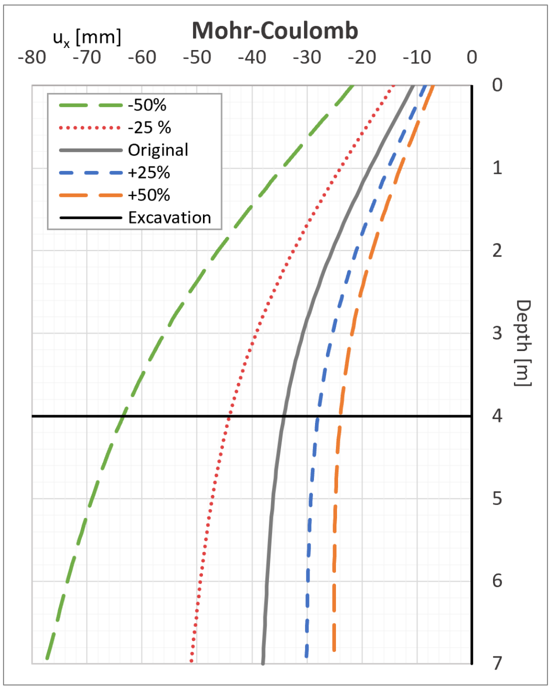

(a) Sheet pile wall displacements calculated using the MC material model

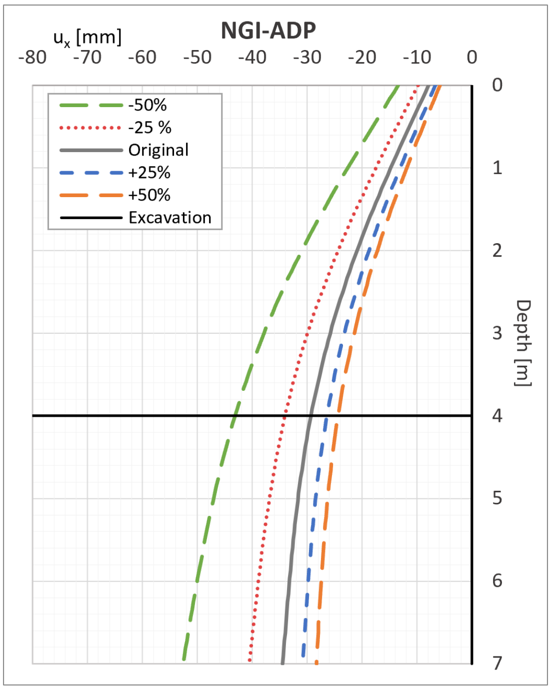

(b) Sheet pile wall displacements calculated using the NGI-ADP material model

Figure 6.3: Results on the horizontal displacements varying the soil stiffness

It can be noted that although displacements are more affected, the wall curvature is relatively similar across all stiffnesses. This shows, as expected, that the horizontal displacement is more sensitive to changes in stiffness or the surrounding soil. The shape of the sheet pile wall, however, is more influenced by the bending stiffness.

Waler forces

The results from the study can be found in Table 6.4, and the largest differences can be found in the MC model when the stiffness is reduced by 50%. Consistent with the results above, the comparison of horizontal displacements indicates that the NGI-ADP is less sensitive to stiffness variation.

In contrast to the sheet pile stiffness study, decreasing soil stiffness increased the resulting waler force, which then decreased as stiffness increased. This is not unexpected, since softer soil allows larger wall movements and larger waler forces, while a softer plate element reduces displacements at the top support and redistributes the load differently.

The results also resemble the previous observations when increasing the stiffness. The changes in waler forces are not as large as when stiffness is decreased, indicating that the system is already relatively stiff.

Table 6.4: Results for the waler forces for varying soil stiffness.

Parametric study					
MC					
Soil stiffness [kPa]	1875	2813	3750	4688	5625
Increase	163	244	325	406	488
Change [%]	-50	-25	±0	+25	+50
Waler force [kN/m]	64	58	54	51	49
Relative change [%]	+17	+7	0	-6	-11
NGI-ADP					
Stiffness ratio [-]	80	120	160	200	240
Change [%]	-50	-25	±0	+25	+50
Waler force [kN/m]	52	48	46	45	44
Relative change [%]	+11	+4	0	-3	-6

Earth pressures

Similar to the earth pressures calculated in the sheet pile stiffness study, there is not much variation. The small differences suggest that soil stiffness also has a limited effect on the earth pressure. The earth pressures can be found in Figure 6.4.

It could be debated whether active earth pressures should decrease as soil stiffness decreases, since displacements increase. This is not the case, as shown in the figure above, where cases with decreased soil stiffness generally have larger active earth pressures. However, the global response appears more complex as increased deformation may lead to the redistribution of stresses.

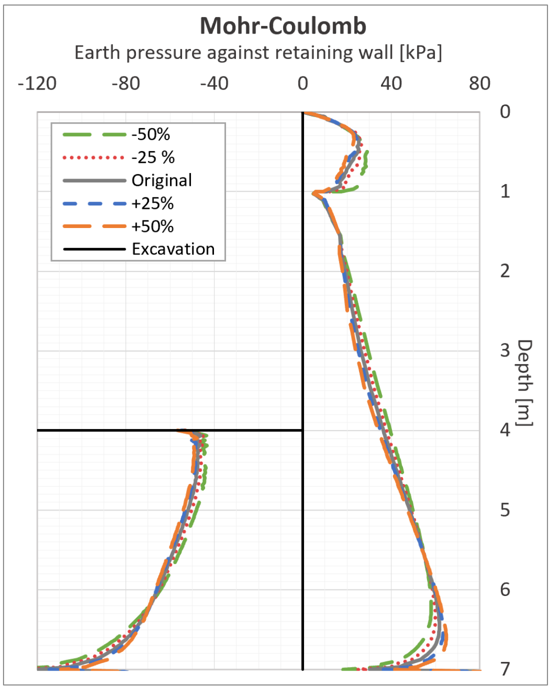

(a) Earth pressures calculated with the MC material model

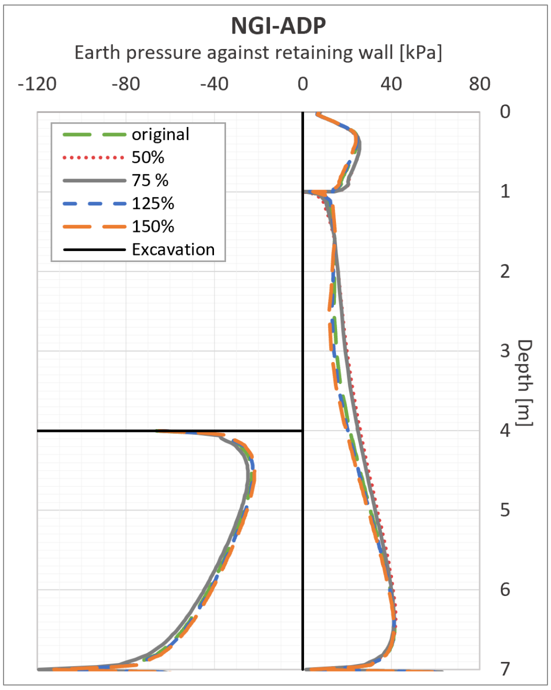

(b) Earth pressures calculated with the NGI-ADP material model

Figure 6.4: Effect of varying the soil stiffness on the earth pressure distribution.

Overall, the results indicate that soil stiffness has a limited influence on the calculated earth pressure distribution compared to its effect on the horizontal displacements.

Although lower soil stiffness results in larger wall movements, this does not directly lead to lower active earth pressures. Instead, the results suggest that the earth pressure distribution is governed by a more complex interaction between wall deformation, soil stiffness and stress redistribution. Therefore, the effect of soil stiffness is more clearly reflected in the displacements and waler forces than in the earth pressure distribution.

6.1.3 Varying the spring stiffness of fixed-end anchor

The anchor in the numerical model is defined by an axial stiffness that represents the support stiffness in the system. By varying the spring stiffness of the fixed-end anchor, the influence on the sheet pile wall can be investigated.

A lower spring stiffness represents a more flexible support, which is expected to allow for larger displacements, reducing the horizontal earth pressures and increasing the reaction forces in the supports.

Results

The parametric study shows that the axial stiffness of the fixed-end anchor has no influence on either the earth pressures, waler forces or the displacement. This was unexpected and could be caused by the stiffness being too high to start with. However, if the axial stiffness had had an impact, there would still have been slight differences that could not have been observed in this case.

As mentioned previously, the models are deformation-dependent. Therefore, as there is no change in deformations in the fixed-end anchor, there is consequently no change in the waler forces.

From this, it can be concluded that in the case studied, the earth pressures, waler forces and displacements are governed by other parameters rather than by the stiffness of the fixed-end anchor. Consequently, this parameter has been excluded from the following parametric studies, as the results indicate that its influence is negligible in the studied case.

6.2 Multiple-strut excavation

The same parametric study as above has been conducted for the theoretical case with an additional strut level in the excavation. For this specific task, the depth of the excavation was increased to 7 m and a second strut level was added at a depth of 3.5 m. The new geometry of the excavation can be found in Figure 3.1.

6.2.1 Varying the sheet pile stiffness

In this part of the parametric study, the bending stiffness of the sheet pile wall is varied exactly as for the previous study. Similar behaviour is expected, in which the stiffness mainly influences the wall's curvature with respect to the displacement profile. The waler forces are also likely to vary, since deformations and force distribution may be affected by stiffness variations. The earth pressures may also vary slightly, as in the previous results, although the influence is expected to be less obvious than for the displacements.

Displacements

The results are presented in Table 6.5, and the displacements are relatively similar between the two models. Both models show similar magnitudes for the displacements and relative changes. While the MC shows slightly larger displacements, the wall profiles are relatively similar, shown in Figure 6.5.

As discussed previously, for this parameter, the bottom displacement is also studied. For cases with reduced bending stiffness, they tend to have larger curvature in the middle and towards the bottom of the wall, and reduced displacements. The opposite is observed for cases with increased stiffness, the sheet pile wall behaves more rigidly, has less curvature in the middle, but shows increased displacement at the bottom. This may be explained by a redistribution of the wall deformation. When the bending stiffness is reduced, the wall is more flexible, and a larger part of the deformation occurs as bending in the middle of the wall. When the stiffness is increased, the wall behaves more like a rigid body, reducing curvature but potentially leading to rotation and larger movements near the bottom of the wall.

Table 6.5: Results of the horizontal displacements from varying the bending stiffness of the sheet pile wall

Parametric study					
Bending stiffness [kNm^2/m]	22680	34020	45360	56700	68040
Change [%]	-50	-25	±0	+25	+50
MC					
Mean displacement [mm]	43.8	42.2	41.1	40.3	39.7
Relative change [%]	+6.6	+2.6	0	-1.9	-3.5
Maximum mid disp. [mm]	+5.5	+2.2	-	-1.6	-2.9
Relative change [%]	+10.8	+4.4	0	-3.2	-5.8
Bottom disp. [mm]	-2.0	-0.8	-	+0.7	+1.1
Relative change [%]	-3.3	-1.4	0	+1.2	+1.9
NGI-ADP					
Mean displacement [mm]	41.1	39.7	38.7	37.9	37.2
Relative change [%]	+6.4	+2.6	0	-2.0	-3.8
Maximum mid disp. [mm]	+5.0	+2.0	-	-1.5	-2.8
Relative change [%]	+10.3	+4.2	0	-3.2	-5.8
Bottom disp. [mm]	-2.2	-0.5	-	+0.3	+0.4
Relative change [%]	-2.2	-0.8	0	+0.5	+0.6

As mentioned previously, the MC model appears more sensitive to variations in the wall's bending stiffness. The NGI-ADP model appears to be more stable, possibly due to different definitions of stiffness for the models.

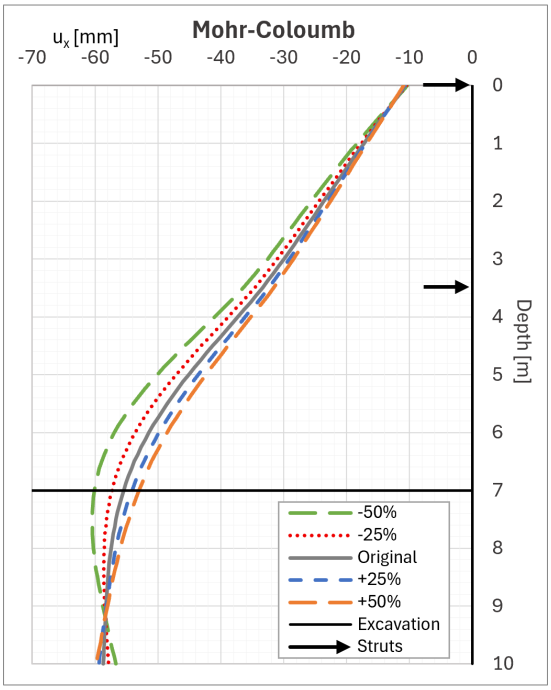

(a) Horizontal displacements calculated using the MC material model

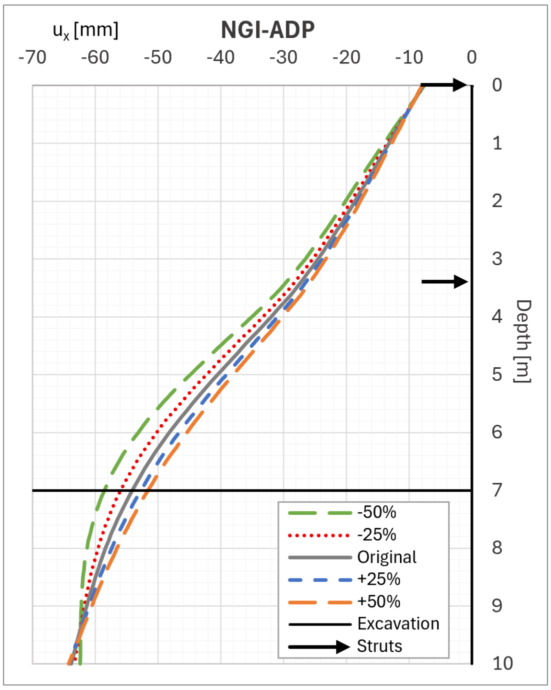

(b) Horizontal displacements calculated using the NGI-ADP material model

Figure 6.5: Results on the horizontal displacements varying bending stiffness of the sheet pile wall

Waler forces

The results in Table 6.6 show that waler forces are affected differently depending on the strut level. For the upper strut, the force decreases as the sheet pile stiffness increases. This trend is observed for both material models, although the relative change is considerably larger in the NGI-ADP model due to the small reference value at the original stiffness. For the lower strut, the opposite trend can be observed, where the waler force increases with increasing sheet pile stiffness.

Based on the results, the NGI-ADP model appears more sensitive to the stiffness of the retaining wall. This is most clearly observed in the upper strut, where the relative changes exceed 100% for some investigated stiffnesses. The strut will also experience extension when the stiffness has been increased by 50 %, which indicates a stiffer response in the soil-structure interaction closer to the ground surface and rotation of the wall.

While the relative change is very large, the magnitude of the actual change is approximately the same. This should be taken into account since the MC model most likely experienced a larger translation and probably experienced the same rotation as the NGI-ADP model, but it is not as clear when only observing the output forces.

Table 6.6: Results for the waler forces for varying the bending stiffness of the sheet pile wall.

Parametric study					
Bending stiffness [kNm^2/m]	22680	34020	45360	56700	68040
Change [%]	-50	-25	0	+25	+50
MC					
Waler force, strut 1 [kN/m]	30.4	27.1	24.1	21.3	18.7
Relative change [%]	+25.8	+12.1	0	-11.6	-22.6
Waler force, strut 2 [kN/m]	206.8	217.8	226.4	234.0	240.4
Relative change [%]	-8.6	-3.8	0	+3.4	+6.2
NGI-ADP					
Waler force, strut 1 [kN/m]	13.6	9.2	5.0	1.1	-2.7
Relative change [%]	+168.9	+82.0	0	-78.8	-154.1
Waler force, strut 2 [kN/m]	213.8	224.8	234.1	242.6	250.2
Relative change [%]	-8.7	-4.0	0	+3.6	+6.8

Earth pressures

The earth pressures in the study show little to no difference near the ground surface until the second strut at a depth of 3.5 m. The MC model shows no variation with changes in the stiffness of the wall above the bottom strut. Since the bottom strut provides global rotational stability, there should be little to no bending of the wall. This provides no particular wall displacements for the earth pressures to act upon in the numerical models. The NGI-ADP model also acts linearly over the same range, but earth pressure shows only small changes in the parametric study.

The passive earth pressures also appear to have very little variation, particularly in the MC model, and the differences between the models is generally small.

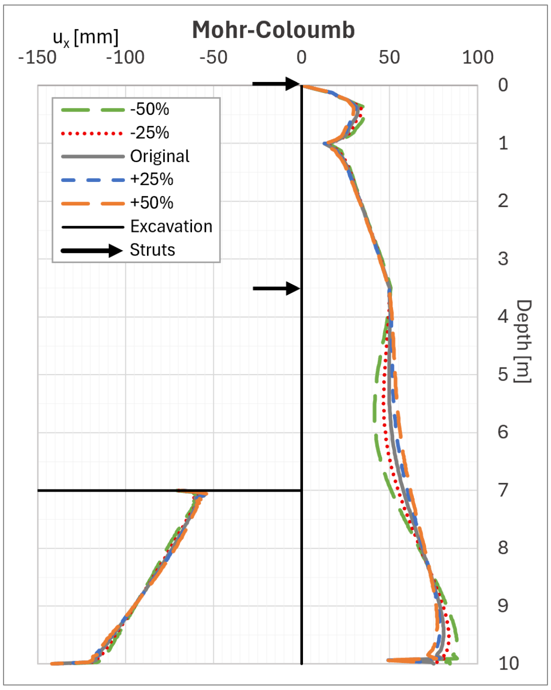

(a) Earth pressures calculated with the MC material model

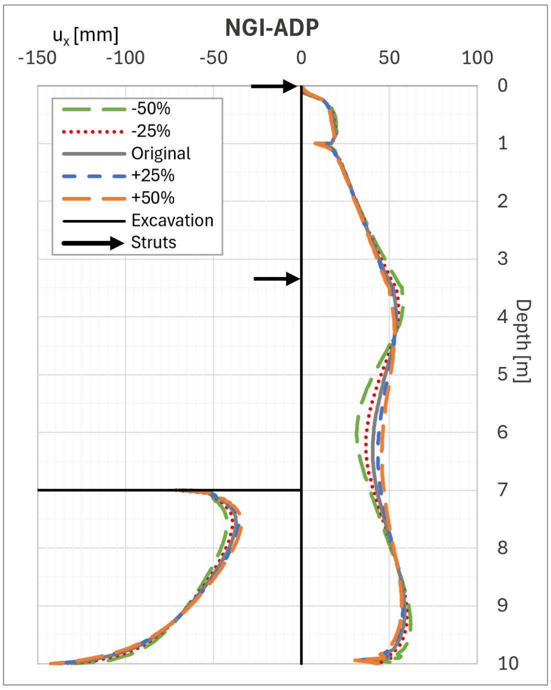

(b) Earth pressures calculated with the NGI-ADP material model

Figure 6.6: Results on the earth pressures for varying the bending stiffness of the sheet pile wall.

6.2.2 Varying the soil stiffness

The soil stiffness input parameters have been varied by ± 25 and 50 %. The sections below present results and discussion from the parametric study for the deeper excavation case.

Displacements

Final displacements depending on soil stiffness are presented in Table 6.7. The difference between the MC model with the original soil stiffness and the 50% lower soil stiffness is 61 mm, whereas in the NGI-ADP model it is 27 mm. This represents an increase of 103% against 46%, and it is clear that the MC model is more affected by changes in the soil stiffness input. This can also be concluded by looking at Figure 6.7.

The study confirms previous results and the conclusion that the NGI-ADP model defines its soil stiffness as anisotropic based on input soil strengths and failure strains, in addition to the varied stiffness ratio. The Mohr-Coulomb model has only one stiffness input parameter that affects the final results. However, the models define stiffness differently, which may also explain the large differences.

Table 6.7: Results on the horizontal displacements for varying the soil stiffness

Parametric study					
Change [%]	-50	-25	±0	+25	+50
MC					
Soil stiffness [kPa]	1875	2813	3750	4688	5625
Increase [kPa/m]	163	244	325	406	488
Mean displacement [mm]	76	53	41	34	29
Relative change [%]	+86	+29	± 0	-18	-34
Maximum disp. [mm]	+61	+20	-	-12	-20
Relative change [%]	+103	+35	0	-21	-34
NGI-ADP					
Stiffness ratio [-]	80	120	160	200	240
Mean displacement [mm]	55	44	39	35	33
Relative change [%]	+33	+7	± 0	-14	-20
Maximum mid disp. [mm]	+27	+9	-	-6	-9
Relative change [%]	+46	+16	± 0	-9	-16

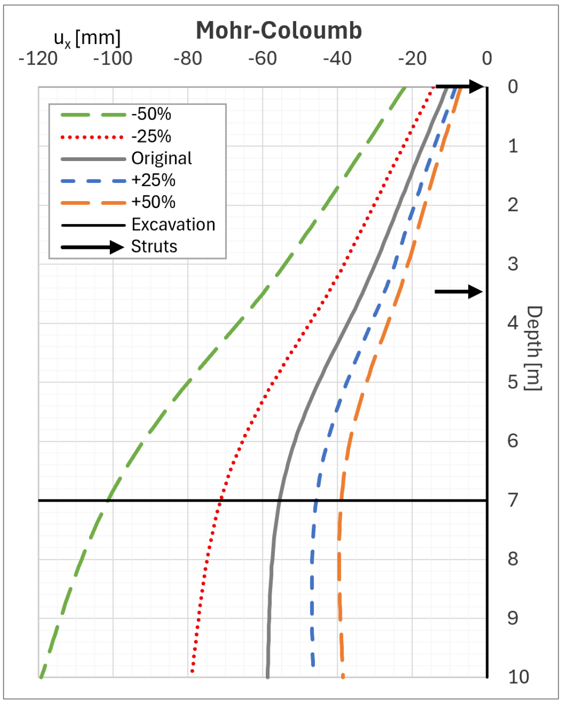

(a) Horizontal displacement calculated using the Mohr-Coulomb model

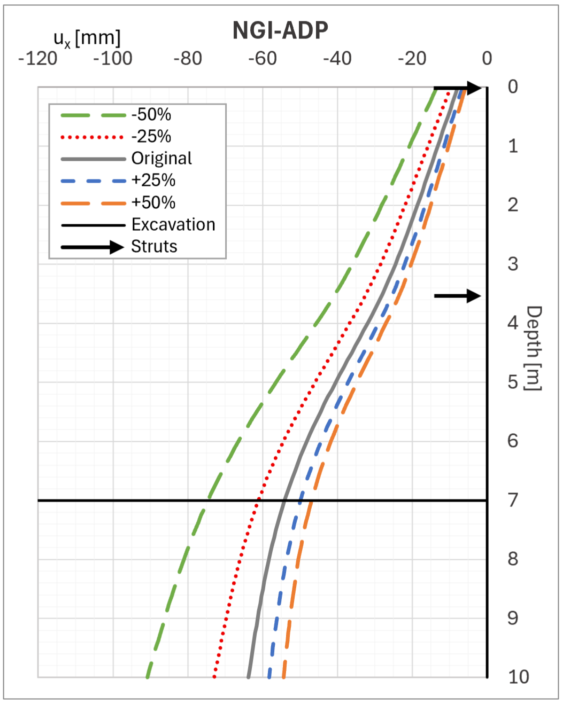

(b) Horizontal displacement calculated using the NGI-ADP model

Figure 6.7: Results on the horizontal displacements for varying the soil stiffness

Waler forces

The result of the parametric study containing waler forces is presented in Table 6.8. It should be noted that the force from the MC model decreases in the top waler and increases in the bottom waler as soil stiffness decreases. Whereas the NGI-ADP model behaves in the opposite way.

The effects may be due to the NGI-ADP model having a higher shear strength in the active zone. This causes the soil to "carry itself" better, and, combined with increased stiffness, the non-linear elasticity of the stress-strain curve becomes steeper. Another possible explanation is that the wall behaves differently, such as by rotating or moving horizontally.

Table 6.8: Results showing the changes in waler force from the soil stiffness sensitivity analysis

Parametric study					
Change [%]	-50	-25	±0	+25	+50
MC					
Soil stiffness [kPa]	1875	2813	3750	4688	5625
Increase [kPa/m]	163	244	325	406	488
Waler force, strut 1 [kN/m]	18	22	24	25	26
Relative change [%]	-25	-7	± 0	+4	+6
Waler force, strut 2 [kN/m]	253	236	226	219	214
Relative change [%]	+12	+4	± 0	-3	-5
NGI-ADP					
Stiffness ratio [-]	80	120	160	200	240
Waler force, strut 1 [kN/m]	8	7	5	4	3
Relative change [%]	+56	+31	± 0	-28	-49
Waler force, strut 2 [kN/m]	229	230	234	239	243
Relative change [%]	-2.4	-1.7	± 0	+2.0	+3.7

Earth pressures

The active and passive earth pressures from the study are presented in Figure 6.8. The active pressure in the Mohr-Coulomb model is not very affected by the change in stiffness above the top and bottom strut, while the NGI-ADP model is changed by ± 10 kPa at 4 m. This difference between the models raises questions about how they redistribute the earth pressure.

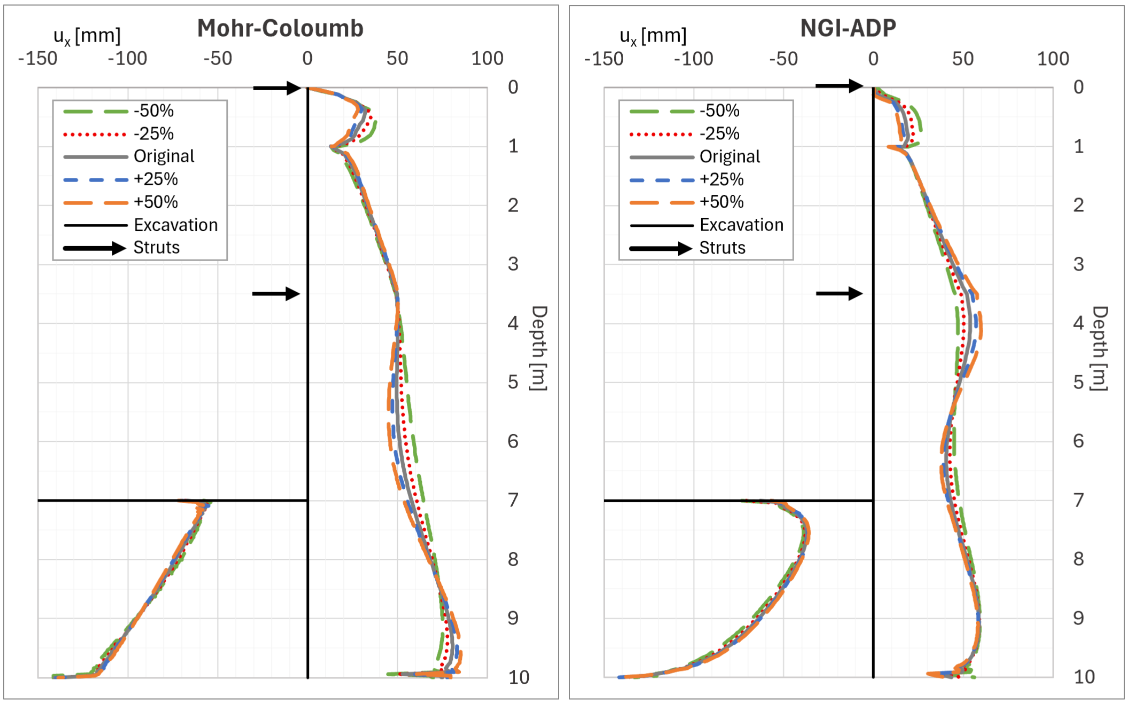

(a) Earth pressures calculated using the Mohr-Coulomb model

Figure 6.8: Results of the earth pressures for of varying the soil stiffness

In Figure 6.8, the earth pressure distribution is relatively similar between the two models until approximately 3 m depth. After that, the NGI-ADP model shows a larger variation in earth pressures around the depth of the second waler, while the MC model shows no variation at that depth. Afterwards, the earth pressures in the MC model will decrease and show more variation down to 8 m depth. The NGI-ADP model will show similar variation, but not as evident as the MC model.

This may be explained by how the models redistribute stresses as the wall deforms. NGI-ADP have anisotropic undrained shear strengths, which may lead to a more local redistribution of stresses around the supports. In contrast, the MC model appear to transfer stresses further down the wall. Overall, the results show that changes in soil stiffness not only affects the magnitude of earth pressures but also the where along the wall the largest redistribution occurs.

7

Parametric study of Lindome case

A parametric study has also been conducted for the Lindome case, with the same changes in soil and sheet pile wall stiffness as above.

The original parameters in the Lindome case are based on on-site measurements and assumptions from empirical relations. Via the parametric study, the aim is to assess the importance of accurate input data.

7.1 Varying bending stiffness of sheet pile wall

Similar assumptions and variations have been used in this parametric study as for the theoretical cases in Chapter 6.

Displacements

Table 7.1 shows mean deflections from the parametric study of both numerical models. Furthermore, the differences in maximum displacements and in bottom displacements are presented.

In general, the results have large similarities to the general scenario and changing the stiffness of the sheet pile wall has a small impact on the final results.

Table 7.1: Results for the horizontal displacement in the Lindome case study for varying the sheet pile wall bending stiffness

Parametric study					
Bending stiffness [kNm^2/m]	22680	34020	45360	56700	68040
Change [%]	-50	-25	±0	+25	+50
MC					
Mean displacement [mm]	43	41	40	39	38
Relative change [%]	+9	+4	±0	-3	-5
Max. mid displacement [mm]	+6.4	+2.7	-	-2.0	-35
Relative change [%]	+13.8	+5.7	±0	-4.4	-8.1
Bottom displacement [mm]	-0.4	-0.2	-	0.3	0.7
Relative change [%]	-1.2	-0.8	±0	+1.1	+2.1
NGI-ADP					
Mean displacement [mm]	47.6	46.4	45.4	44.6	44.0
Relative change [%]	+4.9	+2.1	±0	-1.7	-3.1
Max. mid displacement [mm]	+4.1	+1.8	-	-1.4	-2.6
Relative change [%]	+8.5	+3.6	±0	-2.9	-5.3
Bottom displacement [mm]	-0.9	-0.5	-	0.4	0.8
Relative change [%]	-1.8	-0.9	±0	+0.8	+1.7

The parametric study is shown in Figure 7.1. The MC model shows more curved graphs and a bigger spread than the NGI-ADP model, indicating that it is more sensitive to the wall's bending stiffness.

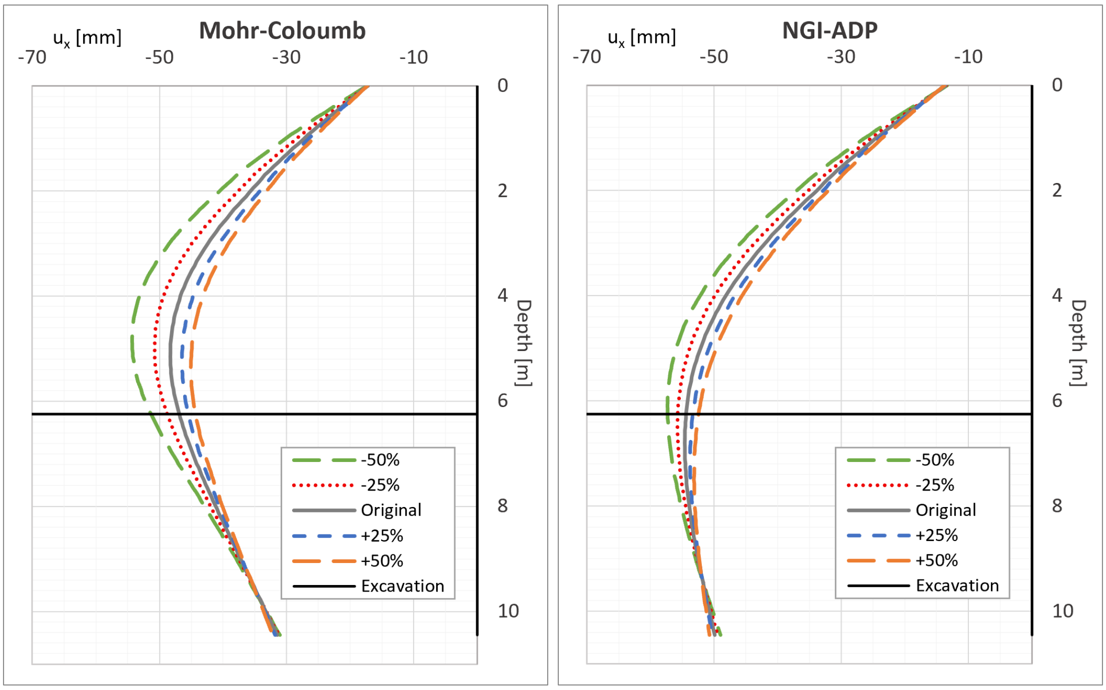

(a) Horizontal displacements from the Mohr-Coulomb model

(b) Horizontal displacements from the NGI-ADP model

Figure 7.1: Results on the horizontal displacements in the Lindome case study for varying the sheet pile wall bending stiffness

Waler forces

The result changes in reaction forces in the waler are presented in Table 5.6. Changing the bending stiffness of the wall has about the same impact on the reaction in both models.

Table 7.2: Results for the waler forces in the Lindome case study for varying the sheet pile wall bending stiffness.

Parametric study					
Bending stiffness [kNm^2/m]	22680	34020	45360	56700	68040
Change [%]	-50	-25	±0	+25	+50
MC					
Waler force [kN/m]	68	74	79	83	86
Relative change [%]	-13	-6	±0	+5	+8
NGI-ADP					
Waler force [kN/m]	64	69	74	77	80
Relative change [%]	-14	-6	0	+5	+9

Earth pressure

The effect that the bending stiffness has on the active and earth pressures is displayed in Figure 7.2. The results are plotted against the measured earth pressures to assess whether the stiffness could have yielded more accurate results.

Below the excavation depth, the differences in active earth pressures between the two models are negligible. The plots show that changes in wall stiffness do not have a substantial effect on the accuracy of the results.

In the MC model in Figure 7.2a, the increase is quite linear between the top of the clay and the excavation bottom. The nonlinear response in the NGI-ADP model is clearer and is reflected in the results, especially between 2 and 6 m depth. However, the magnitude appear to be affected by the bending stiffness in the same way.

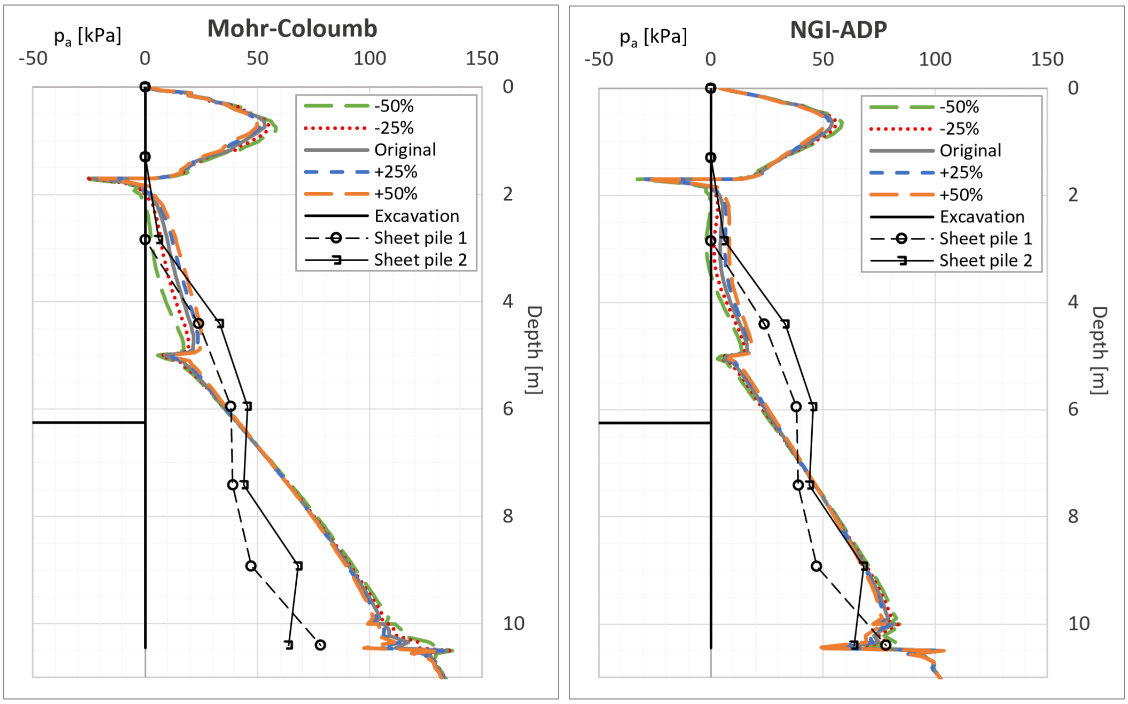

(a) Active earth pressure distribution from Mohr-Coloumb material model

(b) Active earth pressure distribution from NGI-ADP material model

Figure 7.2: Results for the active earth pressure in the Lindome case study for varying the sheet pile wall bending stiffness

7.2 Varying stiffness of soil

In this section, the stiffnesses of the soil layers have been varied rather than the wall stiffness. They have been changed using the same variations as before, ±50% and ±25%. All three clay layers have been varied with the same percentage points.

Displacements

Table 7.3 presents the results of the horizontal displacements with different soil stiffnesses. The results are similar to those from studies of theoretical cases when comparing deformation sizes. The MC model is, as previously, more sensitive to variation in soil stiffness than the NGI-ADP model.

Table 7.3: Results for the horizontal displacement in the Lindome case study for varying the soil stiffness

Parametric study						
Change [%]		-50	-25	±0	+25	+50
MC						
Soil stiffness [kNm^2/m]	Clay 1	2800	4200	5600	7000	8400
	Clay 2	4300	6450	8600	10750	12900
	Clay 3	5650	8475	11300	14125	16950
Mean displacement [mm]		73	51	40	33	28
Relative change [%]		+85	+30	±0	-16	-28
Max. mid displacement [mm]		+39	+14	-	-7	-13
Relative change [%]		+85	+29	±0	-16	-27
Bottom displacement [mm]		+35	+12	-	-6	0.7
Relative change [%]		+111	+38	±0	-18	-32
NGI-ADP						
Stiffness ratio [-]	Clay 1	60	90	120	150	180
	Clay 2	90	135	180	225	270
	Clay 3	120	180	240	300	360
Mean displacement [mm]		62	51	45	42	40
Relative change [%]		+37	+13	±0	-7	-12
Max. mid displacement [mm]		+19	+7	-	-4	-6
Relative change [%]		+35	+12	±0	-7	-12
Bottom displacement [mm]		+16	+5	-	-2	-4
Relative change [%]		+33	+11	±0	-4	-9

In Figure 7.3, the shape and deflections are shown, indicating that the MC model is more influenced than the NGI-ADP model. However, when compared to the measured values in Chapter 5, none of the models shows the same deflection observed close to the ground surface as the measured values show. This suggests that the accuracy of the soil stiffnesses remains important, but for this case, the large differences between the calculated displacements and the measured values likely depend on other external factors.

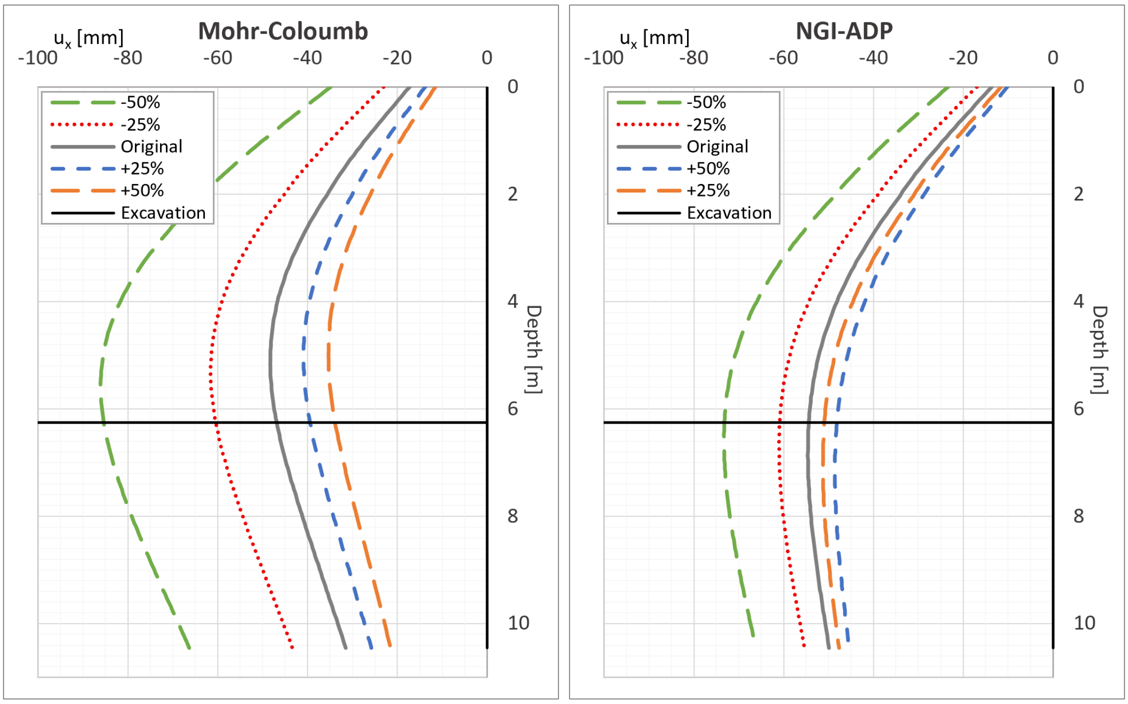

(a) Horizontal displacements from the Mohr-Coulomb model

(b) Horizontal displacements from the NGI-ADP model

Figure 7.3: Results on the horizontal displacements in the Lindome case study for varying the soil stiffness

Waler forces

The waler forces in Table 7.4 also show that the MC model is more sensitive than the NGI-ADP model. This can be connected to Table 7.3 since a bigger variation in displacements should indicate a bigger variation in reaction forces in the structural parts as well. The general trend of the results is very similar to the pattern observed in Section 6.1.2.

Table 7.4: Results of waler force in the Lindome case study if the soil stiffness is varied

Parametric study						
Change [%]		-50 %	-25 %	±0 %	+25 %	+50 %
MC						
Soil stiffness [kNm^2/m]	Clay 1	2800	4200	5600	7000	8400
	Clay 2	4300	6450	8600	10750	12900
	Clay 3	5650	8475	11300	14125	16950
Waler force [kN/m]		97	86	79	74	69
Relative change [%]		+23	+9	0	-7	-12
NGI-ADP						
Stiffness ratio [-]	Clay 1	60	90	120	150	180
	Clay 2	90	135	180	225	270
	Clay 3	120	180	240	300	360
Waler force [kN/m]		84	78	74	71	69
Relative change [%]		+13	+5	± 0	-3	-6

Earth pressure

The earth pressures do not show a significantly varied result in either of the material models in Figure 7.4. Reducing the stiffness by -50% gives slightly higher earth pressures in the first clay layer with the MC model while the NGI-ADP model provides a more linear distribution in the same span. Increasing the stiffness in the NGI-ADP model provides a more curved behaviour, which have been observed previously in Sections 6.1.2 and 6.2.2.

However, the change of soil stiffness does not affect the result against the measurements, the causes for different results are more likely to be caused by the effects from direct surroundings that have note been captured by the plane strain model.

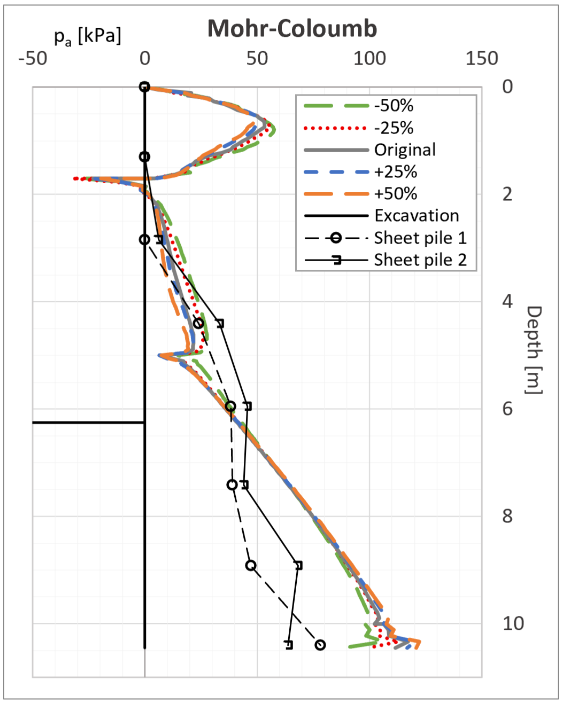

(a) Active earth pressure distribution from Mohr-Coloumb material model

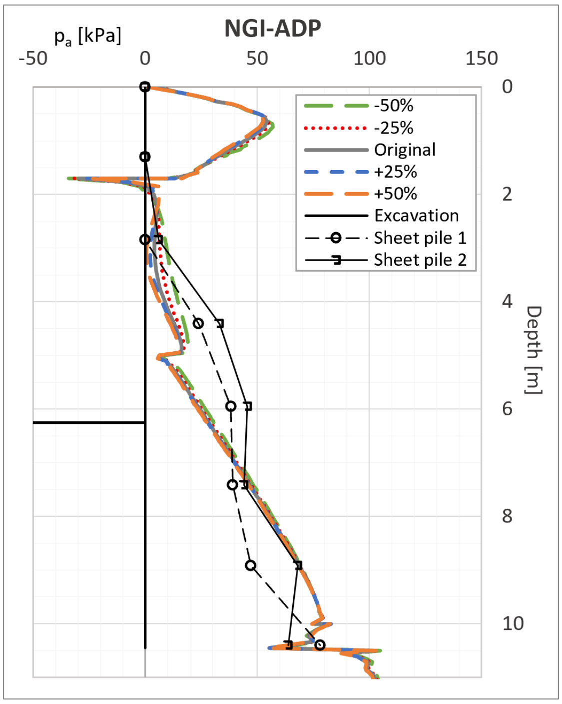

(b) Active earth pressure distribution from NGI-ADP material model

Figure 7.4: Results for the active earth pressure in the Lindome case study for varying the sheet pile wall bending stiffness

8

Conclusions

The aim of the study was to compare analytical and numerical methods for excavations in soft clays and evaluate under which conditions numerical analyses provide additional value. The methods included hand calculations, Spontprogrammet, and numerical analyses in PLAXIS 2D using the MC and NGI-ADP material models.

The results show that the analytical methods are sufficient when the main purpose is to estimate the earth pressures required for wall length and waler strength. For the single-supported theoretical case, the hand calculations and Spontprogrammet showed very similar results. Indicating that both methods are reliable when the same simplifications, assumptions and calculation principles are applied. The numerical models, however, provided additional information about wall displacements and stress distributions that cannot be calculated analytically.

For the multiple-supported theoretical case, the differences became more evident. This implies that the advantage of numerical analyses increases when the structural system of the excavation becomes more complex. The additional support level creates a case in which stress distribution and deformation behaviour become more complex. In this case, numerical analyses provided a more detailed prediction of the soil-structure interaction.

The comparison of the Lindome field measurements showed that none of the calculation methods could describe the wall deformation. The calculated earth pressures partly aligned with the measured values, but the measured behaviour was not fully captured. This was likely due to external factors such as construction-related effects, measurement uncertainties or limitations in modelling.

The modified soil properties used to account for the 3D-effects did not appear to negatively affect the calculated results. The parametric study also concluded that the earth pressure is insensitive to the studied input parameters. However, the modified properties are a simplified representation of the stabilising effects which could not be accounted for in a 2D analysis. They should not be interpreted as representative values but as a modelling assumption to achieve stability in the analysis.

The MC model provides a simpler representation of soil behaviour, whereas the NGI-ADP model accounts for anisotropic undrained shear strength in clay. Results showed that the choice of material model influences the calculated response, especially regarding wall displacement and earth pressures. However, the NGI-ADP model did not consistently provide results closer to the measured data. The results show that a more advanced numerical model does not automatically provide a better representation, especially when only limited field data are available.

The parametric study showed that the earth pressure distribution was relatively insensitive to changes in stiffness parameters. In contrast, the horizontal displacements and the waler forces were more affected, especially by variations in the soil stiffness. Soil stiffness had the greatest influence on all parameters, especially sheet pile displacements. However, the axial force of the struts was negligibly affected by all of the studied inputs. Varying the sheet pile wall stiffness primarily affected the wall's shape and deflection, but the differences were relatively small. This indicates that a good approximation of the soil stiffness is important when using numerical methods to evaluate the deformations.

Overall, analytical methods remain useful and reliable when the geometry and loading conditions are relatively simple. Results can also be transferred into other simple programs for further calculations. Numerical models requires carefully evaluated input parameters, realistic modelling assumptions, and a clear understanding of the limitations. However, when used correctly, PLAXIS provides more informative results when the excavation geometry is more complex, when the deformations are important or when earth pressures need to be evaluated in detail. In the end it becomes a question of preferring to work with several simpler calculation tools or one more complex.

Finally, several possible uncertainties may have influenced the results of this study. This includes simplifications of soil properties and stratigraphy, limitations of 2D modelling, and assumptions regarding field measurements.

Despite these uncertainties, the study provides a clear indication of when numerical analyses can add value beyond analytical methods. Numerical methods can provide more detailed insight into soil-structure interaction, but their reliability depends on the quality of the input data and modelling assumptions. Therefore, the choice of calculation method should be based on the complexity of the problem, the available field data and the required level of detail. Ultimately, engineering judgement is required to evaluate the results for the specific design situation.

It should be noted that this study aimed to come close to measured values and replicate the conditions of the studied excavation. When working with design, the aim is to account for unfavourable conditions that may occur with a certain probability under certain modelling assumptions.

8.1 Further studies

Further studies could include more detailed modelling of the construction stages, 3D effects and long-term behaviour by including additional numerical material models.

A more extensive study can be done on the NGI-ADP model. For instance, a comparison based on a complete set of inputs from field investigations and inputs from empirical relations. More extensive field measurements would allow for better validation of the numerical results and a clearer evaluation of the model's accuracy. Also, the NGI-ADP model could be tested further by applying fully isotropic soil parameters.

References

ArchelorMittal Sheet Piling. (2026). *Pu 12 - PU®/ U sections*. https://sheetpiling.arcelormittal.com/products/u-sections/pu-sections/pu-12 Retrieved 2026, March 10.

Bjerrum, L., & Aitchison, G. (1973). Problems of soil mechanics and construction on soft clays and structurally unstable soils (collapsible, expansive and others). *8th International Conference on Soil Mechanics and Foundation Engineering*, 111–159. https://www.issmge.org/publications/online-library

Broo, H., Lundgren, K., & Plos, M. (2008). *A guide to non-linear finite element modelling of shear and torsion in concrete bridges*. Chalmers University of Technology.

Edstam, T., & Jendeby, L. (1993). Behaviour of a braced sheet pile wall in soft clay. *International Conference on Case Histories in Geotechnical Engineering*.

Edstam, T., & Jendeby, L. (1992). *Spont i anslutning till djupa schakt i lös lera* (tech. rep.). Chalmers university of technology.

Fredriksson, A., Kullingsjö, A., Ryner, A., & Stille, H. (2024). *Sponthandboken rapport 107* (tech. rep.). Pålkommissionen. https://www.palkommissionen.org.

Grimstad, G., Andresen, L., & Jostad, H. P. (2012). Ngi-adp: Anisotropic shear strength model for clay. *International Journal for Numerical and Analytical Methods in Geomechanics*, *36*. https://doi.org/10.1002/nag.1016

Jasoliya, D., Untaroiu, A., & Untaroiu, C. (2024). A review of soil modelling for numerical simulations of soil-tire/agricultural tools interaction. *Journal of Terramechanics*, *111*, 41–64. https://doi.org/10.1016/j.jterra.2023.09.003

Karstunen, M., & Amavasai, A. (2017, November). *Best soil: Soft soil modelling and parameter determination*. Chalmers University of Technology.

Knappett, J. A., & Craig, R. F. (2012). *Craig's soil mechanics* (8th ed.). Spon Press.

Ladd, C., & Foott, R. (1974). New design procedure for stability of soft clays. *Journal of the geotechnical engineering division*, *100*(7).

Lees, A. (2016). *Geotechnical finite element analysis*. ICE Publishing.

Lundström, K., Andersson, M., Dehlbom, B., & Vesterberg, B. (2025). *Egenskapsförändringar i lös lera under provfyllningar: Förändringar efter 60 år i skåedeby* (tech. rep.). Statens Geotekniska Institut,SGI.

Ottosen, N. S., & Petersson, H. (1992). *Introduction to the finite element method* (1st ed.). Prentice Hall.

Papavasileiou, S. (2024). https://bentleysystems.service-now.com/community?id=kb_article&sysparm_article=KB0108936

Plevris, V., & Markeset, G. (2018). Educational challenges in computer-based Finite Element Analysis and design of structures. *Journal of Computer Science*, *14*, 1351–1362. https://doi.org/10.3844/jcssp.2018.1351.1362

Rankine, W. J. M. (1857). On the stability of loose earth. *Philosophical Transactions of the Royal Society of London*.

Ryner, A. (2022). *Manual spontprogrammet*. RySoft AB.

Sahlström, P. O., & Stille, H. (1979). *Förankrade sponter*. Svensk Byggtjänst.

Seequent. (2022). *Stability modelling with geostudio*. Seequent.

Seequent. (2025a). *Plaxis 2d 2025.1 general information manual*. Bentley systems.

Seequent. (2025b). *Plaxis 2d 2025.1 materials models manual*. Bentley systems.

Seequent. (2025c). *Plaxis 2d 2025.1 reference manual*. Bentley systems.

Seequent. (2025d). *Plaxis 2d 2025.1 scientific manual*. Bentley systems.

Skredkommissionen. (1995). *Ingenjörsvetenskapsakademien royal swedish academy of engineering sciences* (tech. rep.). Statens Geotekniska Institut (SGI).

Stille, H. (1976). *Behaviour of anchored sheet pile walls* (tech. rep.). Royal Institute of Technology.

Swedish Standards Institute. (2005). *Eurokod 7: Dimensionering av geokonstruktioner-del 1: Allmänna regler eurocode 7: Geotechnical design-part 1: General rules* (tech. rep.). Svenska institutet för standarder (SIS).

Terzaghi, K. (1946). *Theoretical soil mechanics*. John Wiley; Sons, Inc.

Terzaghi, K., & Peck, R. B. (1967). *Soil mechanics in engineering practice.* John Wiley; Sons, Inc.

Tornborg, J. (2024). *Horisontella vilojordtryck i lera sammanställning av mätresultat samt uppdaterade empiriska samband för normal-till svagt överkonsoliderade leror* (tech. rep.). Skanska Sverige AB.

Trafikverket. (2011, June). *Trafikverkets tekniska krav för geokonstruktioner* (tech. rep.). Trafikverket.

Trafikverket. (2025). *Geokonstruktion, dimensionering och utformning* (tech. rep. No. TRVINFRA-00230). Trafikverket.

A

Soil properties from field measurements

A.1 Undrained shear strength and water content

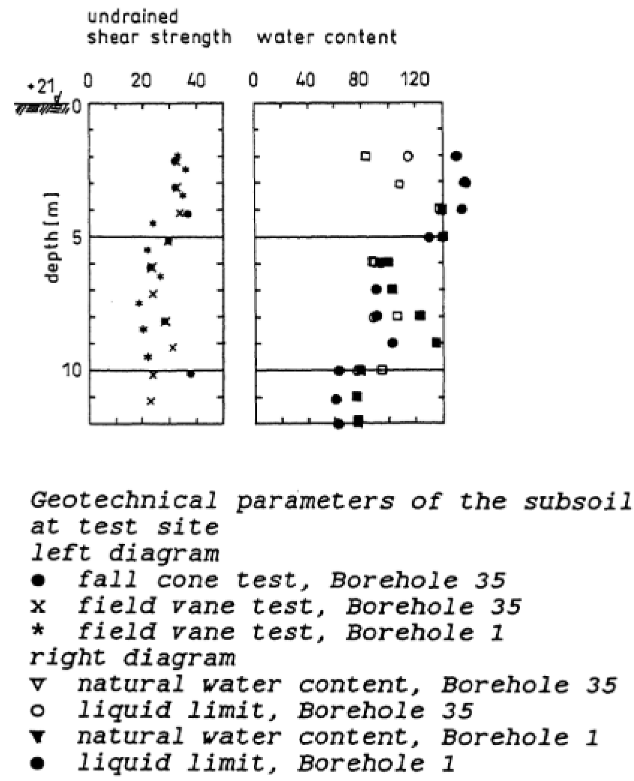

Figure A.1: Uncorrected undrained shear strength on the left and water content and liquid limit on the right (Edstam & Jendeby, 1993).

A.2 Choosing K_0 in Lindome calculation models

K_0 was estimated based on earth pressures measured by pressure cells that were installed on the sheet pile wall. Back-calculations where performed according to Equation (2.2) and the re-calculated initial earth pressure was plotted along with the field measurements in Figure A.2 for evaluation.

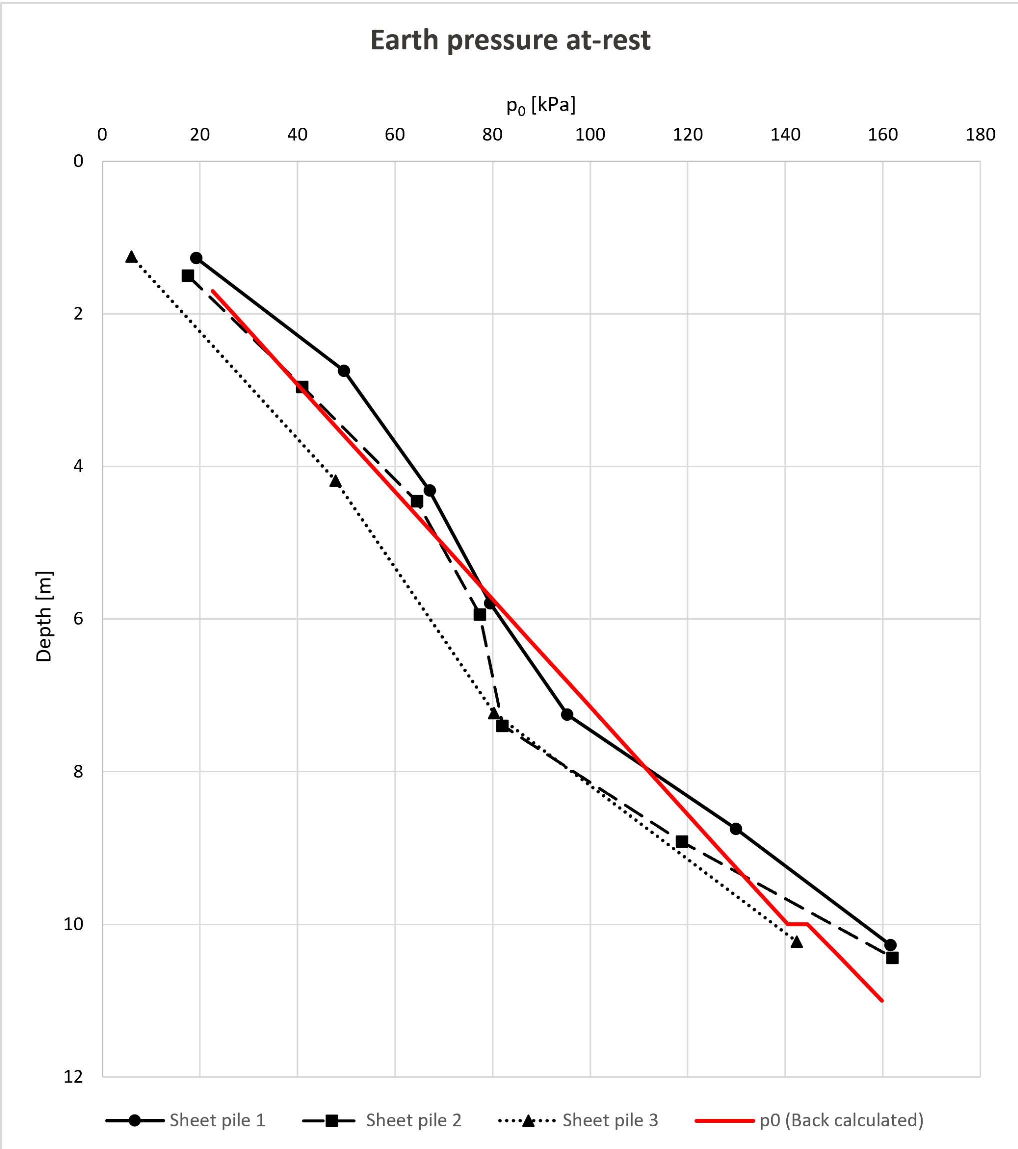

Figure A.2: Comparison of calculated earth pressure at rest and measured rest

B

NGI-ADP material model input parameters

PLAXIS DSS SoilTest was used for both the soil stratigraphies to convert the MC material models to NGI-ADP materials. The DSS test for the theoretical cases is displayed in Figure B.1 and the Lindome soil test is shown in Figure B.2. The aim of the tests was to achieve a material for the NGI-ADP model that can represent the same soil as the MC model. This was done while keeping in mind that the test results are supposed to have differences because of the way the material models are designed.

The soil tests started from assumptions based on empirical relations to undrained shear strength and Poisson's ratio from Trafikverket (2025) according to Equations (B.1) and (B.2). The stiffness raio and the failure strains were varied until satisfactory input paramters were achived.

$$E = 250 \cdot c_u \tag{B.1}$$

$$G = \frac{E}{2 \cdot (1 + \nu)} \tag{B.2}$$

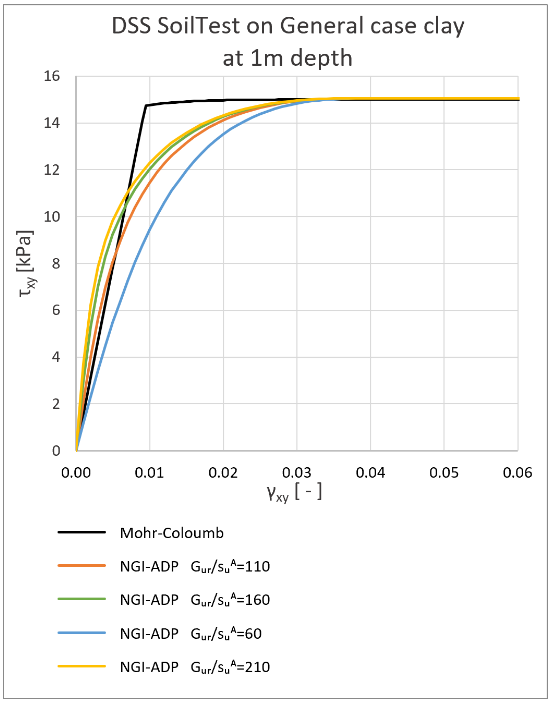

(a) At -1m, $s^{\mathrm{A}}_{\mathrm{u,ref}} = 19.5kPa$, $|\sigma'_{\mathrm{yy}}| = 28kPa$

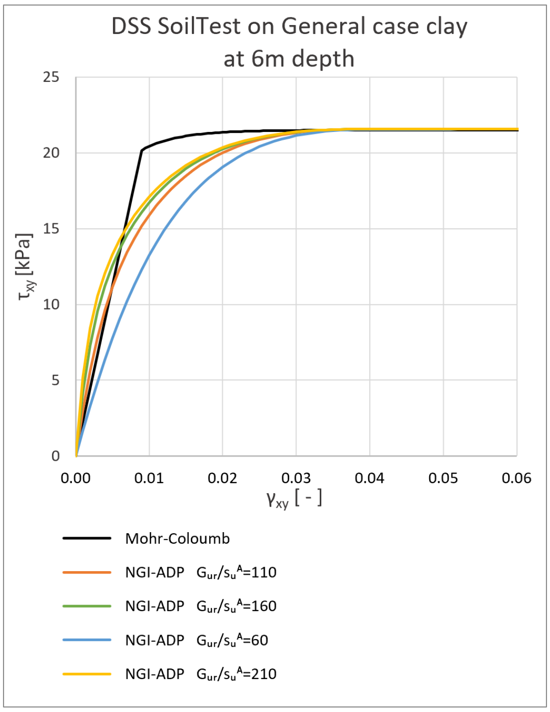

(b) At -6m, $s^{\mathrm{A}}_{\mathrm{u,ref}} = 28kPa$, $|\sigma'_{\mathrm{yy}}| = 108kPa$

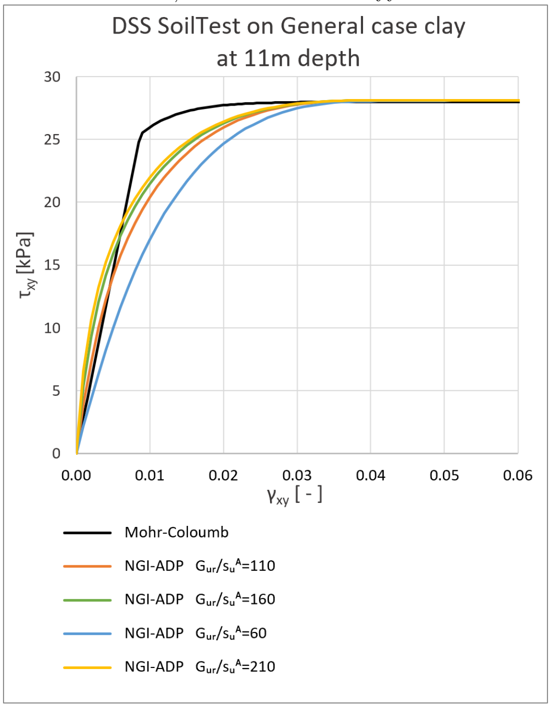

(c) At -11m, $s^{\mathrm{A}}_{\mathrm{u,ref}} = 36.5kPa$, $|\sigma'_{\mathrm{yy}}| = 188kPa$

Figure B.1: Graphs used for determining G_{ur}/s_u^A in the General case study based on DSS SoilTest in PLAXIS 2D. $\gamma^C = 3$, $\gamma^E = 6$, $\gamma^{DSS} = 4$ was assumed in all tests

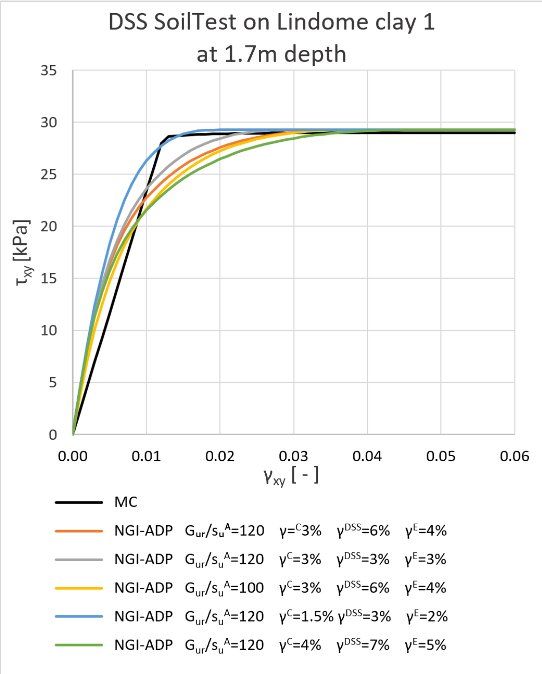

(a) Clay 1 at -1.7m, $s^{\mathrm{A}}_{\mathrm{u,ref}} = 38kPa$, $|\sigma'_{\mathrm{yy}}| = 32kPa$

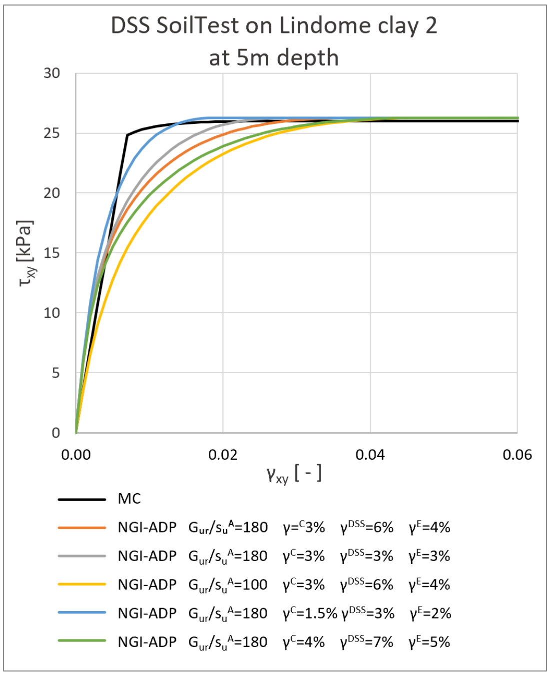

(b) Clay 2 at -5m, $s^{\mathrm{A}}_{\mathrm{u,ref}} = 36kPa$, $|\sigma'_{\mathrm{yy}}| = 52.1kPa$

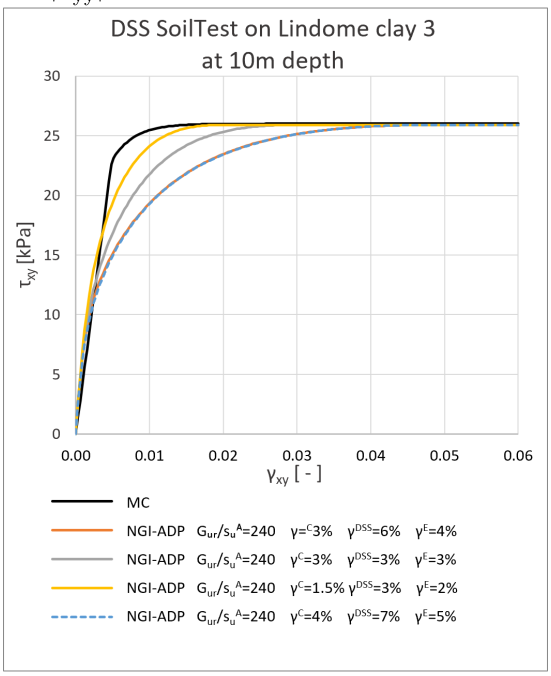

(c) Clay 3 at -10m, $s^{\mathrm{A}}_{\mathrm{u,ref}} = 37kPa$, $|\sigma'_{\mathrm{yy}}| = 82.1kPa$

Figure B.2: Graphs used for determining G_{ur}/s_u^A, γ^C, γ^E, γ^{DSS} in the Lindome case study based on DSS SoilTest in PLAXIS 2D

C

Implementation of SLOPE/W

C.1 Theory

The concept of the Limit Equilibrium Method (LEM) is to be able to calculate the stability of slopes by assessing their slip surface and dividing the sliding mass into parts vertically. It is an old method of numerical analysis that in modern times is commonly performed by computer softwares, such as in this case, Geostudio SLOPE/W (Seequent, 2022).

C.2 Theoretical excavations

SLOPE/W was implemented to obtain a sheet pile wall length that contributes to rotational stability around the single-strut placement. The *grid and radius* option was used to get a satisfactory safety factor (SF) for total stability of the construction. The studied slip surface radius is equal to the sheet pile wall length and the the centre of rotation is as close to the placement of the strut as possible. The wall length was iterated until SF=1 with dimensioning soil parameters. Partial factors that were applied to the soil parameters are presented in table C.1. In order to determine the geometry of the model, partial safety factors were used. These factors are used to transform characteristic values to dimensioning values. The partial factors are applied to increase the load and reduce the shear strength to obtain a lower bound solution. The partial safety factors that were used are presented in table C.1

Table C.1: Partial safety factors applied in SLOPE/W and in analytical calculations

	Magnitude	Application
$\gamma_{\varphi'}$	1.3	Effective friction angle
γ_{cu}	1.5	Undrained shear strength

The soil characteristic soil parameters used are similar to the actual soil of the main case study and follows realistic values for what could be seen as typical Gothenburg clay. Soil parameters used as input to SLOPE/W are presented in table C.2. The unit weight of the sheet pile wall is set according to data from ArchelorMittal Sheet Piling (2026).

Table C.2: Material parameters for stability calculations in SLOPE/W

		Fill	Clay	Sheet pile	
Unit weight	γ_{sat}	18	16	786	$[\frac{kN}{m^3}]$
Effective friction angle	Φ'	42	-	-	$[°]$
c_u at top of layer	$c_{u,ref}$	-	15	-	[kPa]
Rate of change of c_u	$c_{u,inc}$	-	1.3	-	$[\frac{kPa}{m}]$
Soil model	-	Mohr-Coulomb	S=f(datum)	High strength	[-]

The final recommended geometry for the theoretical single-supported excavation can be seen in figure C.1. According to the model, the sheet pile wall needs to be 6.7 m deep to provide rotational stability in ULS calculations. This length have been inserted to the PLAXIS 2D models and confirmed with equilibrium equations in analytical calculations.

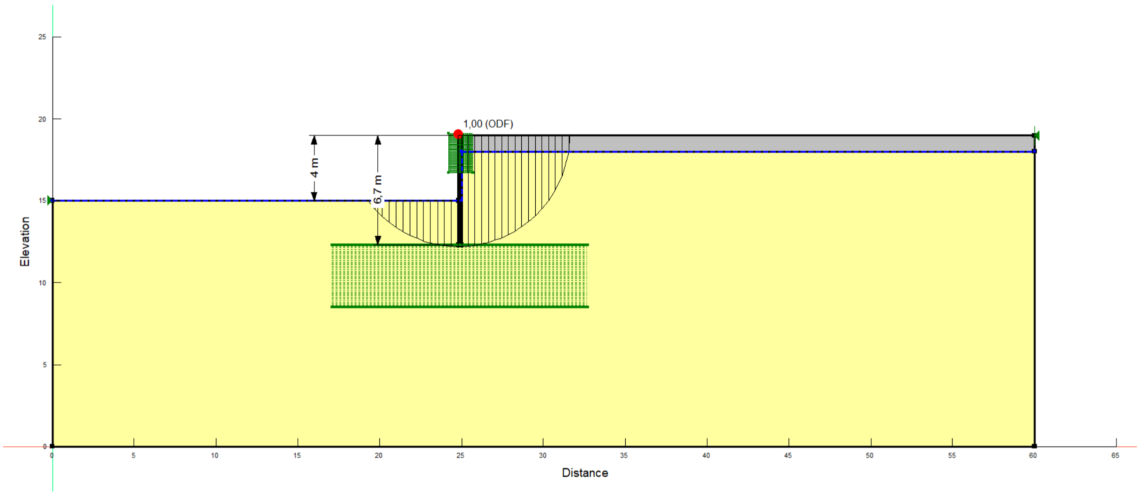

Figure C.1: Results from total stability analysis in SLOPE/W

C.3 Lindome excavation

In the Lindome excavation, the excavation geometry was already known. However, the sectin is not rotationally stable without the surrounding 3D-effects which can not be incorprated in a 2D model. SLOPE/W was then used to increase the undrained shear strength of the soil layers until the global safety factor SF=1.3 was achieved.

Partial factors have not been applied in this analysis since the calculation aims to recreate the actual soil in Lindome. The final SLOPE/W model with chosen c_u-values can be found in Figure C.2.

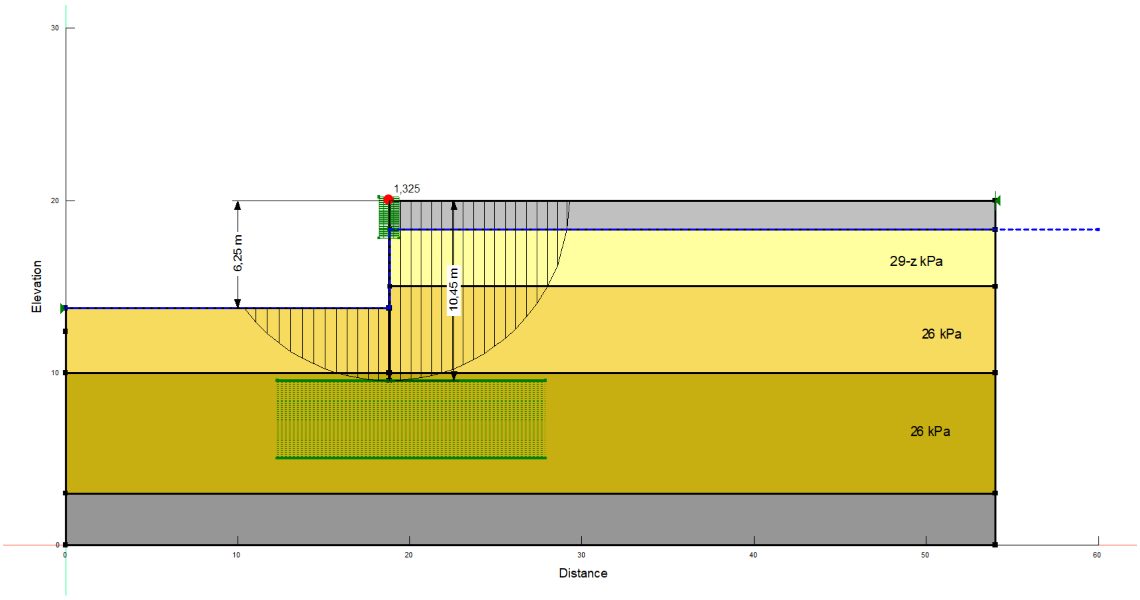

Figure C.2: Results from total stability analysis in SLOPE/W

D

Results from Spontprogrammet

Result outputs from the Spontprogrammet calculations are presented below from all studied cases.

D.1 Theoretical case of single-strutted excavation

Brottlastberäkning enligt EN 1997, SPHB 2018

Säkerhetsklass: 2 $\gamma_{S;d,a,Frik}$: 1,00 $\gamma_{R;d,p,Frik}$: 1,00 Värdena belastar endast de permanenta nettotrycken

γ_d: 0,91 $\gamma_{S;d,a,Lera}$: 1,00 $\gamma_{R;d,p,Lera}$: 1,00

Ncb: 5,7 $\gamma_{S;d}$: 1,274 (vekt konstruktionselement)

Jordartstabell

Jord nr	Jordartstyp	Geokonstruktionens Hållfasthetsvärden Pop-Medelv.	ökning /m	Dimensionerande	ökning /m	Densiteter kN/m³ Torr	Vattenmättad	Partialkoefficient	η-värde
1	Friktionsjord	34 °	0,00	27,4 °	0,00	19	22	1,3	1,00
2	Lera	15 kPa	1,30	10 kPa	0,87	16	16	1,5	1,00

Jordtrycksberäkning

Aktivt tryck

Nivå	σ_v	ϕ_d	C_{ud}	Ka	U_w	σ_a	SBN	HB	VB	σ_{htot}
	Jord						Horisontell intensitet från Lokala Överlaster enl.			
+10,0	0,0	27,4		0,370		0,0				
+9,0	19,0	27,4		0,370		7,0				
+9,0	19,0		10,0			-1,0				
+6,0	67,0		12,6			41,8				
+3,2	111,8		15,0			81,8				
+0,0	163,0		17,8			127,5				

Passivt tryck

Nivå	σ_v	ϕ_d	C_{ud}	Kp	U_w	σ_p
+6,0	0,0		12,6			25,2
+3,2	44,8		15,0			74,9
+0,0	96,0		17,8			131,7

Dimensionerande jordtryck

Nivå	$\sigma_a - \sigma_p$	σ_{netto}	Lokala överlaster	Dim jordtryck inkl överlast
+10,0	0,0		0,0	0,0
+9,0	7,0		0,0	7,0
+9,0	-1,0		0,0	0,0
+6,0	41,8		0,0	41,8
+6,0		-5,1	0,0	-5,1
+3,2		-18,8	0,0	-18,8
+0,0		-34,6	0,0	-34,6
+0,0	-4,2		0,0	-34,6

Beräkningsförutsättningar

Sponten har dimensionerats utan omfördelning av jordtrycket

Sponten har förutsatts slagen så att grundvattnet inte läcker mellan aktiv och passivsida

Beräkningsresultat brottgränsberäkning

Erforderlig spont uk:	+3,2
Pådrivande jordtryck:	64,9 kN/m
Pådrivande jordtryckets moment runt hammarbandet:	181,1 kNm/m
Mothållande jordtryck:	33,1 kN/m
Mothållande jordtryckets moment runt hammarbandet:	184,5 kNm/m
Mothållande jordtryckets hävarm till hammarbandet:	5,6 m
Hammarbandsnivå:	+9,9 m
Horisontell hammarbands last $q_{h,Ed}$:	32,4 kN/m

Dimensionerande moment se sid 55 i Sponthandboken 2018

T=0 på nivå +6,9

h= 3,00 m

hA= 0,89 m

M_{Ed}= 32,37 · (3,00 - 0,89) = 68,4 kNm/m (16,1 %)

Tvärkraft

T_{Ed}: 32,5 kN/m på nivå 6,0

Brottgräns beräkning enligt EN-1997, SPHB 2018 i Säkerhetsklass: 2
Vald spont: PU 12

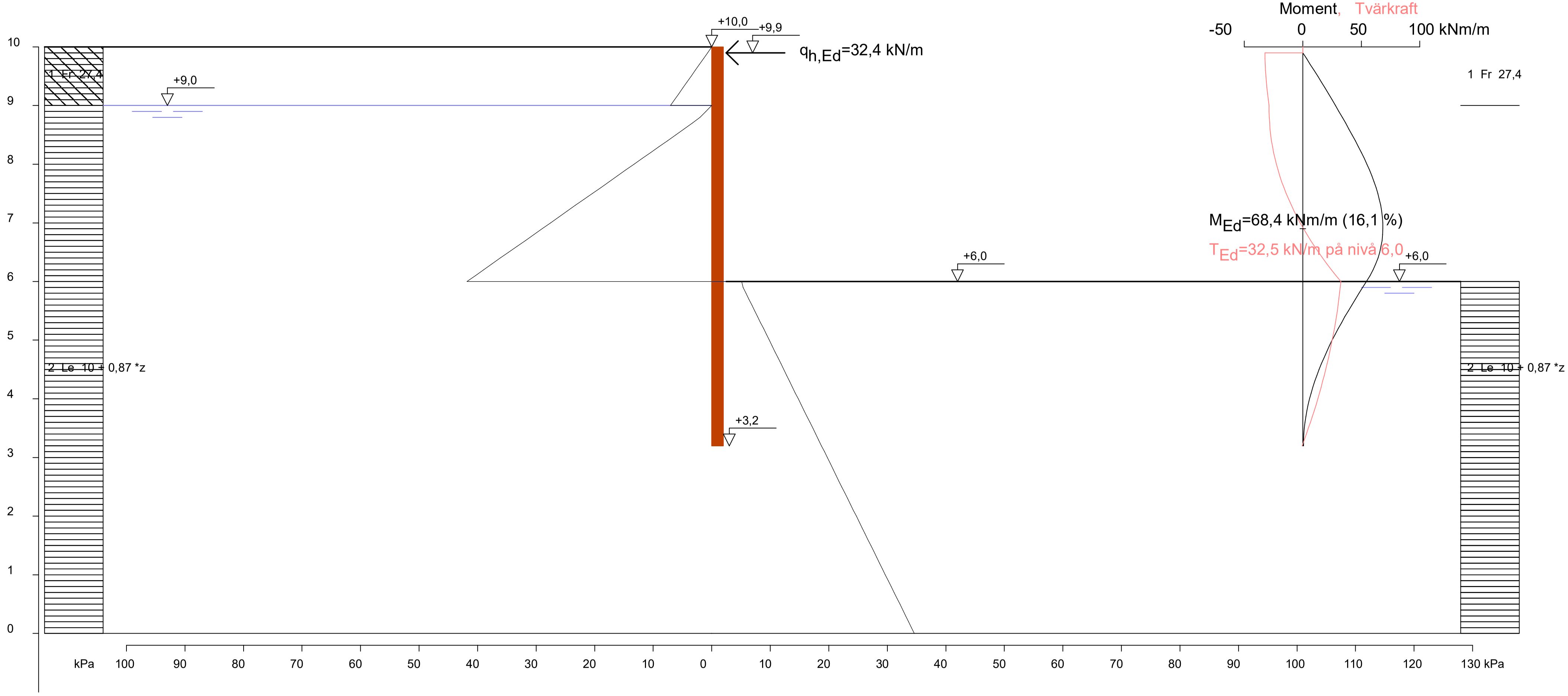

Skala 1:100

Uppdragsnr		Sektion	Sid nr
1	Examensarbete	Case	

Spontprogrammet Ver: 3,63 Datum: 2026-05-19 09:37:24 Konstruktör: Elin Johansson & Erica Larsson Chalmers tekniska högskola

D.2 Theoretical case of multiple-strutted excavation

Brottlastberäkning enligt EN 1997, SPHB 2018

Säkerhetsklass: 2 $\gamma_{S;d,a,Frik}$: 1,00 $\gamma_{R;d,p,Frik}$: 1,00 Värdena belastar endast de permanenta nettotrycken
γ_d: 0,91 $\gamma_{S;d,a,Lera}$: 1,00 $\gamma_{R;d,p,Lera}$: 1,00
Ncb: 5,7 $\gamma_{S;d}$: 1,274 (vekt konstruktionselement)

Jordartstabell

Jord nr	Jordartstyp	Geokonstruktionens Hållfasthetsvärden: Pop-Medelv.	ökning /m	Dimensionerande	ökning /m	Densiteter kN/m³: Torr	Vatten-mättad	Partial-koefficient	η-värde
1	Friktionsjord	41,2 °	0,00	34 °	0,00	19	22	1,3	1,00
2	Lera	22,5 kPa	1,95	15 kPa	1,30	16	16	1,5	1,00

Jordtrycksberäkning

Aktivt tryck — Jord — Horisontell intensitet från Lokala Överlaster enl.

Nivå	σ_v	ϕ_d	C_{ud}	Ka	U_w	σ_a	SBN	HB	VB	σ_{htot}
+10,0	0,0	34,0		0,283		0,0				
+9,0	19,0	34,0		0,283		5,4				
+9,0	19,0		15,0			-11,0				
+3,0	115,0		22,8			69,5				
+0,0	163,0		26,7			109,7				
- 3,7	222,2		31,5			159,3				

Passivt tryck

Nivå	σ_v	ϕ_d	C_{ud}	Kp	U_w	σ_p
+3,0	0,0		22,8			45,6
+0,0	48,0		26,7			101,4
- 3,7	107,2		31,5			170,2

Dimensionerande jordtryck

Nivå	$\sigma_a - \sigma_p$	σ_{netto}	Lokala överlaster	Dim jordtryck inkl överlast
+10,0	0,0		0,0	0,0
+9,0	5,4		0,0	5,4
+9,0	-11,0		0,0	0,0
+3,0	69,5		0,0	69,5
+3,0		-15,3	0,0	-5,0
+0,0		-37,2	0,0	-34,1
- 3,7		-64,6	0,0	-64,6
- 3,7	-10,9		0,0	-64,6

Beräkningsförutsättningar

Sponten har dimensionerats för omfördelat jordtryck

Sponten har förutsatts slagen så att grundvattnet inte läcker mellan aktiv och passivsida

Beräkningsresultat brottgränsberäkning

Vald spont uk:	+0,0
d-nivå:	+3,9
Intensitet omfördelat jordtryck:	25,7 kN/m²
Summa pådrivande jordtryck över d-nivån exkl vatten:	138,7 kN/m
Summa pådrivande vattentryck över d-nivån:	0,0 kN/m
Summa pådrivande jordtryck under d-nivån:	57,1 kN/m
Summa mothållande jordtryck under d-nivån:	57,6 kN/m

Horisontella hammarbandslaster

Nivå:	+9,9	$q_{h,Ed}$:	28,3 kN/m
Nivå:	+6,5	$q_{h,Ed}$:	110,5 kN/m

Moment i spontväggen:

Övre konsol:	0,0 kNm/m
Max fältmoment mellan stagnivåer:	20,4 kNm/m
Moment under understa hammarbandet(fritt upplagt):	50,2 kNm/m

Momentet under understa hammarbandet har dimensionerats för dimensionerande icke omfördelat jordtryck, se prickad linje

Dimensionerande moment M_{Ed}:	50,2 kNm/m (11,8 %)

Brottgräns beräkning enligt EN-1997, SPHB 2018 i Säkerhetsklass: 2
Vald spont: PU 12

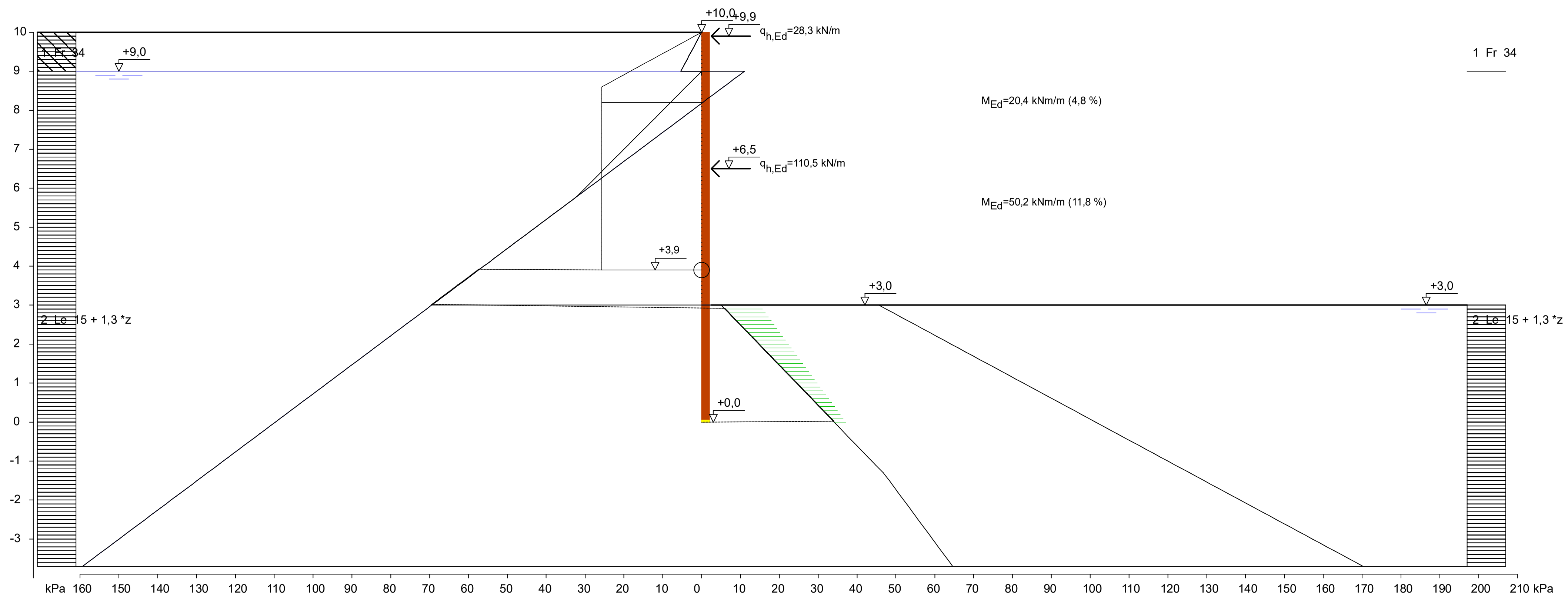

Skala 1:150

Uppdragsnr		Sektion	Sid nr
1	Examensarbete	Case_flerband_uppräknad	

Spontprogrammet Ver: 3,63 | Datum: 2026-05-22 09:23:18 | Konstruktör: Elin Johansson & Erica Larsson | Chalmers tekniska högskola

D.3 Lindome excavation

Brottlastberäkning enligt EN 1997, SPHB 2018

Säkerhetsklass: 2 $\gamma_{S;d,a,Frik}$: 1,00 $\gamma_{R;d,p,Frik}$: 1,00 Värdena belastar de permanenta jordtrycken
γ_d: 0,91 $\gamma_{S;d,a,Lera}$: 1,00 $\gamma_{R;d,p,Lera}$: 1,00
Ncb: 5,7 $\gamma_{S;d}$: 1,274 (vekt konstruktionselement)

Jordartstabell

Jord nr	Jordartstyp	Geokonstruktionens Hållfasthetsvärden Pop-Medelv.	ökning /m	Dimensionerande	ökning /m	Densiteter kN/m³ Torr	Vattenmättad	Partialkoefficient	η-värde
1	Friktionsjord	41,2 °	0,00	34 °	0,00	19	22	1,3	1,00
2	Lera	43,5 kPa	-1,50	29 kPa	-1,00	16	16	1,5	1,00
3	Lera	39 kPa	0,00	26 kPa	0,00	16	16	1,5	1,00
4	Lera	39 kPa	0,00	26 kPa	0,00	17	17	1,5	1,00
5	Friktionsjord	47,5 °	0,00	40 °	0,00	21	21	1,3	1,00

Jordtrycksberäkning

Aktivt tryck — Jord — Horisontell intensitet från Lokala Överlaster enl.

Nivå	σ_v	ϕ_d	C_{ud}	Ka	U_w	σ_a	SBN	HB	VB	σ_{htot}
+20,0	0,0	34,0		0,283		0,0				
+18,3	32,3	34,0		0,283		9,1				
+18,3	32,3		29,0			-25,7				
+15,0	85,1		25,7			33,7				
+15,0	85,1		26,0			33,1				
+13,7	105,9		26,0			54,0				
+10,0	165,1		26,0			113,2				
+10,0	165,1		26,0			113,2				
+9,5	173,6		26,0			121,7				
+7,0	216,1		26,0			164,3				

Passivt tryck

Nivå	σ_v	ϕ_d	C_{ud}	Kp	U_w	σ_p
+13,7	0,0		26,0			52,0
+10,0	59,2		26,0			111,2
+10,0	59,2		26,0			111,2
+9,5	67,7		26,0			119,7
+7,0	110,2		26,0			162,2

Dimensionerande jordtryck

Nivå	$\sigma_a - \sigma_p$	σ_{netto}	Lokala överlaster	Dim jordtryck inkl överlast
+20,0	0,0		0,0	0,0
+18,3	9,1		0,0	9,1
+18,3	-25,7		0,0	0,0
+15,0	33,7		0,0	33,7
+15,0	33,1		0,0	33,1
+13,7	54,0		0,0	54,0
+13,7		-42,3	0,0	-28,1
+10,0		-42,3	0,0	-42,3
+10,0		-42,3	0,0	-42,3
+9,5		-42,3	0,0	-42,3
+7,0		-42,3	0,0	-42,3
+7,0	2,1		0,0	-42,3

Beräkningsförutsättningar
Sponten har dimensionerats utan omfördelning av jordtrycket

Sponten har förutsatts slagen så att grundvattnet inte läcker mellan aktiv och passivsida

Beräkningsresultat brottgränsberäkning

Erforderlig spont uk:	+9,5
Pådrivande jordtryck:	118,9 kN/m
Pådrivande jordtryckets moment runt hammarbandet:	532,2 kNm/m
Mothållande jordtryck:	160,9 kN/m
Mothållande jordtryckets moment runt hammarbandet:	1357,1 kNm/m
Mothållande jordtryckets hävarm till hammarbandet:	7,4 m
Hammarbandsnivå:	+19,9 m
Horisontell hammarbands last $q_{h,Ed}$:	46,7 kN/m

Dimensionerande moment se sid 55 i Sponthandboken 2018

T=0 på nivå +15,5

h= 4,40 m

hA= 1,35 m

M_{Ed}= 46,65 · (4,40 - 1,35) = 142,5 kNm/m (33,4 %)

Tvärkraft

T_{Ed}: 72,2 kN/m på nivå 13,7

E

Mesh sensitivity study

A mesh sensitivity study was conducted to determine an acceptable mesh size for the numerical analyses. The study aimed to determine a mesh size where the results show convergence, meaning further refinement of the mesh does not lead to significant changes in the result. See the mesh study in Figures E.1 to E.3. The plot at the very front i each figure was chosen as the final mesh.

The final mesh size was decided by comparing the earth pressures that are taken from the interfaces of the wall and comparing the abnormal and anomalies in the earth pressure profile. When the anomalies and the values converged, the mesh was sufficiently refined and was considered to provide an acceptable level of accuracy while maintaining reasonable computational cost and energy.

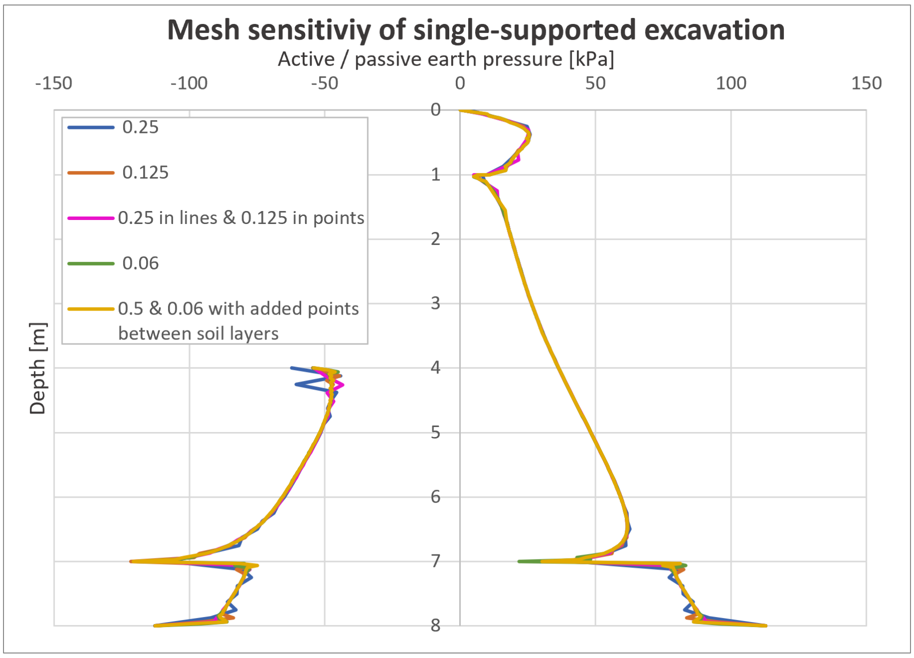

Figure E.1: Mesh sensitivity study on the theoretical single-supported excavaion

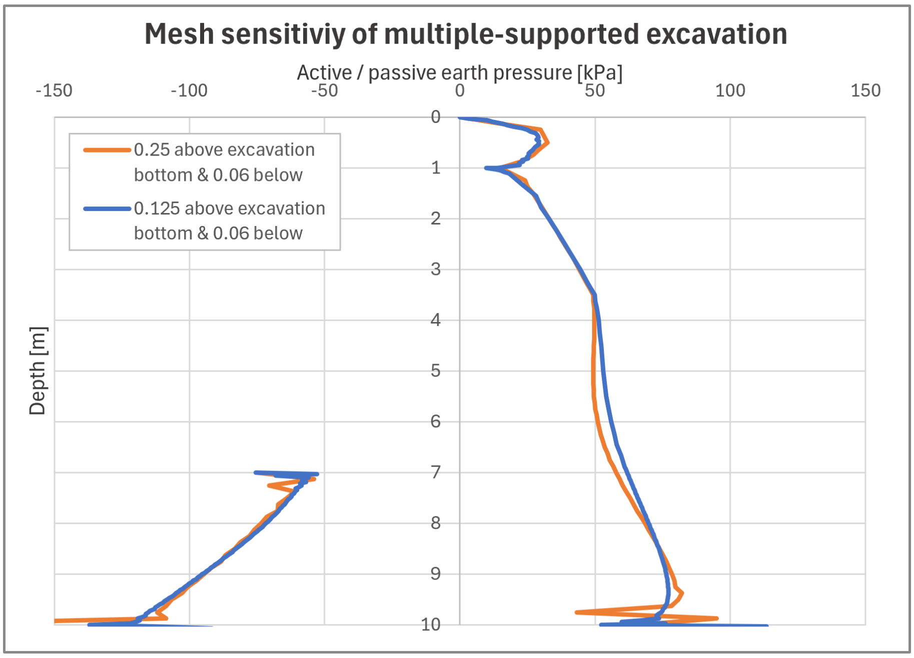

Figure E.2: Mesh sensitivity study on the theoretical multiple-supported excavation

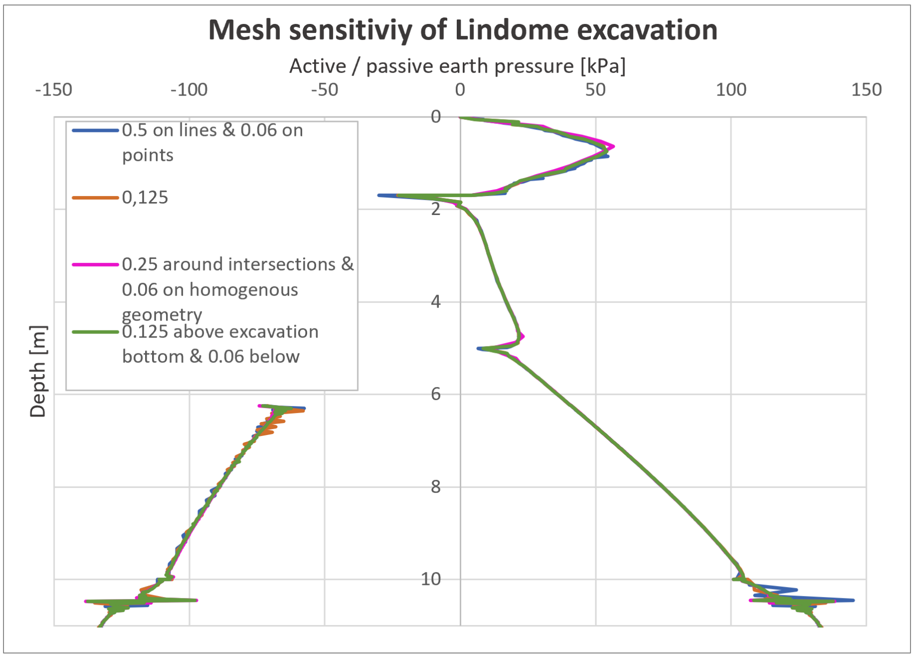

Figure E.3: Mesh sensitivity study on the Lindome excavation